Monitoring induced seismicity near the Wellington oil field, South-Central Kansas

By:

Keith A. Nolte

Submitted to the graduate degree program in Geology and the Graduate Faculty of the University of Kansas in partial fulfillment of the requirements for the degree of Master of Science.

_____

Chairperson, Dr. George P. Tsoflias

_____

Dr. Ross A. Black

_____

Dr. Evan K. Franseen

Date Defended:

The thesis committee for Keith Nolte

certifies that this is the approved version of the following thesis:

Monitoring induced seismicity near the Wellington oil field, South-Central Kansas

_____

Chairperson, Dr. George P. Tsoflias

Date Approved:

ABSTRACT

Seismicity in the United States midcontinent has increased by orders of magnitude over the past decade. Spatiotemporal correlations of seismicity to wastewater injection operations have suggested that injection-related pore fluid pressure increases are inducing the earthquakes. In this investigation, I examine earthquake occurrence in southern Kansas and northern Oklahoma and its relation to the change in pore pressure. The main source of data comes from the Wellington Array in the Wellington oil field, in Sumner County, KS, which has monitored for earthquakes in central Sumner County, KS since early 2015. A catalog of earthquakes was built from this data. These earthquakes were then analyzed for spatial and temporal changes, stress information, and anisotropy information. The region of seismic concern has been shown to be expanding through use of the Wellington earthquake catalog, and has revealed a northward progression of earthquake activity reaching the metropolitan area of Wichita. The stress orientation was also calculated from this earthquake catalog through focal mechanism inversion. The calculated stress orientation was confirmed through comparison to other stress measurements from well data and previous earthquake studies in the region. With this knowledge of the stress orientation, the anisotropy in the basement could be understood. This allowed for the anisotropy measurements to be correlated to pore pressure increases. The increase in pore pressure is monitored through time-lapse shear-wave anisotropy analysis. Since the onset of the observation period in 2010, the orientation of the fast shear-wave has rotated 90°, indicating a change associated with critical pore pressure build up. The time delay between fast and slow shear wave arrivals has increased, indicating a corresponding increase in anisotropy induced by pore pressure rise. *In-situ* near-basement fluid pressure measurements corroborate the continuous pore pressure increase revealed by the shear-wave anisotropy analysis over the earthquake-monitoring period.

This research is the first to identify a change in pore fluid pressure in the basement using seismological data. The shear-wave splitting analysis is a novel application of the technique, which can be used in other regions to identify an increase in pore pressure. This increasing pore fluid pressure has become more regionally extensive as earthquakes are occurring in southern Kansas, where they previously were absent. These monitoring techniques and analyses provide new insight into mitigating induced seismicity's impact to society.

ACKNOWLEDGEMENTS

This research was supported by the Kansas Interdisciplinary Carbonates Consortium (KICC) and the Kansas Geological Survey (KGS) through a grant from the US Department of Energy National Energy Technology Laboratory (DOE-NETL) and cost-sharing partners.

I would like to thank my mentor Dr. George Tsoflias for his support on this project. Many hours of discussion and thought went into the creation of this project, and it could not have been done without him. Thank you to my committee members Dr. Ross Black and Dr. Evan Franseen for their valuable insights on laying out the project and the writing of this thesis.

Additionally, I would like to thank Dr. Lynn Watney and Dr. Tandis Bidgoli for their work on this project through the KGS. Thank you to Jenn Hallenbach and the rest of the KGS staff for supporting this work. I am grateful for the many discussions with all of the students in my department, especially those who have worked for me: Lauren Haga, Betina Sodre, LingHao Chen, and Zelma Molina.

I would like to thank my fiancé Erika Northcutt; without her support I could not have finished this degree. Additionally I would like to thank my family for supporting me throughout my educational career.

TABLE OF CONTENTS

LIST OF FIGURES

Chapter 1: Introduction and Background

Section 1.1: Induced Seismicity

The seismicity being felt in Kansas and Oklahoma is a recent issue, starting in late 2000's, but other regions have been afflicted by man-made seismicity long before. The first documented case of injection-induced seismicity occurred at the Rocky Mountain Arsenal, near Denver, Colorado. Injection of chemical waste began in 1962 at the Rocky Mountain Arsenal [Evans, 1966; Healy et al., 1968]. Residents near the arsenal began to feel earthquakes a few months after injection began and the largest earthquake to occur was an M_w 4.8 in 1967 [Healy et al., 1968]. These earthquakes correlated very closely with injection volumes and the seismicity stopped shortly after injection was halted [Evans, 1966; Healy et al., 1968]. After the induced earthquakes occurred at the Rocky Mountain Arsenal, researchers wanted to confirm the hypothesis that increased pore fluid pressure can cause slip on faults. This hypothesis was proven at Rangely, Colorado in the late 1960s, where fluid was purposefully injected with the objective being to create induced earthquakes [Raleigh et al., 1976]. This study did create earthquakes and monitored fluid pressure, which was then correlated to seismicity. The work by Raleigh et al. (1976) has been furthered in an effort to predict the seismic hazard associated with fluid injection through seismic moment correlation to fluid volume injection [McGarr, 2014]. This study stated that the maximum seismic moment (earthquake size) is directly related to the volume of fluid injected, through some simplifications.

All of these previous studies have produced an understanding of how and why seismicity can be induced, and identified two major mechanisms. The first is that of loading, where the mass on a fault is increased to the point that the fault fails [Ellsworth, 2013]. This occurs by adding weight above the fault, such as constructing a dam or injecting into a reservoir above the

fault. The second scenario is one where fluid pressure increases on the fault to the point where the effective stress is reduced to the point of failure [Ellsworth, 2013; McGarr, 2014; Raleigh et al., 1976]. This is the cause of most injection-induced seismicity.

Induced seismicity is a growing concern in many regions worldwide. Recently, Arkansas [Horton, 2012], Oklahoma [Keranen et al., 2013], Ohio [Kim, 2014], and Texas [Frohlich, 2012; Frohlich et al., 2014] have all seen injection-induced seismicity.

This project focuses on injection-induced seismicity in Kansas and Oklahoma, which is a current problem that has emerged from new oilfield development methods. The United States Midcontinent has seen a drastic increase in seismicity from an historical average of 21 magnitude (M) 3 and greater earthquakes a year to 188 M3 or greater earthquakes in 2011 [Ellsworth, 2013]. This increase became even more significant in 2014, when there were 688 M 3 or greater events [Rubinstein, 2015].

This project focuses on the induced seismicity potentially associated with the Mississippian limestone play, which produces significant volumes of water during oil extraction [Ellsworth, 2015; Buchanan, 2015]. The large water volume is reinjected into deeper formations, commonly the Arbuckle, which lies directly above the granitic basement. Reinjection of fluids into deeper formations causes a pore pressure increase, which can facilitate slip on existing faults that are oriented optimally to subsurface stress fields [Ellsworth, 2013; Morris et al., 1996]. The base of the Arbuckle is considered unconfined, and injected fluids could be infiltrating the basement causing an increase in pore pressure and a scenario prone to faults slipping in the shallow basement [Keranen, 2014]. Many questions remain to be answered about how the injection of fluids causes earthquakes temporally and spatially, as little is known about the stress regime and its interactions with the fault networks that exist in the shallow basement. Most

earthquakes are difficult to tie directly to injection wells and only a small percentage of injection wells appear to have created earthquakes based on spatial correlation [Ellsworth, 2013]. This work aims to test the hypothesis that increased pore fluid pressure in the basement causes earthquakes at large distances (10-100 km) from high-rate saltwater disposal wells.

Section 1.2: The Wellington CO_2 Project

The Kansas Geological Survey (KGS) is currently testing the viability of injecting CO_2 into the Mississippian and Arbuckle formations in the Wellington oil field, which has been in production since 1929 and has produced over 20 million barrels of oil. There are currently 55 active wells in the field operated by Berexco, LLC [KGS, 2016]. The KGS has operated a seismic monitoring network in the Wellington oil field (network code ZA) since early 2015. This network consists of 15 stations on loan from the Incorporated Research Institutions for Seismology (IRIS) and 3 Nanometrics seismometer stations, owned by the KGS. The objective of the network was to monitor the seismic hazard of CO_2 injections in the Wellington oil field. These stations are spread throughout the southern part of the field, as shown in *Figure 1.1*. The seismometers are installed in shallow vaults approximately four feet beneath the surface (*Figure 1.2)*. The Wellington field network is the primary source of data for this project of monitoring seismicity in the region. Other IRIS networks in the region have been utilized to support the Wellington Array. These include the Earthscope Transportable Array (TA) that moved through the region in 2010 and 2011, the Nanometrics Research Network (NX) and the United States Geological Survey (USGS) Network in southern Kansas and Northern Oklahoma (GS).

The large volume (18 stations at 200 samples per second) of high quality data from the Wellington networks has made it possible to look at earthquake attributes, such as shear-wave splitting, to better understand the increase in seismicity. Events were detectable down to a

Moment Magnitude (M_w) of 0.4, with a magnitude of completeness near the field of ~M_w 1.2 (Chapter 3). Earthquakes of M_w 2 and greater were seen progressing northward into southern Kansas. Larger M_w 2 and greater events in Sumner County were used in a focal mechanism inversion to calculate the stress orientation (Chapter 4). The maximum horizontal stress was calculated to be approximately 75°, which correlates with borehole observations and other seismic studies in the region. The confirmation of the maximum horizontal stress direction allowed for an analysis of shear-wave splitting orientations (Chapter 5) that provides strong evidence of a critical pore pressure fluid change in the basement over the last 5 years. This is confirmed in data from a pressure monitor at the Arbuckle in the KGS 1-28 well.

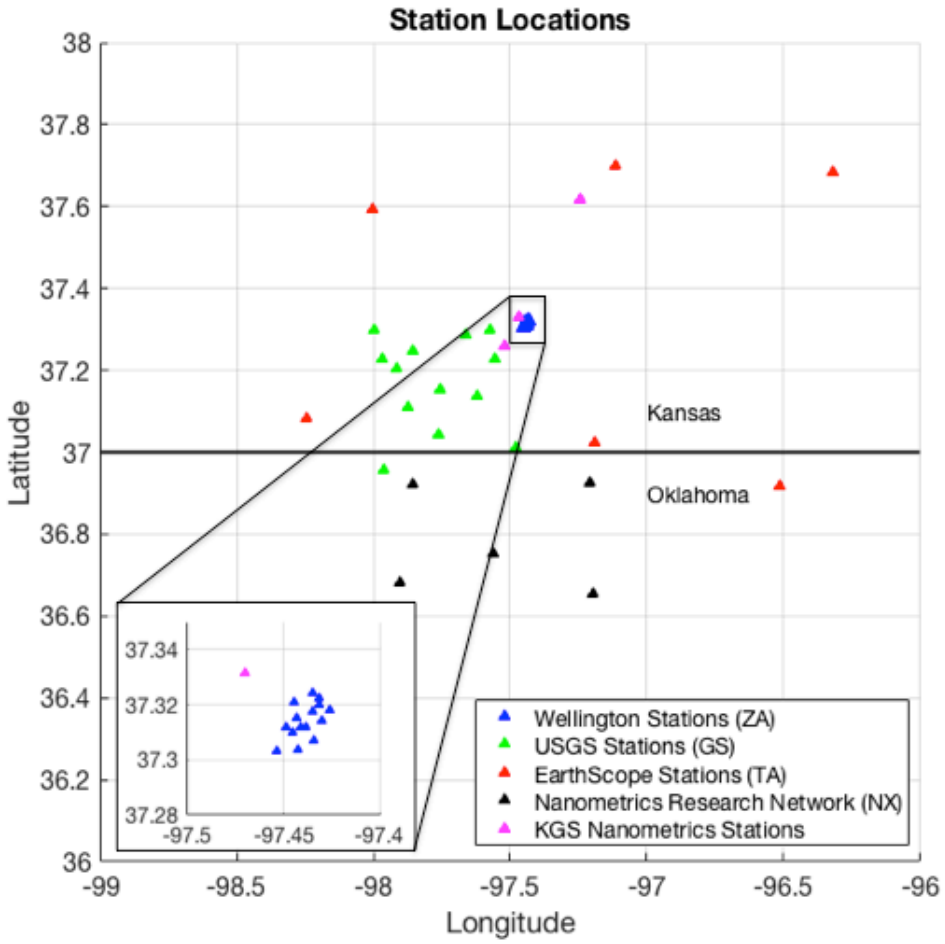

Figure 1.1 Map showing the locations of seismometers used in this study.

Figure 1.2 Photograph of seismometer vault installation at Wellington field showing Sercel L-22 seismometer, Data Acquisition System (DAS) Reftek RT-130, and power supply. (Peterie, 2014, Personal Communication).

Chapter 2: Geologic Setting

Section 2.1: Field Site

The KGS seismometer network is located mostly within the Wellington oil field, approximately 5 km northwest of Wellington, KS, in Sumner County. More than 250 wells have been drilled in the field of approximately 23 square kilometers. The field has produced over 20 million barrels of oil from the Mississippian [KGS, 2016], but production has been declining. The field was chosen as a pilot study for CO_2 enhanced oil recovery (EOR) in the Mississippian and CO_2 sequestration in the Arbuckle. The seismometer network was installed to monitor seismicity associated with these injections. Locations of seismometers and injection wells can be seen in *Figure 2.1.1*.

Section 2.2: Geologic Setting

The North American plate has an average crustal thickness of 36.7 km, and the mid-continental rift/Great Plains region is even thicker, at more than 40 km thick [Chulick and Mooney, 2002]. Since there is no recent deep tectonic activity in the US midcontinent, most models for the earthquake activity are constrained to the uppermost part of the crust, including the upper granitic basement and overlying sedimentary rocks. It is widely believed that the base of the Arbuckle is hydrologically unconfined (Keranen et al., 2014). The Arbuckle has a fluid connection to the fractures in the basement, which allows for a pore pressure increase on ancient fault systems in the basement causing reactivation [Keranen, 2014]. The large fault systems in the United States midcontinent are most likely remnants of the failed Midcontinent Rift System, which extends for 100's of kilometers [Baars, 1995]. Sumner County sits at the south end of the Midcontinent Rift System and to the southeast of the Nemaha uplift. The Midcontinent Rift System contains two conjugate wrench fault zones which have created fault blocks in Sumner

County [Baars, 1995], as seen in *Figure 2.2.1*. These faults are contained mostly in the shallow granite-rhyolite basement which is Precambrian and underlies most of Kansas and Oklahoma [Johnson, 2008]. The layered Paleozoic stratigraphy of Kansas is relatively easy to model in seismicity studies through a 1-dimensional velocity model. This layered stratigraphy consists of alternating shallow marine limestones and shales, along with some evaporites [Merriam, 1963; Johnson, 2008]. These regionally extensive units were deposited within and marginal to the shallow seas that covered the area during much of the Paleozoic [Merriam, 1963].

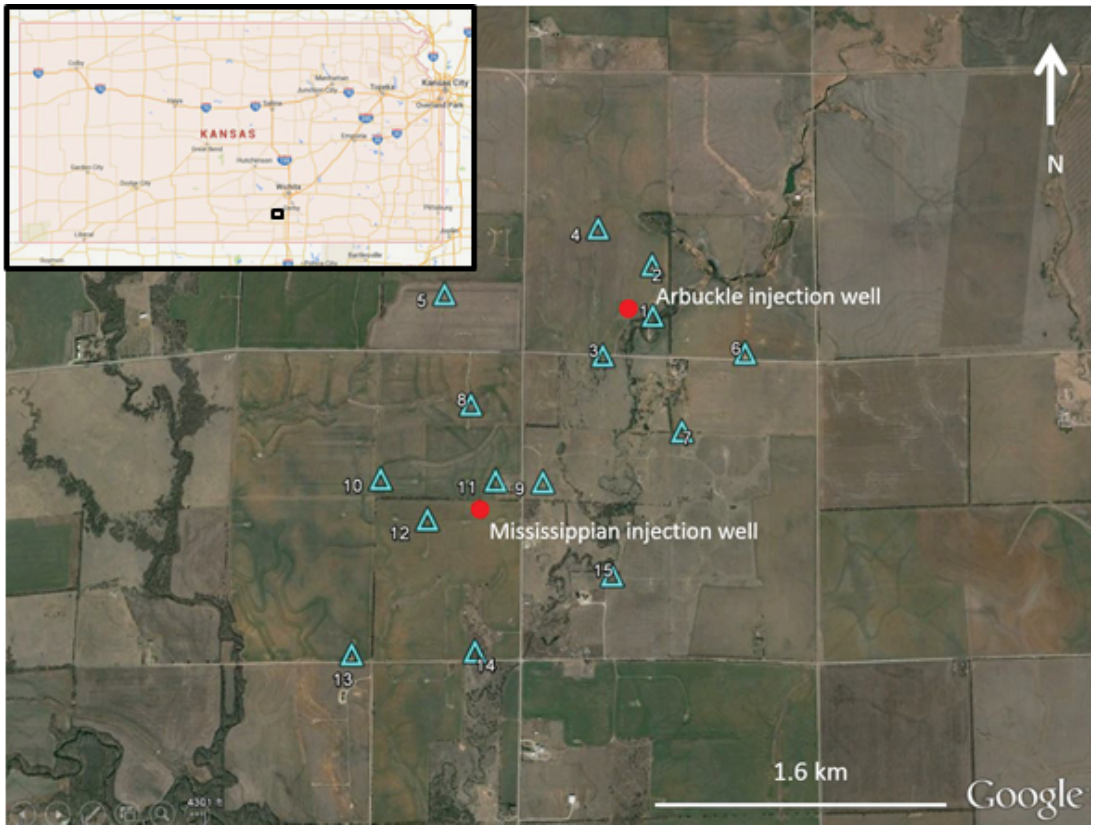

Figure 2.1.1: Map of the Wellington seismometer locations (blue triangles) with respect to the injection wells (red circles). Inset regional map shows the location of Wellington field as a black square.

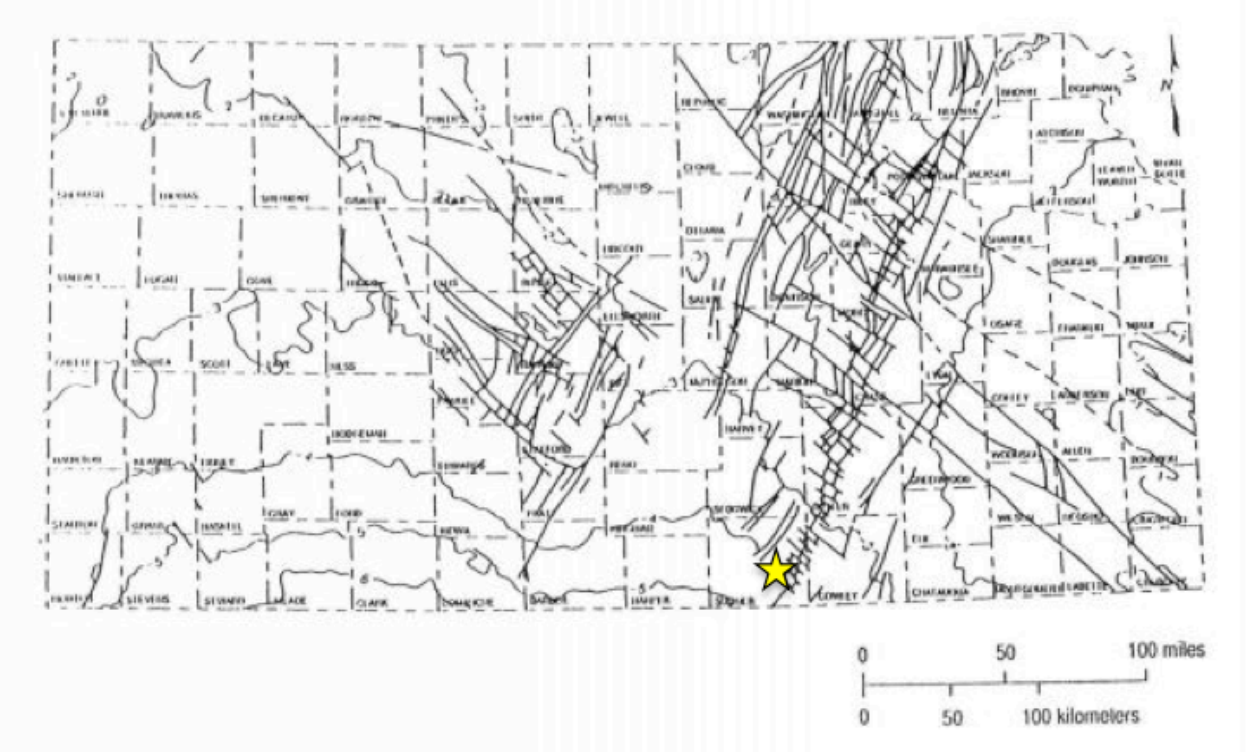

Figure 2.2.1: Map of Kansas with general fault patterns in the basement and Wellington field identified by yellow star (modified from Baars, 1995).

Chapter 3: Cataloging Earthquakes Near Wellington Oil Field

Section 3.1: Passive Seismic Data

My research has accumulated a vast amount (~6 Tb) of passive seismic data in southern Kansas and Northern Oklahoma. The volume of data available through IRIS has also grown significantly over the past five years as other studies have moved seismic equipment into the region. The Wellington Array (network code ZA) consists of 15 Sercel L-22 three-component short period seismometers, recording at 200 samples per second. There are also three Nanometrics Trillium Compact Posthole Seismometers that are three-component and record at 250 samples per second. The Wellington Array seismometers were installed in late September of 2014, but the array struggled with data continuity and flooding in the region. It was subsequently delayed and became fully operational with 14 stations in May of 2015, and with an extra seismometer used as an equipment backup. The additional three Nanometrics seismometers have been moved to locations outside of the Wellington oil field to provide better coverage for the area (Figure 1.1). Instrumentation relocation occurred in the summer of 2016. This seismometer array is mostly inside Sumner County, but other regional arrays have recorded data that is applicable for the study. The EarthScope Transportable Array (TA) was available from 2010 to 2011. The Nanometrics Research Network (NX) in northern Oklahoma and the USGS temporary array (GS) in southern Kansas have been used when the Wellington Array data has not been sufficient. The TA recorded at 40 samples per second on three-component seismometers and the NX and GS arrays recorded at 200 samples per second on three-component seismometers [IRIS, 2016]. The locations for the stations utilized in this study can be seen in *Figure 1.1.*

The Wellington Array has eight stations that are telemeterd to a server at the KGS. All other station data are retrieved manually. The telemetered data are often analyzed first and are used as the primary dataset in the weekly picking of earthquakes. Two of the most eastern USGS temporary array stations are also used to reduce the location error from the weekly Wellington array telemetered data. The nanometrics stations are added into the catalog at a later date. The remaining Wellington array data as well as the data from other arrays are used on events that are not accurately located with the weekly array data. All available stations are used in focal mechanism analysis.

Section 3.2 Identifying and Locating Local Earthquakes

Section 3.2.1 Identifying Local Earthquakes

Earthquakes near the Wellington oil field have been recorded and cataologed since April of 2015. Earthquakes are identified on a weekly basis after the raw data has been processed to miniSEED format, as described in [RT2MS to SEED]. After this processing the data is in hour-long files in miniSEED format, which is read by Seisan, the software used in the earthquake analysis [Ottemoller et al., 2016]. The weekly dataset is searched in hour format for anomalies such as high amplitude spikes in higher frequencies, a very common earthquake signature for the region. These anomalies are identified as earthquakes or as noise by hand. Noise sources include pump jacks (*Figure 3.2.1)*, which are identified as a continuous pattern and thunder, which looks nearly identical to an earthquake except that the speed of sound in air (~343 m/s) is significantly slower than rock seismic velocities (~2 – 6 km/s), creating a much larger time separation between stations (*Figure 3.2.2*). Neither of these common noise sources contain both a p- and s-wave arrivals, which are normally identifiable in local earthquakes (*Figure 3.2.3*).

Once an earthquake is identified in the weekly dataset it is cut into a smaller, more easily manipulated file that still contains all the earthquake arrivals and energy, as well as enough background data before and after the event to visually identify these arrivals. These smaller files are loaded into the earthquake database.

Section 3.2.2 Locating Local Earthquakes

The first step of cataloging the earthquake is to identify the p- and s-wave arrivals of the earthquake. The p-wave is the wave with motion in the direction of propogation and is the first energy arrival of the earthquake; it is often of smaller amplitude than the s-wave, but is usually visually identifiable in small, local earthquakes. The s-arrival is the transverse wave arrival and is the largest amplitude arrival for small, local earthquakes (*Figure 3.2.3*). The seismological standard is to pick the p-arrival on the vertical (Z) channel and the s-arrival on the horizontal channels (1 and 2 or E and N). The p-wave is highest energy on the vertical channel, making it easiest to identify, as is the s-wave in the horizontal channels [Ottemoller et al., 2016].

Once the p- and s-arrivals are picked for all stations on which they are visible, a distance from the station to the earthquake can be calculated. This distance is calculated using the velocity model shown in *Figure 3.2.4*. The velocity model used in the analysis for earthquake location and magnitude is from the KGS 2-32 well, which is in the center of the Wellington oil field. The velocity model was created from blocking the p-wave velocity (sonic log) from the well. The data were used to create four velocity zones down to the bottom of the well. Below the well's maximum depth of 1177 m (3860 ft), two additional velocity zones, down to 20 km, are defined using an average velocity for the granitic basement [Chulick and Mooney, 2002]. The values were initially averages from previous studies [Chulick and Mooney, 2002; Ottemoller et al., 2016], and subsequently refined by inverting the earthquake catalog [Ottemoller et al., 2016].

The S-wave velocity is calculated from the P-wave velocity model multiplied by a Vp/Vs ratio. The Vp/Vs ratio is continuously updated from the arrival times of the earthquakes in the catalog [Ottemoller et al., 2016]. Earthquake distance is calculated directly from the difference in arrivals from the P-wave and S-wave. Having an accurate velocity model and correct Vp/Vs ratio is a key component in correctly locating events, and in calculating magnitudes [Havskov and Alguacil, 2016; Ottemoller et al., 2016].

Section 3.2.3 Calculating Earthquake Magnitude

Seismograph recordings are calibrated with poles and zeros (PAZ), which are corrections for the signal polarity as well as gain factors that convert the raw voltage from the sensor to a displacement in nanometers [Havskov and Alguacil, 2016; Ottemoller et al., 2016]. This corrected signal of ground motion is used in the calculation of earthquake magnitude. The magnitude scale used is the moment magnitude (M_w), which is the standard for very local and induced seismicity [Stork et al., 2014]. Moment magnitude has become the standard due to its robustness in calculating magnitudes at close distances. The moment magnitude is calculated from the energy spectra of the event, which requires higher frequency data than other magnitude estimation methods, but does not exhibit the anomalies that other magnitudes such as Richter (M_L) show at close distances (< 50 km) [Hutton and Boore, 1987]. The energy spectrum calculated from an event is then used along with attenuation factors to correct for the distance from the hypocenter to the station. The corrected energy can then be directly correlated to a magnitude. In SeisAn this is performed by estimating a hyperbolic best-fit of the energy spectra, which is then corrected for attenuation and correlated to magnitude [Ottemoller et al., 2016]. This magnitude calculation is performed on the shear-wave of the horizontal channels. It is

performed on multiple stations, then the average of all the calculated channels is taken and is what is presented as the magnitude of the earthquake.

Section 3.3: Earthquake Catalog

The key components of an earthquake catalog include the basic information required to identify earthquakes in space and time (date, latitude, longitude, and depth), as well as magnitude information (*Appendix A*). The catalog is also presented with a magnitude of completeness (Mc) for the area of interest, shown in *Figure 3.3.1*, which defines the magnitude threshold of the array and region. Many catalogs also include spatial error information, which is available for this catalog, but is not presented here for two reasons: (1) the volume of data, especially in plotting, causes problems visually and computationally and (2) the errors are "well behaved" and are very similar in most events. The errors are on average less than 1 km in both horizontal and vertical directions. The Wellington Array earthquake catalog is available in ***Appendix A*** and contains all earthquake information, ordered in time. The catalog of nearest earthquakes can also be seen in spatial format in *Figure 3.3.1.*

The Mc is a critical component of an earthquake catalog. Usually the Mc is calculated at the end of the study period, however, the Wellington array is being used to monitor the CO_2 injections and must report events larger than M_w 2.5 to regulators. Therefore, it must be proven to regulators that the array is capable of detecting these events. The Mc for the Wellington array is currently approximately 1.2 M_w. This confirms that an event of M_w 2.5 or larger can be detected, since the array can confidently pick all events within a local area of M_w 1.2 and larger. The region this Mc is calculated in is the Area of Interest in *Figure 3.3.1.* A magnitude of completeness is calculated by using the Gutenberg-Richter frequency-magnitude distribution. This law states that for every event of magnitude 2, there were 10 magnitude 1 events and 100

magnitude 0 events [Gutenberg and Richter, 1956]. This relationship can then be turned into the equation:

$$\log(N) = A - bM \qquad \text{(eq. 3.3.1)}$$

Where N is the number of events of magnitude M and A and b are coefficients [Gutenberg and Richter, 1956; Vorobieva et al., 2013]. It is expected that b should be equal to 1 as defined by the Gutenberg-Richter law. Using this equation it can be calculated where the event number diverges from the expected value. This can be seen in *Figure 3.3.2*, where the blue line, the experimental values, diverges from the orange line, the Gutenberg-Richter predictions. This curvature begins at approximately Mw 1.2. However, this curvature occurs with a b-value of close to 1.5, not the standard Gutenberg-Richter b-value of 1.

The deviation in b-value from the expected value of 1 has been theorized to occur in induced seismicity situations, most notably in geothermal operations [Eaton and Maghsoudi, 2015]. Higher than normal b-values are believed to be related to fluid pressure and can be associated with a fluid pressure front moving through the subsurface [Bachmann et al., 2012].

Section 3.4: Northward Advance of Earthquakes

The first induced earthquakes of M_w 2 and greater in Kansas occurred very near the Oklahoma border in Sumner and Harper counties. Earthquakes are now occurring in many more counties in southern Kansas, including Sedgwick County, home to the largest city in Kansas, Wichita with a metropolitan population of >640,000 people [U.S. Census Bureau]. Earthquakes have occurred within the Wichita metro, but have been relatively small and unfelt ($M_w < 2.5$). The Wellington array has already captured this migration of earthquakes, which is caused by the increasing area of critically stressed basement. It is hypothesized that the growing volume of brine water injected into the Arbuckle formation is causing the increase in critically stressed

basement. The advancement of induced seismicity in Kansas is a case study, demonstrating that large-volume injection induced pore-pressure increases can have impacts on regional seismicity. Shallow basement pore pressure increase appears to impact seismicity several 10's of kilometers away from individual injection wells. Far reaching pore pressure changes can be of concern to populated regions from Texas to Ohio that currently face injection induced seismicity.

The northward migration is most evident in smaller earthquakes ($M_w < 2.5$), which occur farther north than larger earthquakes ($M_w > 2$). The overall movement of earthquakes identified by the Wellington Array is most evident in *Figure 3.4.1,* which shows the migration of earthquakes through time.

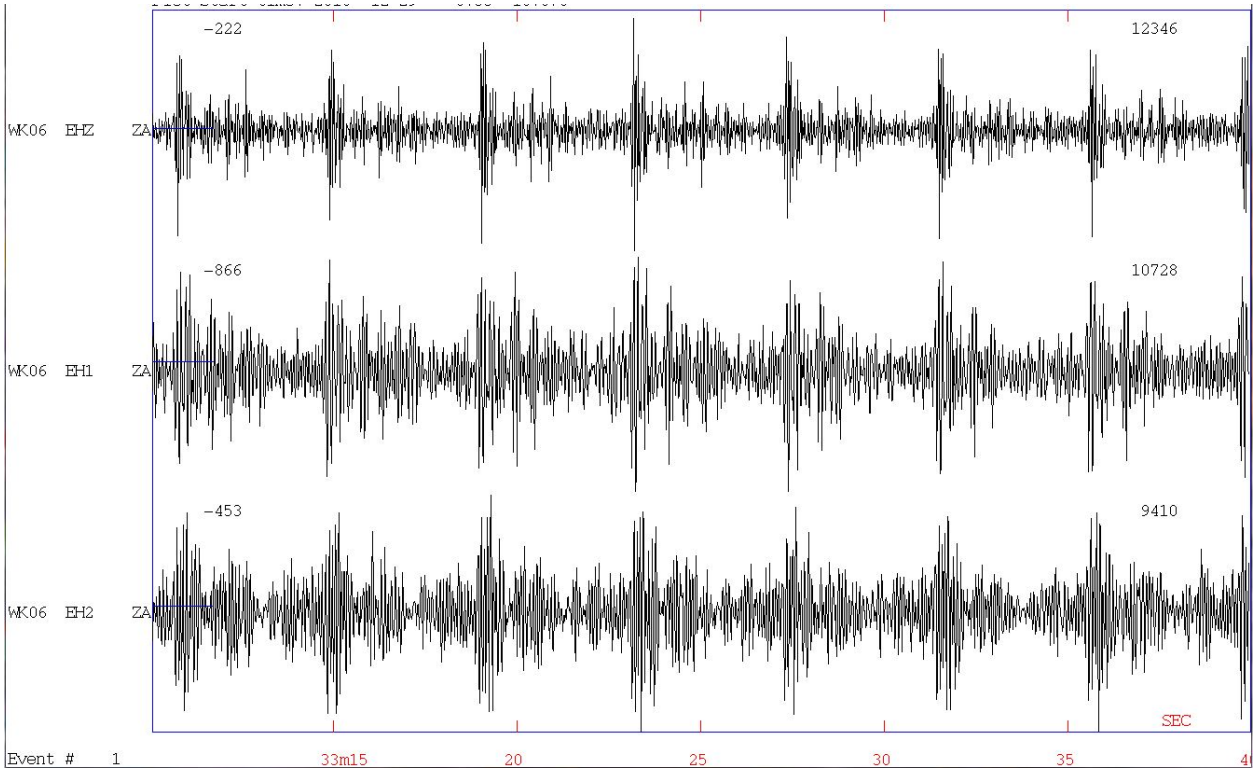

Figure 3.2.1. Example of pump jack noise from one seismometer (WK06) in Wellington oil field. Pump jack noise can be identified through its cyclical pattern. It is often too low energy to be observed across multiple stations.

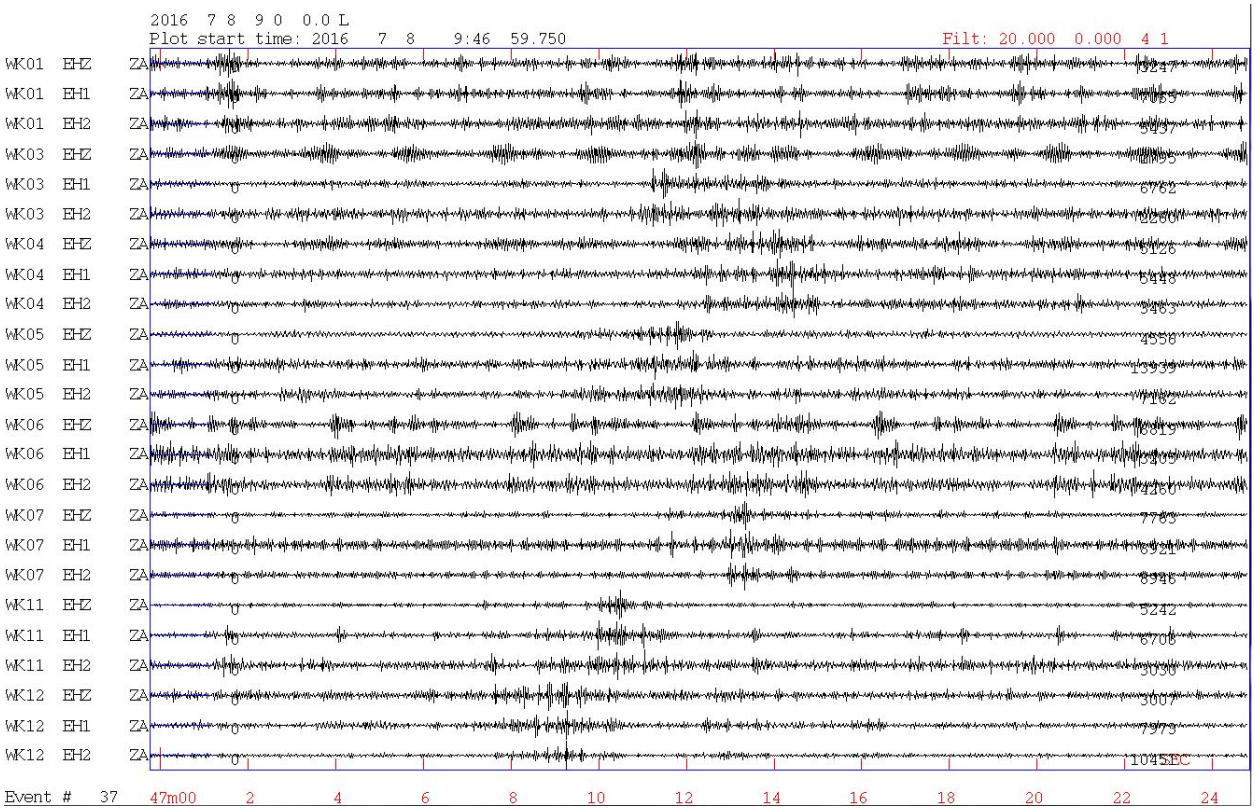

Figure 3.2.2. Example of thunder from seismometers in Wellington oil field. Thunder looks very similar to local earthquakes but can be differentiated by looking at the arrival times across multiple stations. Thunder travels at the speed of sound in air (~343 m/s) so the arrivals are separated by multiple seconds. Here the arrivals can be seen between 8 seconds and 14 seconds.

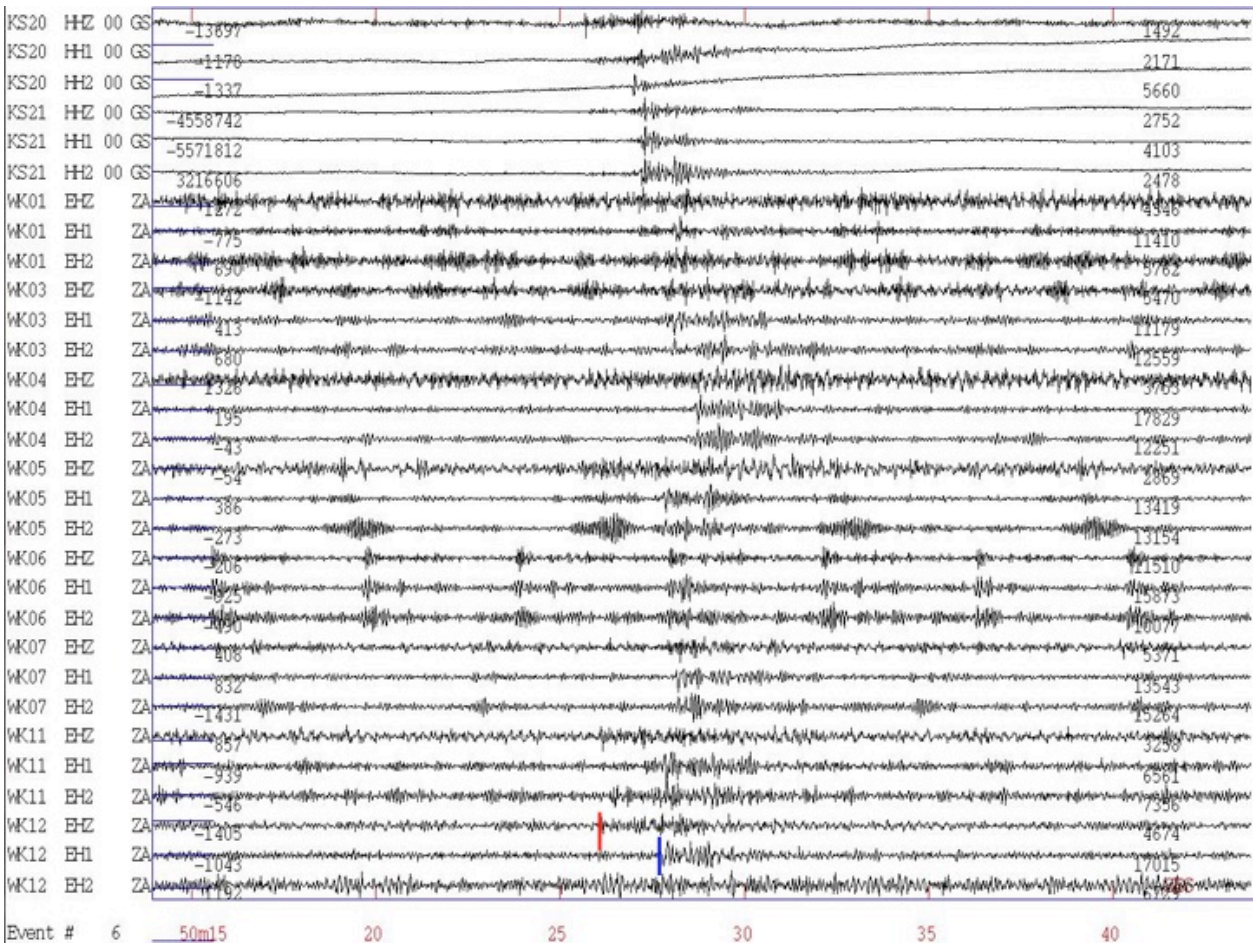

Figure 3.2.3. Example of a local earthquake near Wellington oil field. The P-arrival is at approximately 26 seconds and the S-arrival is at approximately 27-28 seconds. The P-arrival for station WK12 is marked in red and the S-arrival is marked in blue.

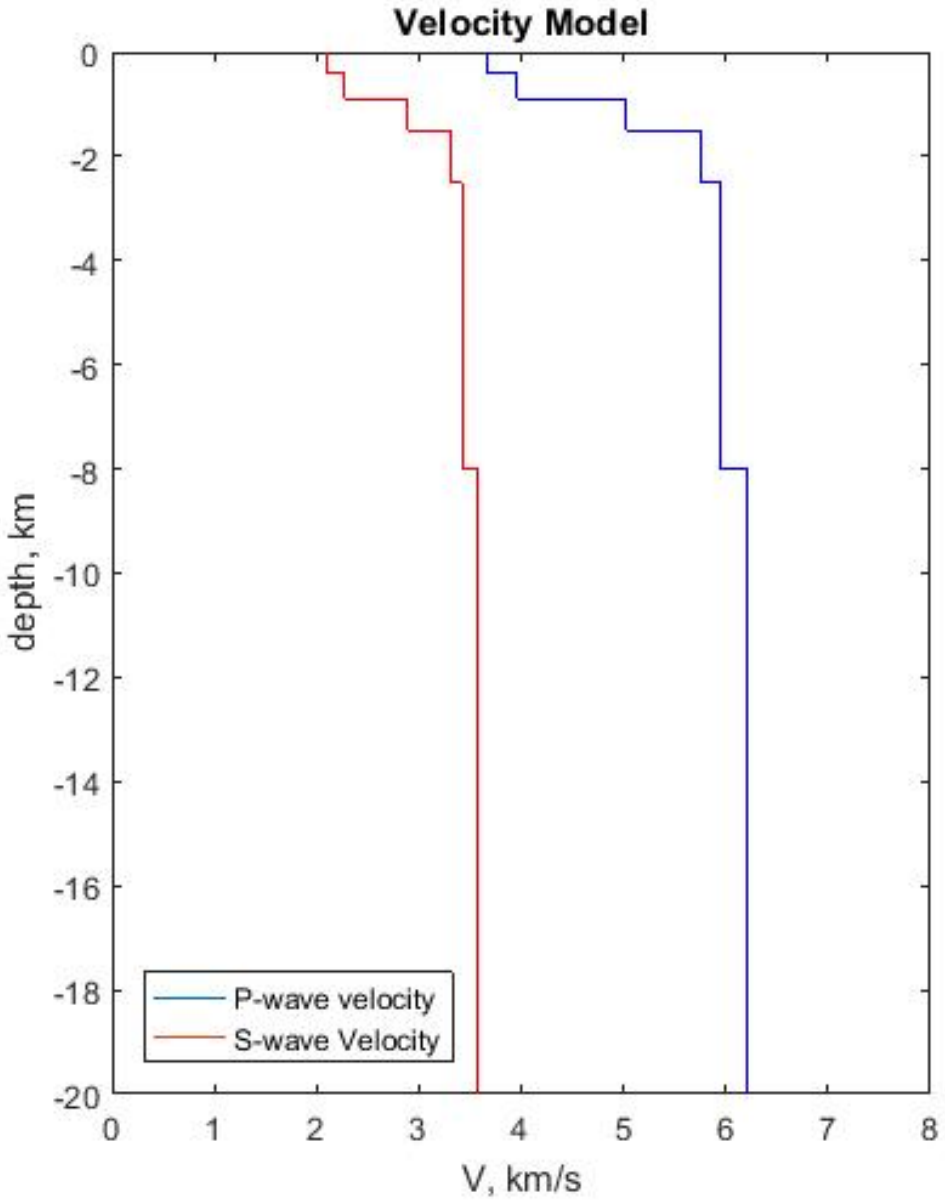

Figure 3.2.4. Velocity model constructed from KGS well 2-32 sonic log. Velocities below well depth (1177 m) were estimated from inversion of local seismic events.

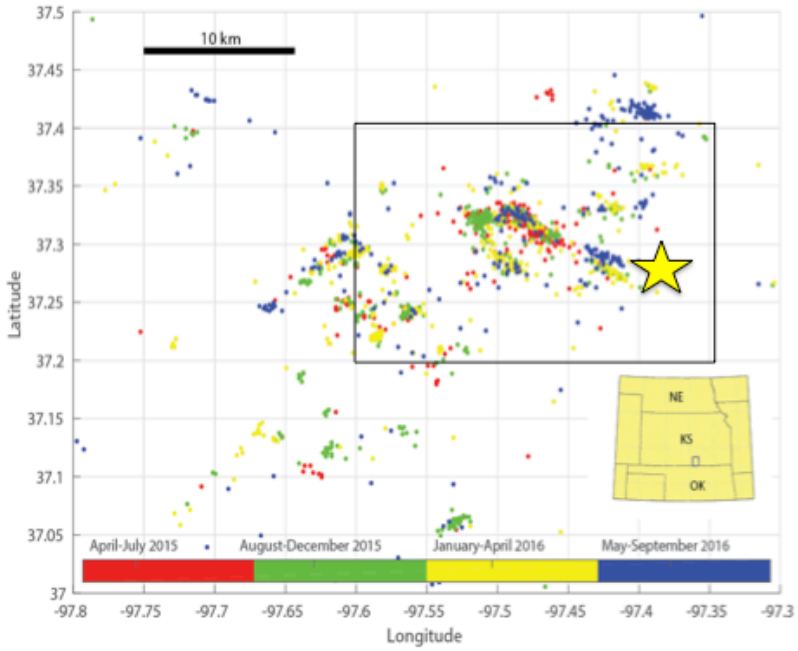

Figure 3.3.1. Locations of nearby earthquakes recorded from Wellington Seismic array between May 2015 and December 2016. Area of Interest is marked by black box around the seismic array. This region was used for the Magnitude of completeness calculation. The color of the earthquake represents the time in which it occurred, with reds being older and blues being most recent. Wellington, KS is marked as the yellow star.

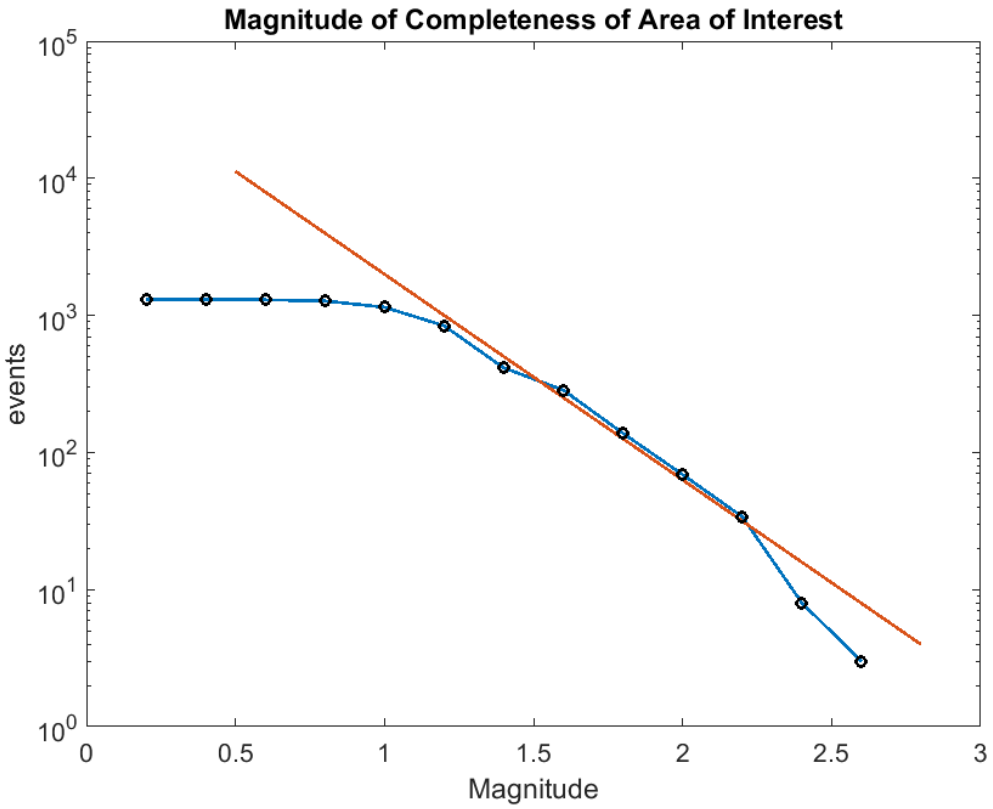

Figure 3.3.2. Graph of the magnitude of completeness from the Gutenberg-Richter law. The blue line with black circles represents events recorded from the seismometer array, and the orange line represents predicted events using the Gutenberg-Richter law, with a b-value of 1.5. The two curves diverge at a magnitude Mc = 1.2.

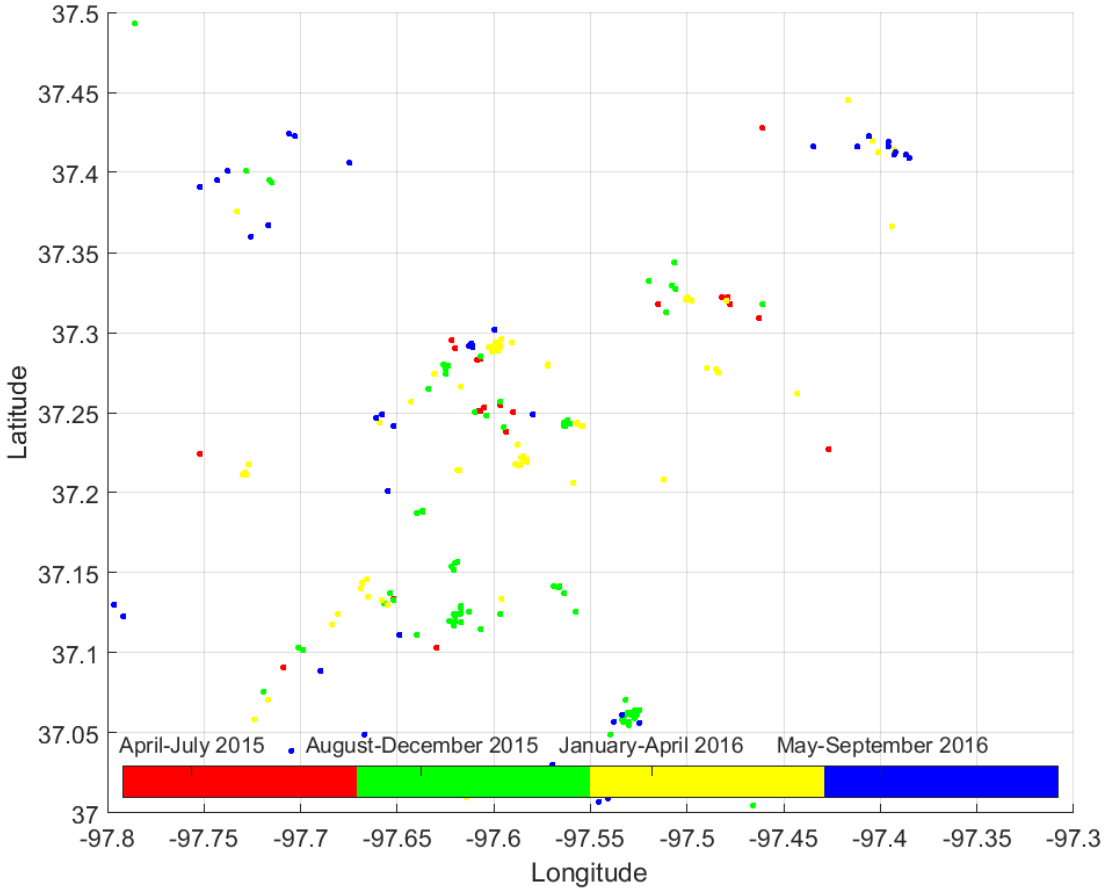

Figure 3.4.1. Image of earthquakes (Mw 2 or greater) from April 2015 to December 2016. The northward progression can be clearly seen from the clustering of green earthquakes in the south to the more north clusters of yellow and blue earthquakes.

Chapter 4: Earthquake Focal Mechanisms

Section 4.1: Calculating Earthquake Focal Mechanisms

Earthquake focal mechanisms are the geometric estimate of the attitude of the fault plane and direction of fault motion. They describe the relative motion between the two sides of the fault surface [Aki and Richards, 1980]. Each side of the fault plane contains a compressional (P) and tensional (T) component, so the focal mechanism contains two potential fault planes that separate the tensional and compression sectors of the focal sphere. There is no way to identify which is the correct fault plane with only one focal mechanism. Focal mechanisms are calculated through waveform analysis of the P-wave polarity and amplitude ratios. P-wave polarities are the best source of data because they retain the seismic character of the section of the focal sphere the raypath begins in at the source of the seismic event. This means that if p-wave polarities are corrected for raypath incidence from the source location, they can be mapped to create the nodal planes of the focal mechanism. The focal mechanism is drawn as a "beach ball" at the source location [Aki and Richards, 1980].

Examples of focal mechanisms for the basic faulting regimes can be seen in *Figure 4.1.1.* Faulting can occur with four types of slip: normal-slip, reverse-slip, strike-slip, and oblique-slip. Normal slip occurs in extensional environments where the fault blocks are pulling away from each other. Reverse faulting occurs in compressional environments where the fault blocks are being pushed against each other enough to cause one block to slide up the other. Strike-slip faulting occurs when one block is pushed past the other, oblique-slip faulting, is a combination of dip-slip and strike-slip motions.

The focal mechanisms calculated from the Wellington earthquake catalog are derived from P-wave arrivals and amplitude ratio of the P-wave and S-wave on the vertical channel (SV).

The amplitude ratio provides additional information that can help to constrain the range of potential fault plane solutions that come from the grid search [Hardebeck and Shearer, 2003; Ottemoller et al., 2016]. P-waves have the highest amplitude at the P and T axes and the lowest at the nodal planes [Hardebeck and Shearer, 2003]. The nodal plane is what separates a compressional regime from a tensional regime. In theory the P-wave amplitude is zero at the nodal plane, making the SV/P ratio very large. At the P and T axes, the P amplitude is the highest, making the SV/P ratio small [Kisslinger, 1980].

Focal mechanisms were calculated for earthquakes in Sumner County with $M_w \geq 2.0$. Since we do not have sufficient azimuthal coverage of the full county, which is essential in calculating accurate focal mechanisms, many solutions are very poor. Full coverage is essential because focal mechanisms are "maps" of the P-wave polarity as it exits at the source location. If there is poor coverage around the source, the P-wave data will not cover the focal sphere adequately, which will give many possible solutions, resulting in poor estimates by the computer. The nodal planes are constrained best by finding the best fit planes that separate the P axis from the T axis, so if there is little data covering the whole axis, the best fit will have a wide range of potential values. The objective of the focal mechanisms presented here is to calculate the stress regime, so the analysis of focal mechanisms was still performed, acknowledging the poor station coverage.

SeisAn employs multiple fault plane solution software packages. These include FOCMEC, HASH, FPFIT and PINV [Ottemoller et al., 2016]. Each one picks the best solution through a slightly different method. FOCMEC allows the user to manually choose the best fit focal mechanism after inputting the width of the grid search and allowed number of p-wave polarity and SV/P errors [Snoke et al., 1984]. The other three software packages calculate the

focal mechanism automatically. The difference is in the error analysis, which leads the computer to the focal mechanism presented as the result. FPFIT finds the best solution from P-wave polarities. It also presents a basic understanding of the error of the fault plane solution by returning the weighted sum error of the P-wave polarity fit as well as a station distribution ratio, which assesses how well spaced the station data are on the focal sphere [Raesenberg and Oppenheimer, 1985]. PINV is similar to FPFIT in that it only uses P-wave polarities [Suetsugu, 1998]. However, it presents no error analysis and returns only the one best-fit fault plane solution. It is therefore expected to be used only to confirm or give an idea if other solutions from the other programs are accurate [Ottemoller, 2016]. HASH uses both P-wave polarities and amplitude ratios. It operates similarly to FOCMEC but the difference is that it returns the best solutions automatically and does not require the user to choose from many potential solutions [Hardebeck and Shearer, 2003].

All four focal mechanism determination methods were used on each earthquake analyzed, and only the earthquakes that had similar solutions for all four programs are presented here. This method was chosen to limit the amount of time required to accurately check the error analysis produced from the programs, while still having a quality control system. A total of 173 focal mechanisms were calculated for earthquakes from May 2015 to September 2016. Their solutions can be seen in *Figure 4.1.2* and *Figure 4.1.3.* The Wellington Array calculated a broad range of fault plane solutions, including some reverse-slip motion. This is an unlikely result, given that the stress regime of the Midwest is not suited for thrust faulting [Alt and Zoback, 2016]. There are wrench faults in the basement, and although the faults in the wrench systems could reactivate, they are no longer under the same stress regime that caused them to form and will likely not exhibit reverse slip motion during reactivation [Baars, 1995]. However, the

midcontinent is known to have both normal and strike-slip faulting [National Earthquake Information Center]. Poor fault plane solutions are a significant concern because there is poor azimuthal station coverage in the area of these solutions.

Section 4.2: Calculating Stress Orientation from Focal Mechanisms

Stress orientation can be calculated through focal mechanism inversion by different methods. The methods used here were developed by Michael, 1984, in which the solution is calculated by a least squares approach to finding the best fit deviatoric stress tensor that would cause the fault slip in the focal mechanisms. This approach assumes that each earthquake is independent, but representative of a constant stress field throughout the area [Angelier, 1979; Gephart and Forsyth, 1984; Michael, 1984; Michael, 1987]. This method is performed by calculating the vector normal to the fault plane, and then calculating the slip vector on that planar surface. These vectors are then used to find the best-fit direction of slip [Gephart and Forsyth, 1984; Michael, 1984]. Since there are two possible fault planes in every focal mechanism, the software takes a bootstrap resampling approach [Michael, 1987], which randomly picks one fault plane from the focal mechanism and recalculates a new solution for the stress tensor. The software then calculates the second fault plane solution. If the second fault solution is inconsistent with the original solution, the first fault plane solution is kept. If it improves the solution more than the first, then the second solution is kept. By this method, it is assumed the best stress tensor solution is calculated, because the proper fault plane is chosen from the focal mechanism. SeisAn uses the SLICK software package, written by Andrew Michael (1984 and 1987) and available through the USGS, to perform the focal mechanism inversion.

Polar histograms of the stress inversion results can be seen in *Figure 4.2.1.* The principle horizontal stress (~75°) matches closely with previous studies of the stress in the region [Zoback and Zoback, 1980; Dart, 1990; Holland, 2013; Alt and Zoback, 2016; Schwab, 2016]. However, the error associated with the inversion is very large, with an average misfit of nearly 60° and standard deviation of 59°. The error is noted as β by Michael [1984] and is the average misfit between the slip vector calculated from the fault plane solution and the calculated slip vector based on the new stress tensor. This large error and standard deviation means that there is a significant range in the direction of slip on faults, which is very unlikely given the stability of the midcontinent region in the United States. Having such a large β value is very indicative of a poorly constrained stress tensor. The solution by itself should be viewed with caution, and the values from previous studies should instead be used when trying to understand the stress regime for the region.

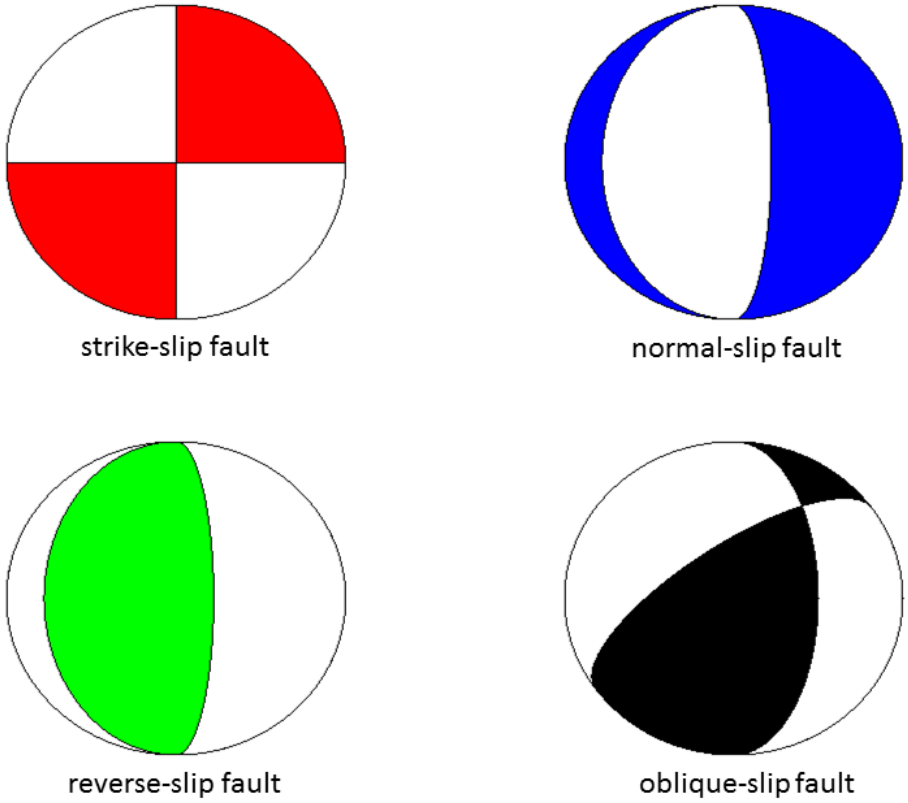

Figure 4.1.1: Examples of a strike-slip fault (red), normal fault (blue), reverse fault (green) and an oblique-slip fault (black). The colored quadrant is compressional, and the white quadrant is the tensional quadrant.

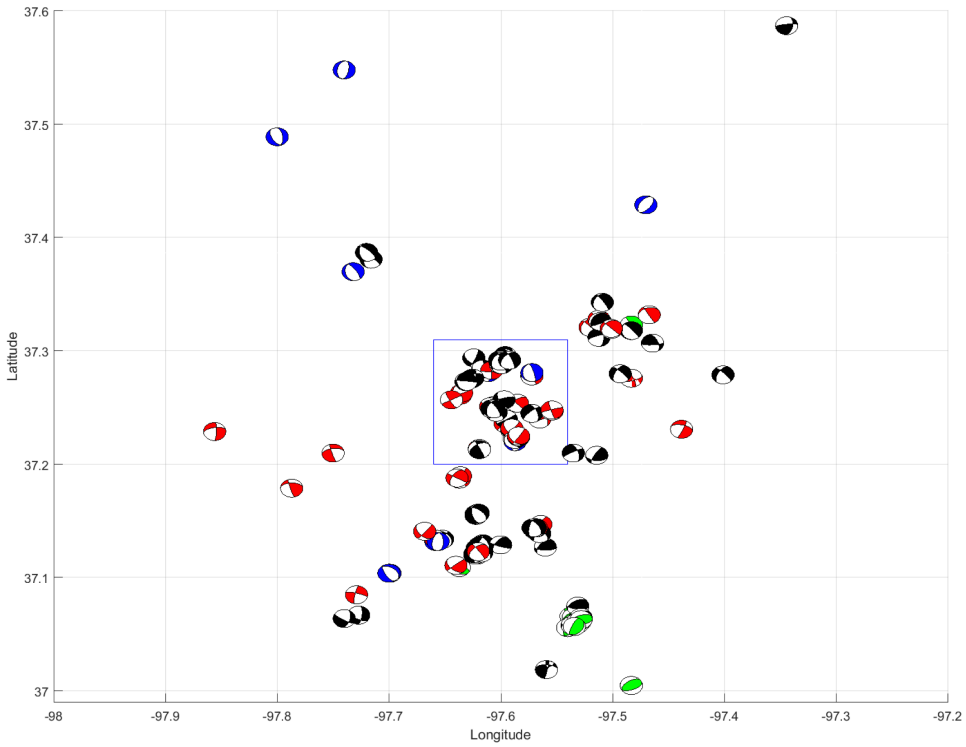

Figure 4.1.2: Beach ball focal mechanisms for earthquakes greater than Mw 2, near the Wellington oil field. The blue square encompasses events nearest to the Wellington array, shown in figure 4.1.3.

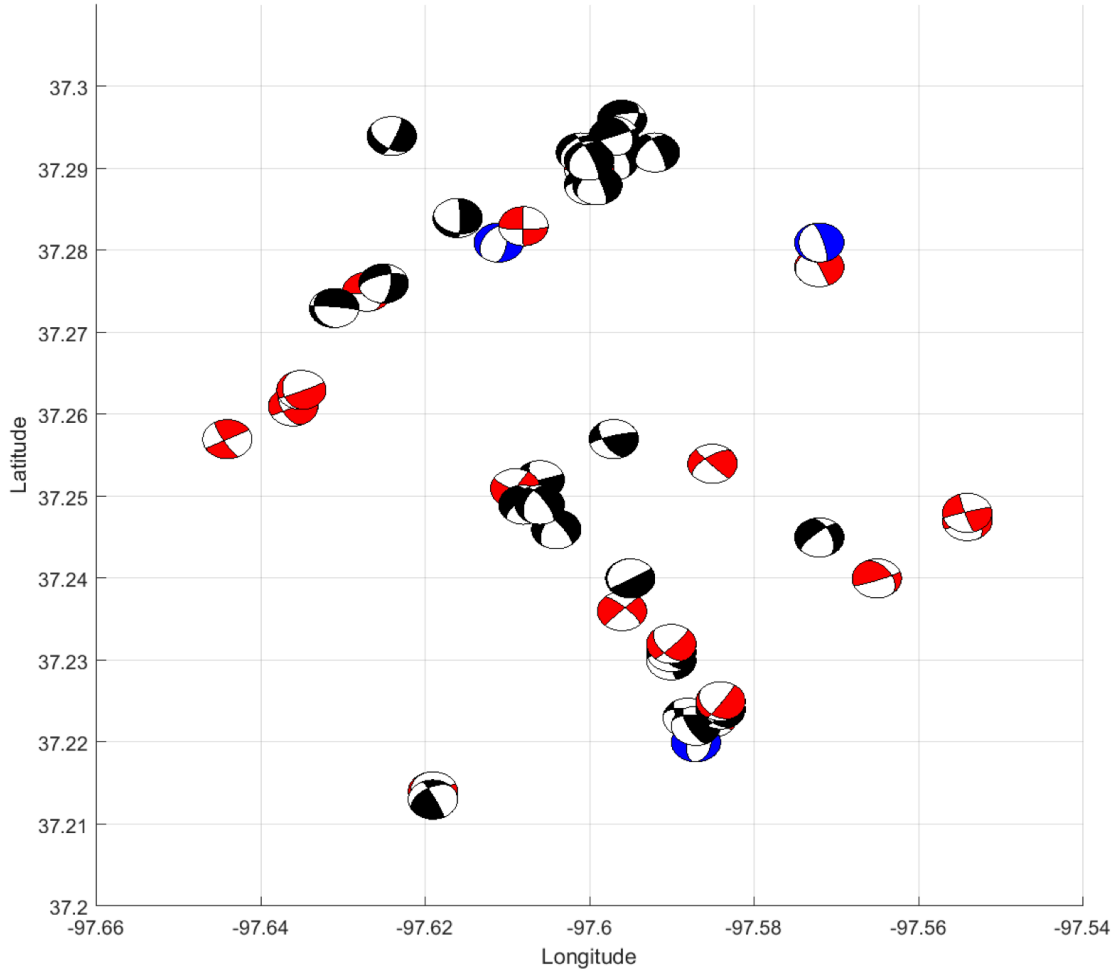

Figure 4.1.3: Beach ball focal mechanisms for earthquakes greater than Mw 2, in the blue box from Figure 4.1.2, showing the focal mechanisms nearest the field.

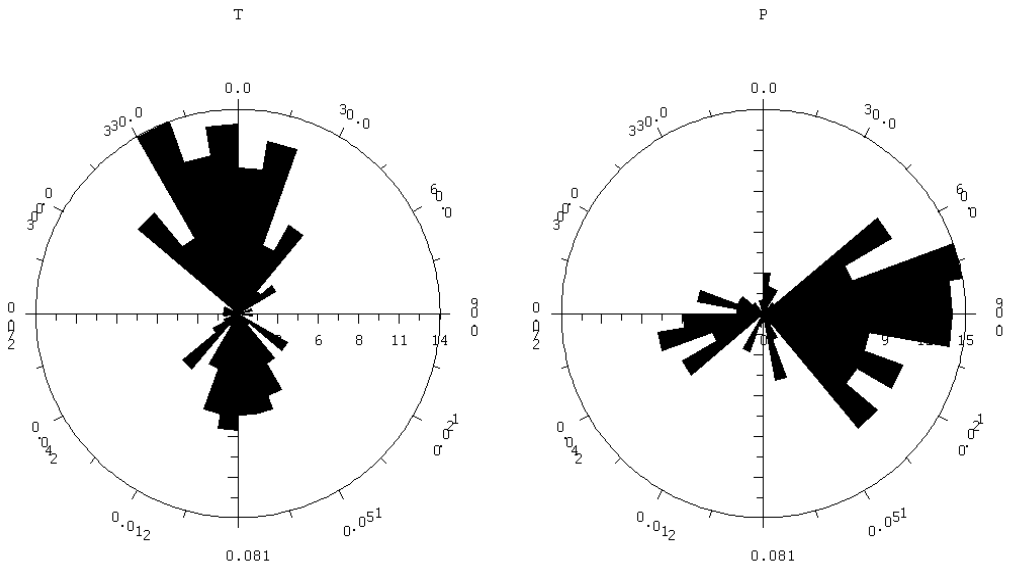

Figure 4.2.1: Rose diagrams depicting the principle horizontal stress (right) and the secondary horizontal stress (left). From SeisAn focal mechanism inversion [Ottemoller et al., 2016], performed by the method of Michael [1984 and 1987].

Chapter 5: Shear-Wave Splitting

Section 5.1: Shear-Wave Splitting Methods

Spatiotemporal analysis of earthquakes and wastewater injection points to pore fluid pressure increases as the cause of increased seismicity across the central US [Ellsworth, 2013; Keranen et al., 2013; Kim, 2013; Frohlich et al., 2014; Keranen et al., 2014; Ellsworth et al., 2015; Mcnamara et al., 2015; Rubinstein and Mahani, 2015; Walsh and Zoback, 2015; Langenbruch and Zoback, 2016; Yeck et al., 2016; Walsh and Zoback, 2016], but direct evidence from seismological data has not been documented [Keranen et al., 2014]. Time-lapse earthquake shear-wave (S-wave) split analysis, presented here, demonstrates that pore fluid pressure in the shallow basement has increased over time to a critical pressure, and is the cause of the increased seismicity. The build-up of critical pore fluid pressure allows for natural fault systems to slip [Crampin and Zatsepin, 1997; Zinke and Zoback, 2000].

Shear-wave splitting occurs when a wave travels through an anisotropic medium [Crampin, 1985; Crampin and Zatsepin, 1997; Crampin, 1999; Crampin and Chastin, 2000; Crampin and Chastin, 2003; Crampin et al., 2003; Gao and Crampin, 2003; Crampin et al., 2004; Crampin and Peacock, 2005; Vecsey et al., 2008; Wustefeld et al., 2008] such as faulted and fractured shallow basement rocks in the US midcontinent [Baars, 1995]. Wave propagation oblique to the anisotropy causes the S-wave to split into two components; a fast S-wave polarized parallel to the fast axis of the anisotropy and a slow S-wave polarized oblique to the fast axis [Crampin, 1985; Crampin and Zatsepin, 1997; Crampin, 1999; Crampin and Chastin, 2000; Crampin and Chastin, 2003; Crampin et al., 2003; Gao and Crampin, 2003; Crampin et al., 2004; Crampin and Peacock, 2005; Vecsey et al., 2008; Wustefeld et al., 2008]. The difference in the arrival times between the two S-waves is δt, and ϕ is the azimuthal angle of the fast S-

wave orientation [Crampin, 1985; Crampin and Zatsepin, 1997; Crampin, 1999; Crampin and Chastin, 2000; Crampin and Chastin, 2003; Crampin et al., 2003; Gao and Crampin, 2003; Crampin et al., 2004; Crampin and Peacock, 2005; Vecsey et al., 2008; Wustefeld et al., 2008].

Shear-wave splitting analysis of naturally occuring earthquakes has been used to identify critically high pore fluid pressure zones through observation of 90° flips in the fast S-wave orientation*(Figure 5.1.1* and *Figure 5.1.2),* causing it to align with the minimum horizontal stress [Zinke and Zoback, 2000; Crampin et al., 2004; Crampin and Peacock, 2005]. Ninety-degree flips in ϕ are seen when the raypath travels a greater distance in high-pore fluid pressure zones, than in normally pressured rock [Crampin et al., 2004]. Change in travel path ratio of high fluid pressure to normal fluid pressure can have significant impact on the range of time delays (δt), with up to an 80% scatter in values [Crampin et al., 2004].

The first observation of induced critical pore fluid pressure change evidenced by S-wave splitting occurred while monitoring the injection of CO_2 in a fractured reservoir using time-lapse 3D reflection seismic [Angerer et al., 2002]. In that study, the fast orientation prior to injection lined up with the maximum horizontal stress; following the injection, which caused a change in the criticality of the pore fluid pressure, the fast S-wave orientation flipped 90°, aligning with the minimum horizontal stress.

Here, I examine if the recent seismicity in northern Oklahoma and southern Kansas exhibits fast S-wave ϕ flips and increased δt scatter, which would constitute direct evidence of critical pore pressure build-up along the raypaths traveled. The time-lapse earthquake data analyzed span the period from 2010 to 2016. Data was obtained from networks hosted through the Incorporated Research Institutions for Seismology (IRIS) including the EarthScope

Transportable Array (TA), which occupied the region in 2010 and 2011, the Nanometrics Research Network (NX), the United States Geological Survey (USGS) Networks (GS), and the Wellington, Kansas CO_2 sequestration monitoring network (ZA).

A total of 120 earthquakes met the criteria and were analyzed. Since 2013, there has been increased seismicity in south-central Kansas (*Figure 5.1.3*). Most events were in the range of M_w 2 – M_w 3, the largest event was an M_w 4.3, and all earthquakes occurred in the shallow basement (1.5-11 km depth) (*Figure 5.1.4 and Figure 5.1.5*). The M_w 2 criterion was chosen so that each earthquake was clearly visible at all monitoring stations with good signal to noise ratio. Earlier events in 2010-2012 came from northern Oklahoma, given the scarcity of earthquakes in southern Kansas at that time. *In-situ* downhole pressure measurements in the Arbuckle Group saline aquifer, approximately 30 m above basement, were obtained from the KGS 1-28 well in the Wellington oil field.

The S-wave splitting analysis was performed by the methods presented in Silver and Chan [Silver and Chan, 1991], using the processing technique of Zinke and Zoback [Zinke and Zoback, 2000]. Matlab code was modified from Splitlab1.0.5 [Wustefeld et al., 2008]. This method performs a grid search for ϕ and δt, which best removes the anisotropy by calculating eigenvalues that correspond to the covariance matrix of the two orthogonal components [Silver and Chan, 1991; Zinke and Zoback, 2000; Wustefeld et al., 2008]. In my study, the calculation minimizes the second eigenvalue (*Figure 5.1.6*). The ϕ and δt are calculated from all stations that had a signal to noise ratio high enough to visually identify the first arrival S-wave in both waveform plots (example in *figure 5.1.7*) as well as in cross-plots (hodograms) of the horizontal channels (*Figure 5.1.1 and Figure 5.1.2*)**.** The hodograms that show the first arrival are cross-correlated to find the minimum second eigenvalue, or the ϕ and δt values which best correct for

the anisotropy [Silver and Chan, 1991]. The calculated δt was corrected for the distance traveled from hypocenter to station, to obtain δt of ms/km. The ϕ values were plotted as individual values for all stations and mirrored across 180 degrees in the polar plot (*Figure 5.1.8*). Values of δt presented in Fig. 3 are averages of all δt values of earthquakes that occurred on the same day to reduce clutter. The ϕ and δt results are presented in *Figure 5.1.8*.

Shear-wave splits were observed in orientations parallel with the maximum horizontal stress and perpendicular to it. An example of S-wave splitting with ϕ parallel to the maximum horizontal stress can be seen in *Figure 5.1.2* and an example with a 90° flip in ϕ orientation along the minimum horizontal stress is shown in Figure 5.1.1.

Section 5.2 Shear-Wave Splitting Analysis

The anisotropy analysis shows a 90° flip in the ϕ of events that occurred in 2015-2016 (*Figure 5.1.8*, A3) compared to events from an earlier time window (2010-2015) (*Figure 5.1.8*, A1, A2). The early (2010-2012) solution of ϕ is primarily in the direction of the maximum horizontal stress in the region (~75°) as calculated from earthquake focal mechanisms and from well-bore sonic log data analysis [Alt and Zoback, 2016]. Flipped ϕ solutions (~330°) are also evident but less common. In the histogram corresponding to the 2015-2016 earthquakes (*Figure 5.1.8*, A3*)*, the fast shear wave orientation ϕ is offset by approximately 90° from the maximum horizontal stress, causing it to align with the minimum horizontal stress. Although natural stress changes are a possible explanation of the change in azimuth, the similarity in stress orientations from well log data and inversion of recent earthquake focal mechanisms suggests that tectonic stresses over this seven-year period have been stable, as would be expected for an intraplate setting, indicating that this is unlikely to be the result of a natural stress change [Alt and Zoback,

2016]. This rotation in ϕ and the narrow timeframe of its occurrence provide evidence of a change that is likely anthropogenic. Such changes in ϕ have previously been identified as an effect of pore fluid pressure increases, where the raypath travels through rock that is critically stressed by pore fluid for a longer distance than rock that is not critically stressed by pore fluid [Crampin et al., 2004; Crampin and Peacock, 2005; Zinke and Zoback, 2000; Crampin et al., 2002]. These studies have also identified large deviation in δt shown to be associated with pore fluid pressure changes.

The analysis shows increasing values, range, and scatter in δt estimates, with nearly a six-fold increase in the range of δt as well from 2012 to 2016 (*Figure 5.1.8 B*). The increase in δt suggests increasing anisotropy of the rock, often associated with the fracture density and aperture width [Crampin, 1999]. It is likely that the basement has become critically stressed by increasing pore fluid pressure. The pore fluid pressure increase reduces the effective stress on the rock, which previously kept fractures that were not parallel to the maximum horizontal stress closed [Crampin et al., 2004]. Increasing pore fluid pressure can cause fractures to shear or dilate, increasing the anisotropy and the magnitude of δt. Large scatter in δt estimation is a recognized issue in critical pore fluid settings, as δt is very sensitive to small pressure changes [Crampin et al., 2004]. Furthermore, the scatter in δt may be an indicator that the pressure field is non-uniform or "patchy", with some regions of the shallow basement critically stressed by fluid pressure and other areas not critically stressed [Crampin et al., 2004].

The observed flip in ϕ as well as the increase in average δt and the increase in δt scatter are interpreted as direct evidence of an increase in pore fluid pressure over the time of the investigation. These changes correlate with downhole pressure data acquired at the KGS 1-28 well in the lower Arbuckle saline aquifer, near the basement. Bottomhole pressure has increased

more than 200 kPa since 2011, when the well was drilled (*Figure 5.1.8* B). The borehole remained idle until April of 2016, when a pressure sensor was installed for continuous monitoring of the lower Arbuckle. The high-resolution pressure measurements since April show that downhole pressures are increasing at a rate of 3-4 kPa per month (*Figure 5.1.8* B1).

The shear-wave splitting analysis presented here, supported by downhole pressure monitoring data, is the first direct evidence of increasing pore pressure in the region detected by seismic observations. This increase in pore fluid pressure is the hypothesized cause of the increase in seismicity in the midcontinent [Ellsworth, 2013; Keranen et al., 2013; Kim, 2013; Frohlich et al., 2014; Keranen et al., 2014; Ellsworth et al., 2015; Mcnamara et al., 2015; Rubinstein and Mahani, 2015; Walsh and Zoback, 2015; Langenbruch and Zoback, 2016; Yeck et al., 2016; Walsh and Zoback, 2016]. Modeling studies have suggested a pressure plume from wastewater injection diffusing through central and northern Oklahoma and southern Kansas is inducing the observed seismicity [Keranen et al., 2014; Yeck et al., 2016]. Earthquake occurrence (*Figure 5.1.3*) suggests a northward progression of seismicity over time, which is also supported by over 1,600 earthquake observations near the Wellington, Kansas CO_2 sequestration monitoring network since 2015 (*Figure 3.3.1*). Much of the observed seismicity near Wellington (*Figure 3.3.1*) has occurred in swarms of earthquakes, as noted in other studies of injection-induced seismicity [Kim, 2013; Yeck et al., 2016]. A "patchy", or heterogeneous, pressure field as opposed to a uniformly expanding pressure pulse may be a more realistic representation of critical pore pressure distribution in the subsurface and its contribution to induced seismicity, which can also help to explain the scatter in δt.

Results of this study show that analyzing the change in anisotropy of the basement is an effective means of identifying critical changes in pore fluid pressure that are the likely cause of

fault reactivation and earthquakes in the region [Ellsworth, 2013; Keranen et al., 2013; Kim, 2013; Frohlich et al., 2014; Keranen et al., 2014; Ellsworth et al., 2015; Mcnamara et al., 2015; Rubinstein and Mahani, 2015; Walsh and Zoback, 2015; Langenbruch and Zoback, 2016; Yeck et al., 2016; Walsh and Zoback, 2016]. This methodology could be applied to other regions of potentially induced seismicity to verify that increasing pore fluid pressure related to deep well injection is the underlying cause of seismicity increases.

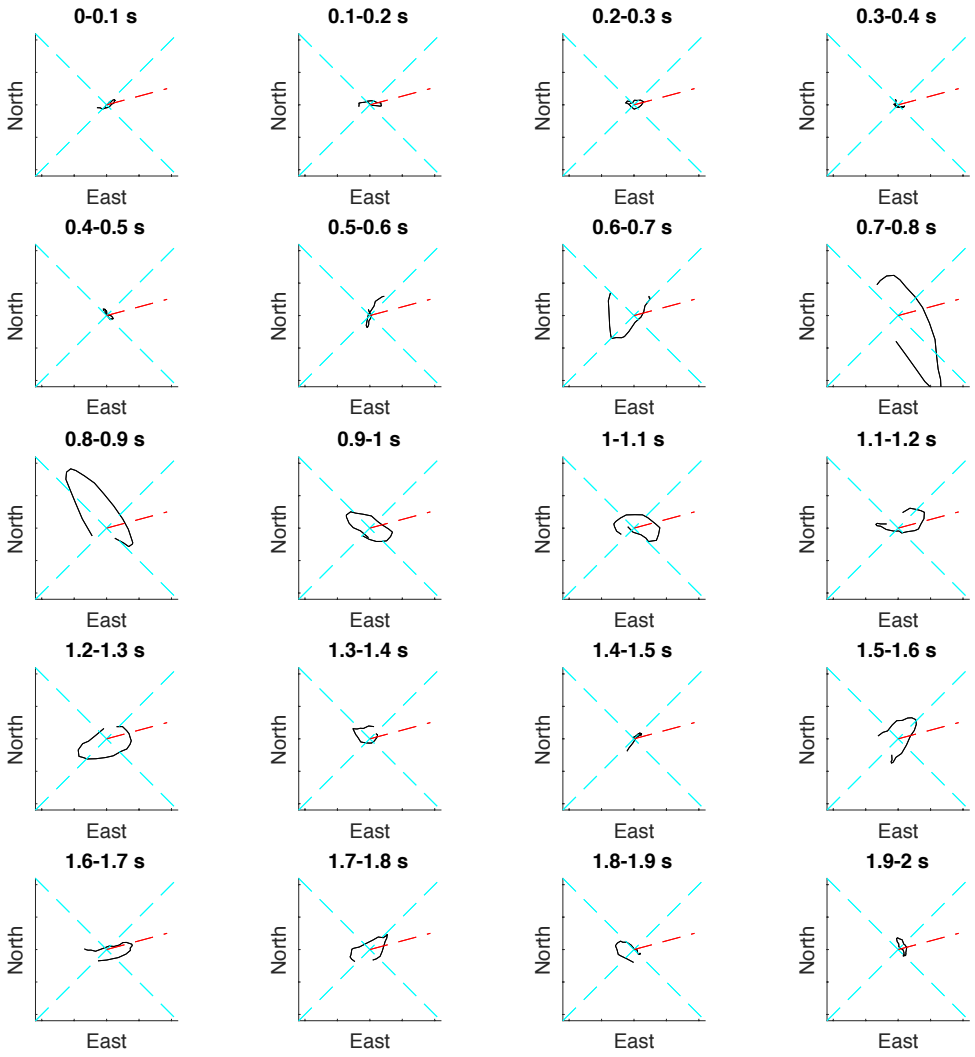

Figure 5.1.1. Hodogram plots of 0.1 seconds increments corresponding to the 2-second time window identified in fig. S3. The time stamp is shown at the top of each hodogram panel. All plots are normalized to the same axis values, making the first arrival often the largest magnitude plot. The first arrival can be seen in hodograms from 0.6 s to 0.9 s. It is identified by the elliptical motion as well as the magnitude of motion. The particle elliptical motion long axis shows a 90° offset from the regional maximum horizontal stress orientation (approximately 75°) marked by the red dashed lines. The first arrival was chosen based on time windows that exhibit the same direction of elliptical motion.

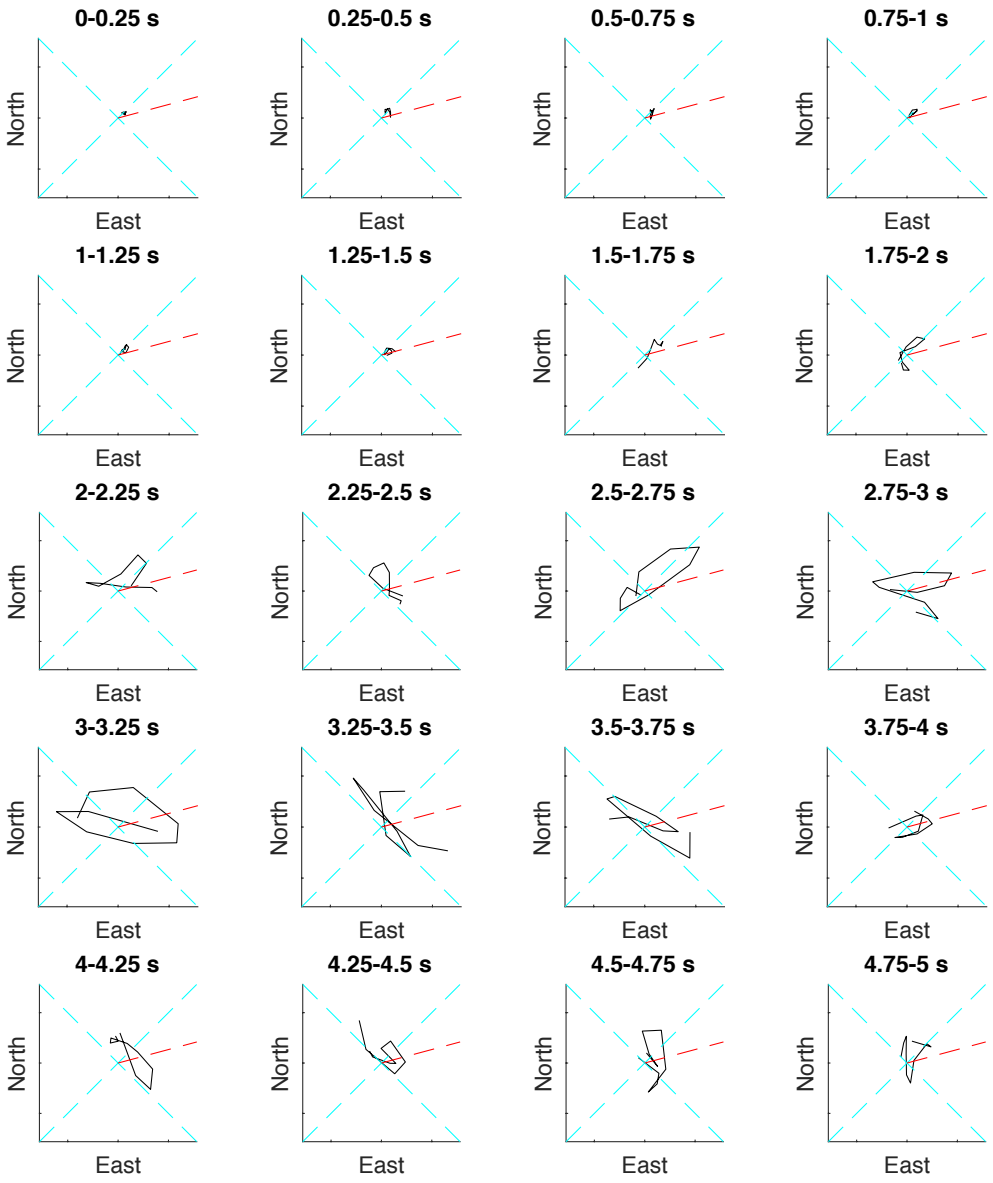

Figure 5.1.2. Hodogram plot of shear-wave splitting that aligns with the maximum horizontal stress at approximately 75°(marked in red dashed line). The first arrival can be seen from 2-3 s. This data corresponds to an Mw 2.7 earthquake in February 2012. Each hodogram displays a 0.25 second increment cross-plot. Cross-plot panels have a longer duration than Figure 5.1.6 because the sampling rate of the waveforms is lower.

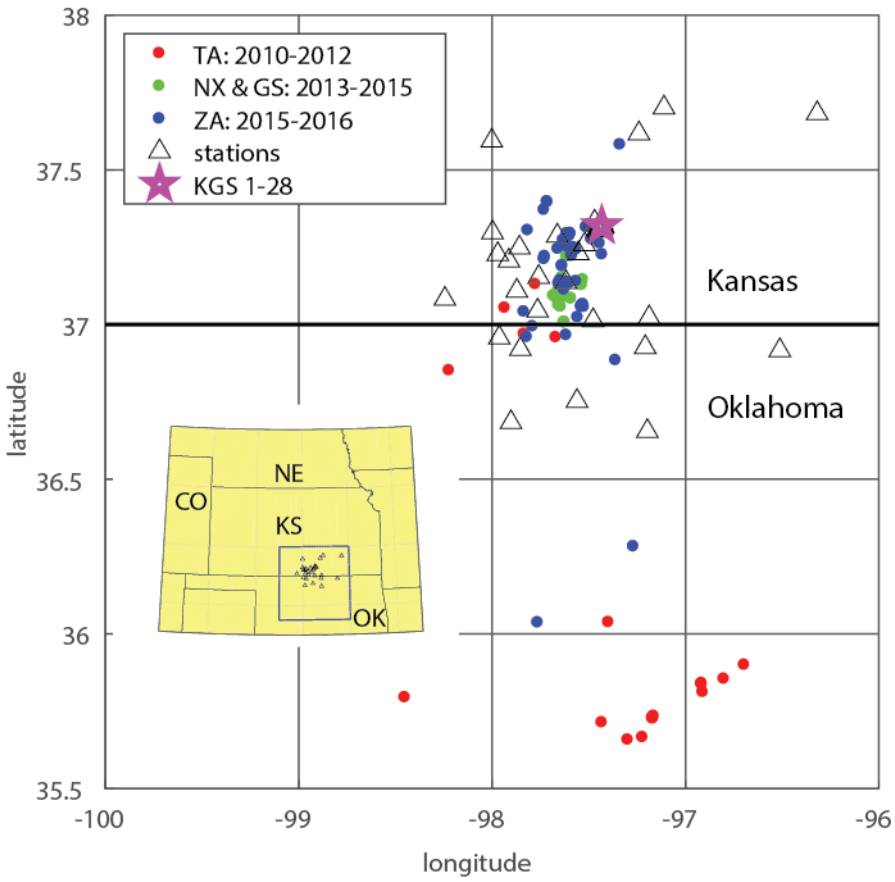

Figure 5.1.3. Map of the study area in south-central Kansas and northern Oklahoma. Black triangles are seismometer station locations; colored circles are earthquake epicenters where color identifies the time period of the earthquake and the source of the data. Red circles: 2010-2012 EarthScope Transportable Array (TA); Green circles: 2013-2015 Nanometrics Research Network (NX) and the USGS network (GS); Blue circles: 2015-2016 Wellington, Kansas CO2 sequestration monitoring network (ZA). Arbuckle pressure measured in well KGS 1-28. Most events used in the study occurred in or near western Sumner County, Kansas. More distant events in northern Oklahoma were incorporated during early time periods when there was very little seismicity in Kansas. The timing of earthquake occurrence suggests a progression of seismicity from south to north over the seven-year period.

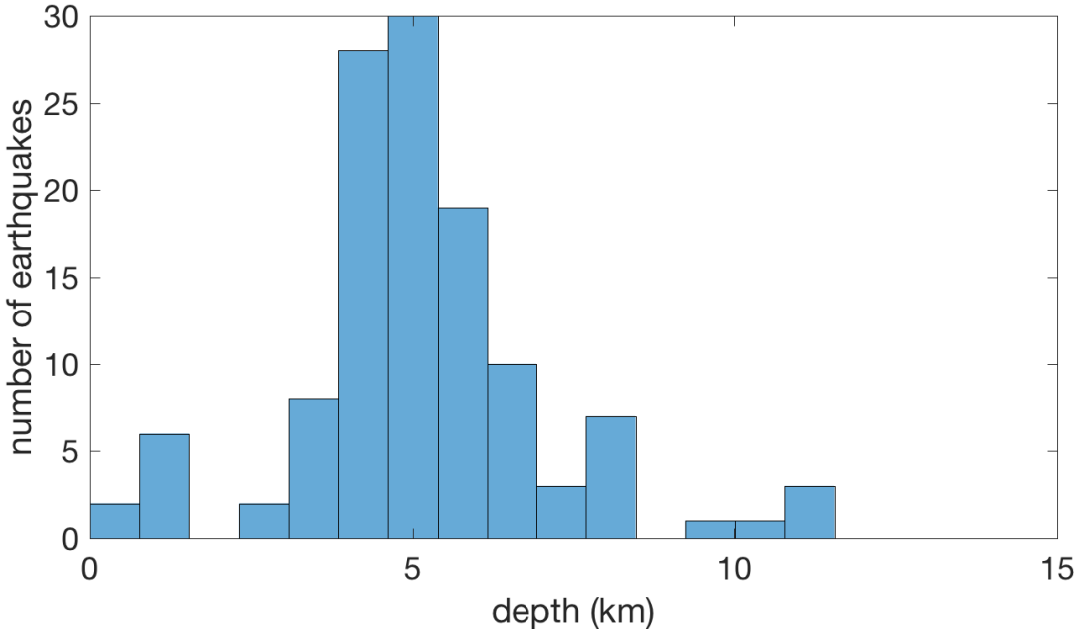

Figure 5.1.4. Histogram plot of the depth distribution of earthquakes used in the study. Earthquake depths were obtained from the USGS earthquake catalog where Wellington catalog depths were unavailable.

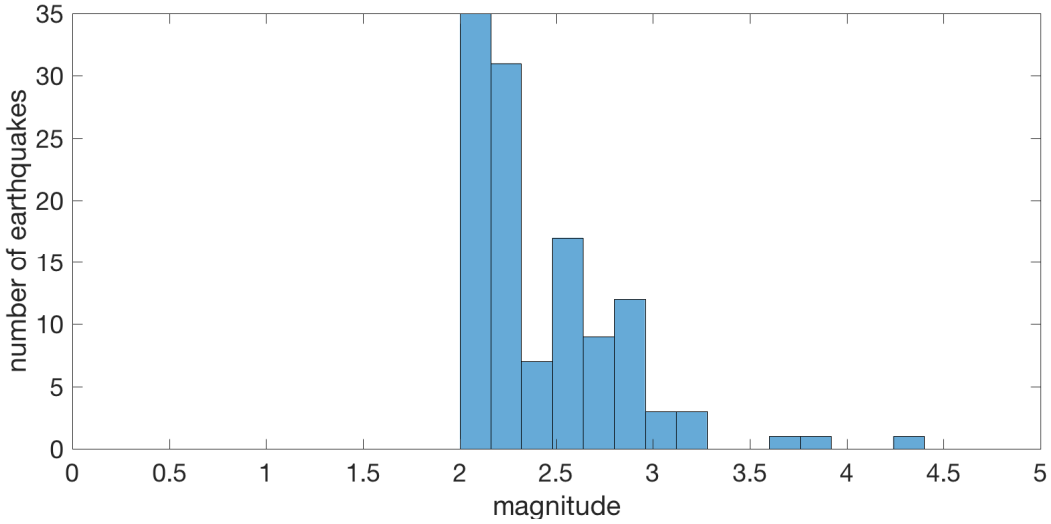

Figure 5.1.5. Histogram plot of the Mw 2.0 or greater distribution of earthquakes used in this study.

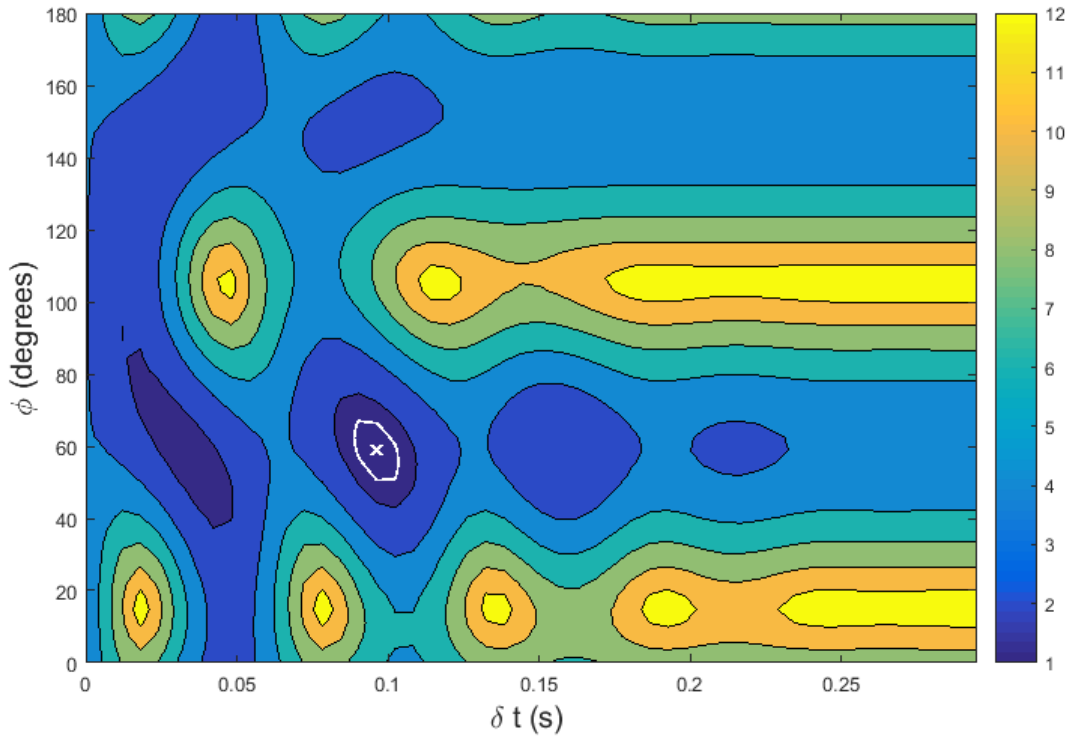

Figure 5.1.6. Plot of the minimization of the second eigenvalue (λ2) from data in Figure 5.1.5 and Figure 5.1.6 in ϕ and δt space. Minimizing λ2 is the chosen mathematical way to return a covariance matrix that is closest to being singular. With no noise the covariance matrix will return λ1 as the only non-zero eigenvalue [31]. The white marker (x) is the best solution and the white line is an estimate of the 95% confidence interval. Angles are from 0° to 180°, where 0° is west and 180° is east. This solution of approximately 60° is therefore 30° west of north or 330°.

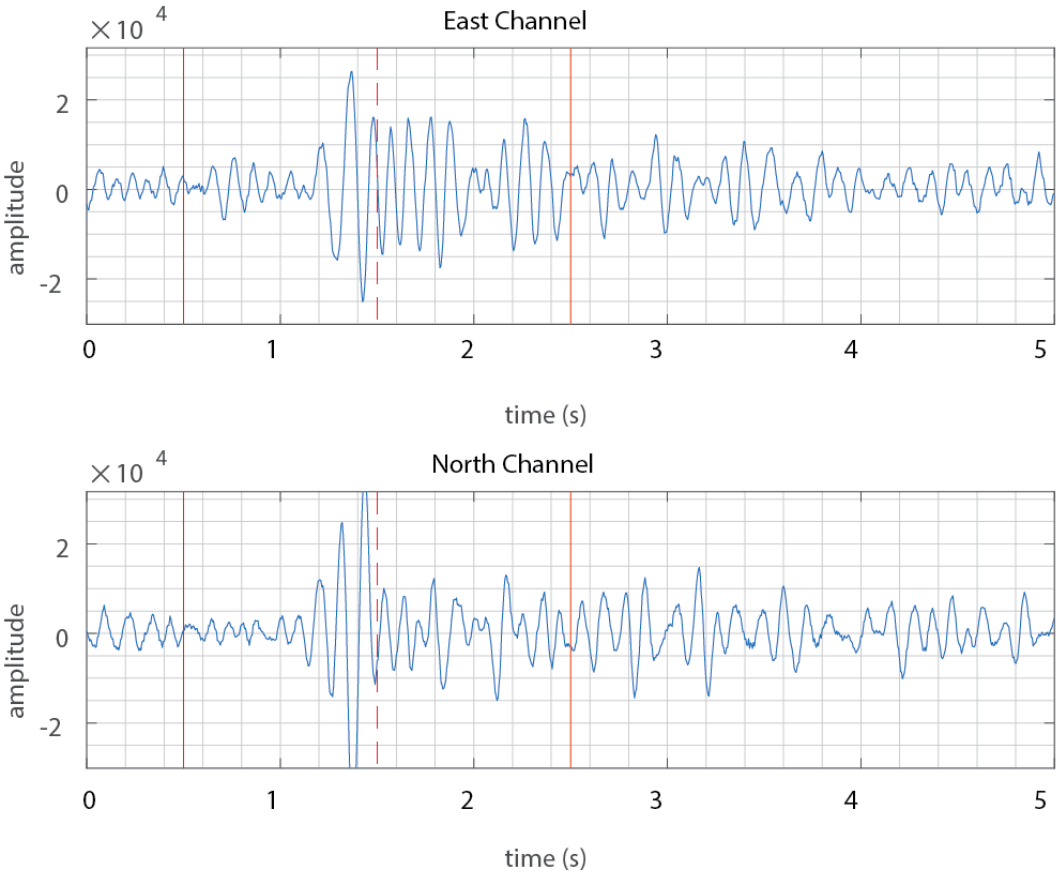

Figure 5.1.7. Plot of raw channel data from station WK15 of a Mw 2.7 earthquake that occurred in July of 2015. Red solid lines indicate the 2-second window seen in hodogram plots of Figure 5.1.6. Red dashed line separates the first 10 plots from the second 10 plots shown in Figure 5.1.6.

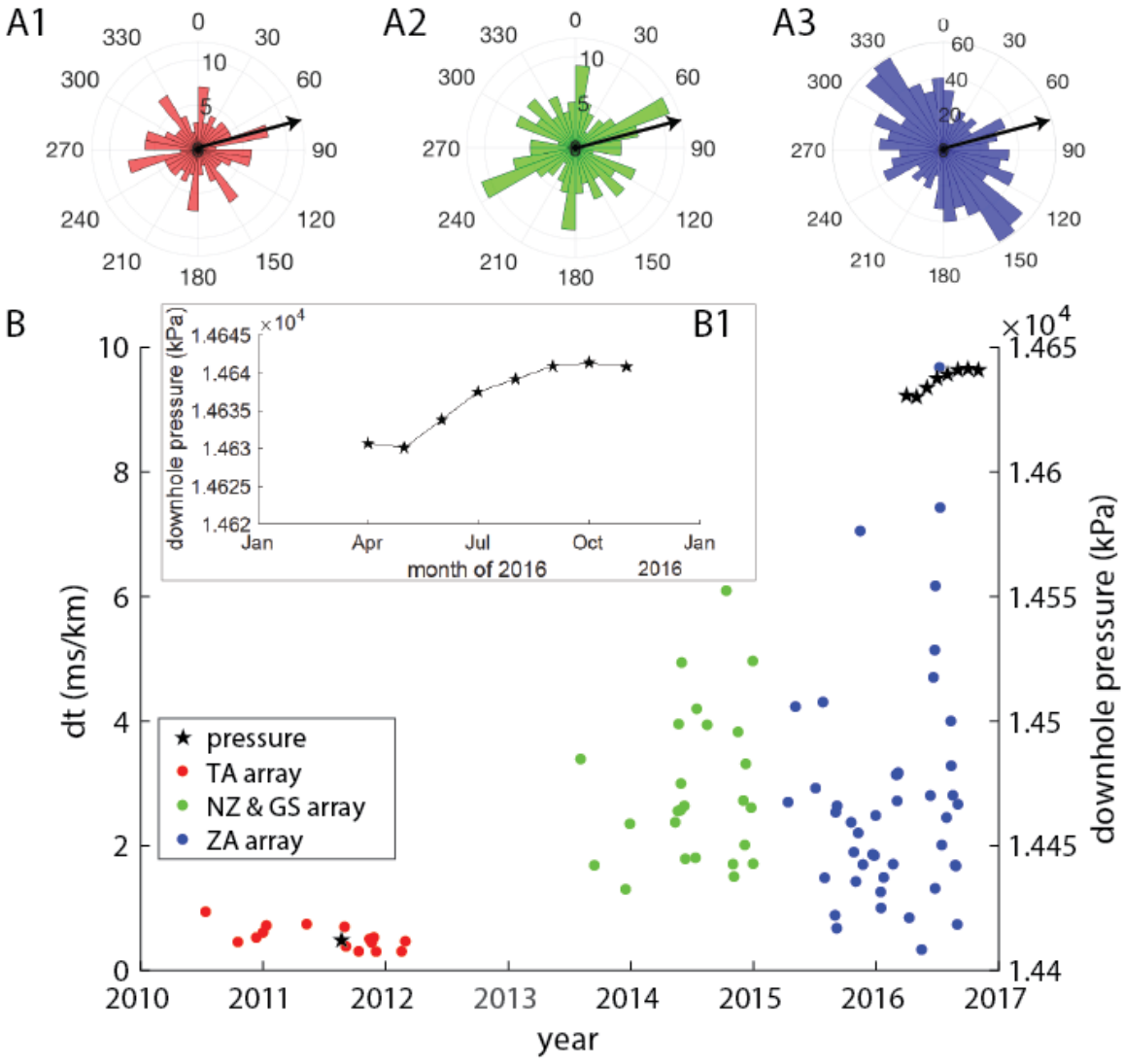

Figure 5.1.8. (A1) Polar histogram of ϕ from TA events 201-2012 (red). The most common ϕ value is near the maximum horizontal stress of ~75° along with flipped values at ~330°. Zero degree values are most often null solutions. (A2) Polar histogram of ϕ from NZ & GS events 2013-2015 (green) showing common solutions in line with maximum horizontal stress as well as solutions 90° off of maximum horizontal stress. (A3) Polar histogram of ϕ from ZA events 2015-2016 (blue) show the most common solution to be 90° off of the maximum horizontal stress, a

direct indicator of critical pore fluid pressure. Arrows indicate the orientation of maximum horizontal stress at 75°. (B) Average *ms*/km of earthquakes from 2010 through 2016, showing a steady increase in magnitude over time as well as an increase in variance. Black stars correspond to average monthly pressure observations in well KGS 1-28, at Wellington Oil field. The initial pressure measurement in August 2011 was obtained when the well was drilled. Inset B1 is an expanded view of monthly average downhole pressures from April to November 2016.

Chapter 6: Discussion and Conclusions

Section 6.1: Discussion

The United States midcontinent has seen a large increase in seismicity from the historical average of 21 magnitude (M) 3 and greater earthquakes a year [Ellsworth, 2013]. This increase in activity now also affects a larger region. The Wellington Array clearly identified movement of the M_w >2 earthquakes in Sumner County. This movement away from the source of the highest rate of fluid injection in Oklahoma is probably indicative of pore fluid pressure increase expanding at great distance from the site of injection.

This expansion of the fluid pore pressure in the shallow basement is also corroborated with the elevated b-value from the earthquake catalog. Having a b-value above 1 is an indicator that the cause of the fault failure is elevated pore pressure [Bachmann et al., 2012]. While models have been generated, little is actually known about the effects of far-field pressurization in the shallow basement, but monitoring the b-value of earthquake occurrences could help to provide information on the pore pressure. This could be possible closer to large volume injection wells, giving insight of the area that is directly affected by high rate injection, versus the area that experiences far-field effects. Having a better understanding of the differences could lead to better injection practices, reducing the risk of earthquakes being triggered by immediate pressure increase, but these near earthquakes are very small and do not pose much risk. Most earthquakes of concern are theorized, through modeling, as being caused by far-field effects, which this methodology is incapable of monitoring. This creates a major drawback to monitoring b-values because the area an array is capable of in-depth analysis of is very small, so monitoring a large region would require a significant number of seismometers, which would be expensive and cumbersome to manage. Another method of monitoring presented here, shear-wave splitting, is likely more economical for monitoring larger regions.

The stress tensor orientation calculated from the Wellington earthquake catalog indicates a maximum horizontal stress of ~75°. This maximum horizontal stress direction aligns well with previous studies [Zoback and Zoback, 1980; Dart, 1990; Holland, 2013; Alt and Zoback, 2016; Schwab, 2016], but the one calculated here is still very poorly constrained. The only reason the value can be used in analyzing the anisotropy results is because other studies have better constrained it at this direction. The stress tensor is so poorly constrained because the focal mechanisms had very poor raypath coverage of the source locations. The Wellington Array was designed to monitor injections directly below it; therefore it cannot obtain good raypath coverage of distant earthquakes. The addition of the three Nanometrics stations drastically increased the coverage nearest the Wellington oil field, and the USGS array helped with more distant earthquakes, but the region where most of the M_w 2 and greater earthquakes occurred was not well covered by existing networks.

Shear-wave splitting results clearly indicate a large increase in anisotropy from 2010 to 2016. Combining the increase in anisotropy with the 90° flip in ϕ provides strong evidence of the basement being critically stressed by pore fluid pressure. The flip in ϕ indicates that the ray traveled at least half the raypath through rock critically stressed from pore fluid pressure. It is expected that the basement is highly fractured and this fracture network is where all of the fluid is going and critically stressing the rock. Having at least half the raypath in a critically stressed pore fluid environment is very likely, given that earthquakes do not just occur close to high-rate injection wells and as previously mentioned, are probably the cause of far-field pressurization. It is then very reasonable that the far-field pressure from any given well interacts with the far-field pressures from other wells, causing most of the region to increase in pore fluid pressure. This hypothesis also correlates with the downhole pressure monitoring that has shown a direct

increase in the pressure at the Arbuckle in the Wellington oil field. The pressure monitoring has shown an increase of ~200 kPa since late 2011. This increase in pressure from 2011 to 2016 would be a reasonable effect if the overall pore fluid pressure in the basement is increasing. However, this pore fluid pressure is not believed to be homogenous through southern Kansas and northern Oklahoma.

The wide variability in the anisotropy measurements from 2014-2016 are associated with critically stressed pore fluid pressure as well. The criticality of the pore fluid pressure appears to be heterogeneous. This heterogeneity is interpreted to be what causes the anisotropy measurements to vary by up to 80% [Crampin et al., 2004]. This wide range of anisotropy measurements is a strong indicator that the basement is not being affected by pore fluid pressure uniformly. There is not currently enough S-wave splitting data to map these regions, but given more data it could be possible to identify regions that are not critically stressed from pore fluid from regions that are. It may also be possible to identify regions of high anisotropy that are not critically stressed from pore fluid pressure. These could be regions that are more highly fractured and capable of holding more fluid without being critically stressed.

Understanding the heterogeneity of the pore pressure in the basement could significantly increase the ability to assess risk associated with induced seismicity. Regions are not equal in potential for large earthquakes. Knowing the heterogeneity would significantly increase the ability to model the seismic risk, as the pore pressure heterogeneity likely has a significant role in the risk, since it is the mechanism for failure. The ability to identify areas that are more prone to high-pressure fluid, and therefore more prone to failure, could provide a better assessment of seismic risk. However, areas with high anisotropy and few earthquakes could also be possible. In this case the anisotropy could be associated with fractures that are able to hold more fluid than

less-fractured crystalline rock. In these situations, knowing the ϕ response would be critical to knowing if the fluid is at a critical pressure or not.

The application of earthquake locations, along with b-values and shear-wave anisotropy, and an understanding of the stress tensor can greatly advance the understanding of induced seismicity. Spatial mapping of the b-value gives strong insight into the cause of pressure-related faulting: whether it is a far-field effect of pressure increase, or if it is near field, high-pressure that is causing the failure. Most studies have found elevated b-values of nearly 2 or higher in near-field high-pressure injections. In the case of southern Kansas and northern Oklahoma it seems much more likely that it is far-field pressure effects that are causing the induced seismicity. The b-value of 1.5 matches the assumption that it is likely fluid pressure, but does not have the higher b-value associated with very high local pressures. This is a reasonable hypothesis, given that the volume of brine disposal in Oklahoma is an order of magnitude greater than in southern Kansas, it would make sense that the activity is a result of far-field effects from the high-rate injection wells in Oklahoma.

The movement of a pressure front from Oklahoma seems to be evident in the shear-wave splitting anisotropy results. The idea that at least half of the raypath must be in critically stressed pore fluid pressure to flip the fast arrival by 90° gives a rough understanding of how far the pressure field has moved. Following the assumption that the increase in pore pressure started in Oklahoma and has moved north, one could conservatively estimate the minimum distance (half the raypath) as the edge of the critical pore fluid pressure in the basement. Using this estimation, it could be seen that initially (~2011) most of northern Oklahoma/southern Kansas was not critically stressed by pore fluid pressure, whereas in 2016, most of this region would be. The earliest shear-wave spit results (2010-2012) show the fast arrival parallel to the maximum

horizontal stress, indicating that at least half of the basement was not critically stressed due to pore fluid pressure. Since the early earthquakes occurred in Oklahoma, it could be reasonably assumed that the increased pore pressure started in that region, and not in southern Kansas. As time went on the fast arrival became flipped, indicating at least half of the raypath was through rock critically stressed by pore fluid pressure. Since the later earthquakes (2015-2016) in the study are closer to the array and more distant to the high-rate injection in Oklahoma, at minimum, half of the raypath that is critically stressed must be located in Kansas, given that both source and receiver are in Kansas. This northward movement of pressure is quite reasonable, supported by the northward movement of earthquakes that are likely caused by the pressure increase (*Figure 3.4.1*).

It is evident that the induced seismicity in Kansas and Oklahoma is from an increase in pore pressure in the basement, and that this pore pressure increase is caused by fluid injection. This increase in pore pressure appears to be spreading through the basement in the region, affecting a larger area, as the injections continue. Identifying regions of higher seismic hazard through S-wave splitting and employing mitigation techniques in those areas could help to reduce the chance of larger earthquakes. The techniques presented here can be used to assist with the mitigation of risk in these areas, both in Kansas and Oklahoma and in other parts of the world experiencing induced seismicity.

Section 6.2: Conclusions

The Wellington array has located 1905 earthquakes from April 2015 through December 2016. The catalog has a Mc of ~ M_w 1.2, with a b-value of ~1.5. From this catalog of earthquakes, 173 were chosen for focal mechanism calculations. The focal mechanisms were

inverted for a stress tensor that indicated a maximum horizontal stress of approximately 75°. This maximum horizontal stress direction matched well with previous studies, and was used to understand the anisotropy of the basement. The anisotropy of the basement was analyzed through shear-wave splitting from earthquakes in Northern Oklahoma and Southern Kansas. The shear-wave splitting results showed that anisotropy has increased significantly since 2011-2012. The direction of the fast shear-wave orientation has also flipped 90°, from in line with the maximum horizontal stress to perpendicular to it. This increase in anisotropy is from an increase in pore fluid pressure from fluid injection, causing the increase in seismicity in southern Kansas and northern Oklahoma.

REFERENCES

Angerer, E., Crampin, S., Xiang-Yang, L., Thomas, D.L. (2002). Processing, modeling and predicting time-lapse effects of overpressured fluid-injection in a fractured reservoir. Geophysical Journal International, 149, 268-281.

Aki, K., Richards, P.G. (1980). Quantitative Seismology. University Science Books, 2nd edition.

Alt II, R.C., Zoback, M.D. (2016). In-situ stress and active faulting in Oklahoma. Bulletin of the Seismological Society of America. 10.1785/0120160156.

Angelier, J. (1979). Determination of the mean principal directions of stresses for a given fault population.

Baars, D.L. (1995). Basement tectonic configuration in Kansas, Kansas Geological Survey, 237.

Bachmann, C.E., Wiemer, S., Goertz-Allmann, B.P., Woessner, J. (2012). Influence of pore-pressure on the event-size distribution of induced earthquakes. Geophysical Research Letters, 39(9).

Buchanan, R. C. (2015). Increased seismicity in Kansas. The Leading Edge, 34(6), 614-617.

Chulick, G.S., Mooney, W.D. (2002). Seismic structure of the crust and uppermost mantle of north America and adjacent oceanic basins: A synthesis. Bulletin of the Seismological Society of America, 92(6), 2478-2492.

Crampin, S. (1985). Evaluation of anisotropy by shear-wave splitting. Geophysics, 50, 142-152.

Crampin, S. (1999). Caclulable fuild-rock interactions. Geological Society, London, 156, 501-514.

Crampin, S. Chastin, S., Gao, Y. (2003). Shear-wave splitting in a critical crust: III. Preliminary report of multi-variable measurements in active tectonics. Journal of Applied Geophysics, 54, 265-277.

Crampin, S. Peacock, S. (2005). A review of shear-wave splitting in the compliant crack-critical

anisotropic earth. Wave Motion, 41, 59-77.

Crampin, S. Peacock, S., Gao, Y., Chastin, S. (2004). The Scatter of time-delays in shear-wave splitting above small earthquakes. Geophysics Journal International, 156, 39-44.

Crampin, S., Chastin, S. (2000). Shear-wave splitting in a critical crust: II. compliant, calculable, controllable, fluid-rock interactions. Anisotropy 2000, 21-48.

Crampin, S., Chastin, S. (2003). A review of shear-wave splitting in the crack-critical crust. Geophysics Journal International, 155, 221-240.

Crampin, S., Gao, Y. (2006). A review of techniques for measuring shear-wave splitting above small earthquakes. Physics of the earth and planetary interiors, 159, 1-14.

Crampin, S., Volti, T., Chastin, S., Gudmundson, A., Stefansson, R. (2002). Indication of high pore-fluid pressures in seismically-active fault zone. Geophysics Journal International, 151, f1-f5.

Crampin, S., Zatsepin, S.V. (1997). Modelling the compliance of crustal rock-II. Response to temporal changes before earthquakes. Geophysical Journal International, 129, 495-506.

Dart, R. L. (1990). In situ stress analysis of wellbore breakouts from Oklahoma and the Texas Panhandle (No. 1866). Department of the Interior, US Geological Survey.

Eaton, D.W., Maghsoudi, S. (2015). 2b… or not 2b? Interpreting magnitude distributions from microseismic catalogs. First break, 33(10), 79-86.

Ellsworth, W.L. (2013). Injection-Induced Earthquakes. Science, 341, 1225942.

Ellsworth, W.L., Llenos, A.L., McGarr, A.F., Michael, A.J., Rubinstein, J.L., Mueller, C.S., Peterson, M.D., Calais, E. (2015). Increasing seismicity in the U.S. midcontinent: implications for earthquake hazard. The Leading Edge, 34, 618-626.

Evans, D. M. (1966). The Denver area earthquakes and the Rocky Mountain Arsenal disposal

well. Mountain Geologist, 3.

Frohlich, C. (2012). Two-year survey comparing earthquake activity and injection-well locations in the Barnett Shale, Texas. Proceedings of the National Academy of Sciences, 109(35), 13934-13938.

Frohlich, C., Ellsworth, W., Brown, W.A., Brunt, M., Luetgert, J., MacDonald, T., Walter, S. (2014). The 17 May 2012 M4.8 earthquake near Timpson, East Texas: an event possibly triggered by fluid injection. Journal of Geophysical Research: Solid Earth, 119.

Gao, Y., Crampin, S. (2003). Temporal variations of shear-wave splitting in field and laboratory studies in China. Journal of Applied Geophysics, 54, 279-287.

Gephart, J. W., and Forsyth, D. W. (1984). An improved method for determining the regional stress tensor using earthquake focal mechanism data: application to the San Fernando earthquake sequence. Journal of Geophysical Research: Solid Earth, 89(B11), 9305-9320.

Gutenberg, B., Richter, C.F. (1956). Earthquake magnitude, intensity, energy, and acceleration. Bulletin of the Seismological Society of America, 46(2), 105-145.

Hardebeck, J.L., Shearer, P.M. (2003). Using S/P amplitude ratios to constrain the focal mechanisms of small earthquakes, Bulletin of the Seismological Society of America, 93(6), 2434-2444.

Havskov, J., Alguacil, G. (2016). Instrumentation in Earthquake Seismology. Springer.

Havskov, J., Ottemoller, L. (1999). SeisAn Earthquake analysis software, Seismological Research Letters, 70.

Healy, J. H., Rubey, W. W., Griggs, D. T., and Raleigh, C. B. (1968). The Denver earthquakes. Science, 161(3848), 1301-1310.

Holland, A. A. (2013). Optimal fault orientations within Oklahoma. Seismological Research

Letters, 84(5), 876-890.

Horton, S. (2012). Disposal of hydrofracking waste fluid by injection into subsurface aquifers triggers earthquake swarm in central Arkansas with potential for damaging earthquake. Seismological Research Letters, 83(2), 250-260.

Hutton, L.K., Boore, D.M. (1987). The ML scale in southern California. Bulletin of the Seismological Society of America. 77(6), 2074-2094.

IRIS, RT2MS to SEED, https://www.passcal.nmt.edu/webfm_send/2592

Johnson, K.S. (2008). Geologic history of Oklahoma. Oklahoma Geological Survey Educational Publication, 9, 2–9.

Keranen, K.M., Savage, H.M., Abers, G.A., Cochran, E.S. (2013). Potentially induced earthquakes in Oklahoma, USA: links between wastewater injection and the 2011 Mw 5.7 earthquake sequence. Geology, 41, 699-702.

Keranen, K.M., Weingarten, M., Abers, G.A., Bekins, B.A., Ge, S. (2014). Sharp increase in central Oklahoma seismicity since 2008 induced by massive wastewater injection. Science, 345, 448-451.

KGS oil and gas wells database, Kansas Geological Survey, http://www.kgs.ku.edu/Magellan/Qualified/, (accessed 10/20/2016).

Kim, W.Y. (2013). Induced Seismicity associated with fluid injection into deep well in Youngstown, Ohio. Journal of Geophysical Research: Solid Earth, 118, 3506-3518.

Kisslinger, C. (1980). Evaulation of S to P ratios for determining focal mechanisms from regional network observations. Bulletin of the Seismological Society of America, 70(4), 999-1014.

Langenbruch, C., Zoback, M.D. (2016). How will induced seismicity in Oklahoma respond to

decreased saltwater injection rates? Science Advances, 2, e1601542.

MATLAB R2016b, The MathWorks, Inc., Natick, Massachusetts, United States.

McGarr, A. (2014). Maximum magnitude earthquakes induced by fluid injection. Journal of Geophysical Research: solid earth, 119(2), 1008-1019.

McNamara, D.E., Hayes, G.P., Benz, H.M., Williams, R.A., McMahon, N.D., Aster, R.C., Holland, A., Sickbert, T., Herrmann, R., Briggs, R., Smoczyk, G., Bergman, E. (2015). Reactivated faulting near Cushing Oklahoma: increased potential for a triggered earthquake in an area of United States strategic infrastructure. Geophysical Research Letters, 42, 8328-8332.

Merriam, D. F. (1963). The geologic history of Kansas. University of Kansas publications.

Michael, A.J. (1984). Determination of stress from slip data: Faults and Folds. Journal of Geophysical Research, 89(B13), 11517-11526.

Michael, A.J. (1987). Use of Focal Mechanisms to determine stress: A control study. Journal of Geophysical Research, 92(B1), 357-368.

Morris, A., Ferrill, D.A., Henderson, D.B. (1996). Slip-tendency analysis and fault reactivation. Geology, 24(3), 275-278.

Ottemoller, L., Voss, P., Havskov, J. (2016). SEISAN EARTHQUAKE ANALYSIS SOFTWARE FOR WINDOWS, SOLARIS, LINUX and MACOSX.

Raesenberg, P., Oppenheimer, D. (1985). Fpfit, fpplot, and fppage: Fortran computer programs for calculating and displaying earthquake fault plane solutions. United States Geological Survey. 85-739.

Raleigh, C. B., Healy, J. H., and Bredehoeft, J. D. (1976). An experiment in earthquake control at Rangely, Colorado, Science, 191, 1230-1237.

Rubinstein, J.L., Mahani, A.B. (2015). Myths and Facts on Wastewater Injection, Hydraulic Fracturing, Enhanced Oil Recovery, and Induced Seismicity. Seismological Research Letters, 86, 1060-1067.

Schwab, D.R. (2016). Characterizing the potential for fault reactivation related to fluid injection through subsurface structural mapping and stress field analysis, Wellington Field, Sumner County, KS. The University of Kansas, Lawrence, Kansas.

Silver, P.G., Chan, W.W. (1991). Shear wave splitting and subcontinental mantle deformation. Journal of Geophysical Research, 96, 16429-16454.

Snoke, J.A., Munsey, J.W., Teague, A.G., Bollinger, G.A., (1984). A program for focal mechanism determination by combined use of polarity and SV-P amplitude ratio data. Earthquake Notes, 55.

Stork, A.L., Verdon, J.P., Kendall, J.M. (2014). The robustness of seismic moment and magnitudes estimated using spectral analysis. Geophysical Prospecting, 62, 862-878.

Suetsugu, D. (1998). Practice on source mechanism, IISEE lecture note. Technical report, Tsukuba, Japan.

Vecsey, L., Plomerova, J., Babuska, V. (2008). Shear-wave splitting measurements- problems and solutions. Tectonophysics, 462, 178-196.

Volti, T., Crampin, S. (2003). A four-year study of shear-wave splitting in Iceland: 1. Background and preliminary analysis. Geological Society, London, special publications, 212, 117-133.

Volti, T., Crampin, S. (2003). A four-year study of shear-wave splitting in Iceland: 2. Temporal changes before earthquakes and volcanic eruptions. Geological Society, London, special publications, 212, 134-149.

Vorobieva, I., Narteau, C., Shebalin, P., Beauducel, F., Nercessian, A., Clouard, V., Bouin, M.P. (2013). Multiscale mapping of completeness magnitude of earthquake catalogs. Bulletin of the Seismological Society of America, 103(4), 2188-2202.

Walsh III, F.R., Zoback, M.D. (2016). Probabilistic assessment of potential fault slip related to injection-induced earthquakes: application to north-central Oklahoma, USA. Geology, 44, 991-994.

Walsh, F.R., Zoback, M.D. (2015). Oklahoma's recent earthquakes and saltwater disposal. Science Advances, 1, e1500195.

Wustefeld, A., Bokelmann, G.,Zaroli, C., Barruol, G. (2008). SplitLab: A shear-wave splitting environment in Matlab. Computers and Geosciences, 34, 515-528.

Yeck, W.L., Weingarten, M., Benz, H.M., McNamara, D.E., Bergman, E.A., Herrman, R.B., Rubinstein, J.L., Earle, P.S. (2016). Far-field pressurization likely caused one of the largest injection induced earthquakes by reactivating a large preexisting basement fault structure. Geophysical Research Letters, 43.

Zinke, J.C., Zoback, M.D. (2000). Structure-related and stress-induced shear-wave velocity anisotropy: observations from microearthquakes near the Calaveras fault in central California. Bulletin of the Seismological Society of America, 90, 1305-1312.

Zoback, M. L., and Zoback, M. (1980). State of stress in the coterminous United States. Journal of Geophysical Research: Solid Earth, 85(B11), 6113-6156.

Appendix A: earthquake Catalog

Year	MMDD	HHmm	ss.s	Latitude	Longitudee	depth (km)	Magnitude
2015	414	1925	53.6	37.227	-97.427	5.6	2.0WTES
2015	414	2127	46.1	37.326	-97.542	6.4	1.3WTES
2015	418	1251	38.2	37.314	-97.467	4.1	1.3WTES
2015	418	1329	25.4	37.306	-97.46	3.8	1.2WTES
2015	418	1331	21.3	37.315	-97.469	3.9	1.3WTES
2015	418	1524	0.8	37.316	-97.48	3.5	1.7WTES
2015	418	1608	13.2	37.308	-97.46	4.4	1.4WTES
2015	418	1627	56.4	37.284	-97.444	0.1	0.8WTES
2015	418	2009	57.1	37.316	-97.471	4.1	1.4WTES
2015	423	815	36.9	37.267	-97.502	4.3	1.5WTES
2015	5 6	2150	30.1	37.283	-97.609	5.2	2.2WTES
2015	5 6	2211	50.1	37.284	-97.607	4.6	2.3WTES
2015	5 9	936	23.1	37.33	-97.439	3.1	0.6WTES
2015	5 9	1448	43.2	37.28	-97.599	5.3	1.1WTES
2015	513	604	10.7	37.238	-97.594	0.9	2.3WTES
2015	518	233	8.6	37.226	-97.579	0.6	1.7WTES
2015	518	324	49	37.295	-97.493	4.7	1.3WTES
2015	520	620	28.9	37.309	-97.515	2.1	1.7WTES
2015	524	1149	44.6	37.31	-97.526	0.1	1.4WTES
2015	524	1950	20.4	37.363	-97.417	3.4	1.3WTES
2015	529	958	45.7	37.21	-97.533	5.7	1.9WTES
2015	531	2310	37.6	37.261	-97.449	3.1	1.2WTES
2015	6 4	116	10.7	37.287	-97.5	3.8	1.3WTES
2015	6 4	311	51.1	37.27	-97.422	1.7	0.9WTES
2015	6 5	1522	25.3	37.255	-97.597	7.6	2.1WTES
2015	629	305	37.1	37.295	-97.622	2.9	2.0WTES
2015	629	342	27	37.29	-97.62	4.1	2.2WTES
2015	629	745	19	37.295	-97.624	4.1	1.5WTES
2015	629	1331	30.6	37.25	-97.59	4.7	2.0WTES
2015	629	1843	40.9	37.25	-97.591	4.4	1.9WTES
2015	630	855	43.6	37.134	-97.652	3.8	2.4WTES
2015	7 2	528	13.1	37.308	-97.472	3.6	0.6WTES
2015	7 2	1227	55.1	37.292	-97.612	4.9	1.8WTES
2015	7 2	2046	0.6	37.288	-97.617	5.7	1.4WTES

2015	7 3	342	44.4	37.29	-97.615	5.1	1.3WTES
2015	7 3	2341	21.4	37.296	-97.621	3.5	1.6WTES
2015	7 3	2352	43.5	37.271	-97.646	15	1.4WTES
2015	7 4	2112	46.8	37.429	-97.464	4.2	1.0WTES
2015	7 4	2206	6.2	37.243	-97.614	5	1.7WTES
2015	7 5	1328	6.9	37.31	-97.466	3.7	1.4WTES
2015	7 5	1330	15.8	37.306	-97.469	3.7	0.6WTES
2015	7 5	1354	13.3	37.251	-97.608	3.8	2.4WTES
2015	7 5	1504	13.1	37.312	-97.466	3.6	0.7WTES
2015	7 5	1509	50.1	37.315	-97.482	3.1	0.5WTES
2015	7 5	2238	55.2	37.317	-97.507	1.9	1.0WTES
2015	7 6	543	59.1	37.424	-97.461	6.7	1.4WTES
2015	7 6	1302	26.3	37.432	-97.462	4.5	1.3WTES
2015	7 7	630	46.8	37.43	-97.465	4.7	1.3WTES
2015	7 7	1707	9	37.221	-97.613	5.8	1.4WTES
2015	7 8	8	23.3	37.277	-97.575	5	1.2WTES
2015	7 8	542	50.3	37.328	-97.494	0.7	0.6WTES
2015	7 8	823	49.2	37.326	-97.482	3.6	0.8WTES
2015	7 8	1716	32.1	37.332	-97.489	1.9	1.0WTES
2015	7 8	2108	44.6	37.32	-97.475	4.2	1.8WTES
2015	7 8	2113	7.2	37.323	-97.484	2.9	0.7WTES
2015	7 8	2126	30.5	37.325	-97.482	3.6	1.4WTES
2015	7 8	2231	12.6	37.328	-97.485	3.1	0.7WTES
2015	7 8	2255	50.9	37.324	-97.479	3.6	1.1WTES
2015	7 8	2322	55.1	37.322	-97.487	3.5	0.7WTES
2015	7 9	141	40.4	37.325	-97.482	3.5	0.9WTES
2015	7 9	203	11.8	37.312	-97.458	3.4	0.5WTES
2015	7 9	250	58	37.285	-97.608	4	1.0WTES
2015	7 9	424	40.4	37.324	-97.481	3.4	1.0WTES
2015	7 9	454	50.2	37.329	-97.49	2.5	0.8WTES
2015	7 9	605	7.8	37.322	-97.479	3.5	2.4WTES
2015	7 9	852	46.6	37.327	-97.48	3.7	0.9WTES
2015	7 9	907	9.3	37.31	-97.466	3.7	1.4WTES
2015	7 9	1459	0	37.31	-97.467	3.8	1.3WTES
2015	7 9	1530	13.6	37.312	-97.467	3.7	1.6WTES
2015	7 9	1531	38.8	37.312	-97.465	4	0.7WTES
2015	7 9	1534	34.4	37.324	-97.484	2.4	1.1WTES

2015	7 9	1629	35.1	37.303	-97.477	4.5	0.6WTES
2015	7 9	1639	13.9	37.286	-97.466	5.4	0.9WTES
2015	7 9	1639	17.2	37.309	-97.47	3.6	0.4WTES
2015	7 9	1646	48.9	37.303	-97.454	4.2	1.3WTES
2015	7 9	1722	13.8	37.308	-97.471	3.5	0.5WTES
2015	7 9	2245	57.1	37.312	-97.467	4	0.8WTES
2015	7 9	2249	46.1	37.317	-97.478	3.8	0.7WTES
2015	7 9	2250	42.3	37.306	-97.472	3.9	0.6WTES
2015	710	11	36.4	37.25	-97.606	3.9	1.7WTES
2015	710	20	37.3	37.249	-97.607	4.2	1.8WTES
2015	710	530	11.4	37.247	-97.606	4.4	1.4WTES
2015	710	1020	1.3	37.309	-97.465	3.9	1.5WTES
2015	710	1235	49.6	37.31	-97.466	3.9	0.7WTES
2015	710	1639	59.2	37.308	-97.469	3.8	0.6WTES
2015	710	1656	41.3	37.303	-97.467	4	0.7WTES
2015	711	56	3.2	37.312	-97.487	3	1.0WTES
2015	711	56	21.1	37.301	-97.472	3.9	0.7WTES
2015	711	709	1.4	37.307	-97.469	4	0.9WTES
2015	711	755	34.7	37.318	-97.486	3.4	1.0WTES
2015	711	2028	4.8	37.293	-97.483	3.5	1.1WTES
2015	712	29	43.9	37.311	-97.473	3.8	0.9WTES
2015	712	1601	29.7	37.428	-97.461	5.3	2.3WTES
2015	712	1727	48.9	37.284	-97.62	3.2	1.6WTES
2015	712	1946	54.5	37.155	-97.614	7	1.8WTES
2015	713	10	1.8	37.309	-97.463	3.8	2.3WTES
2015	713	16	50	37.308	-97.473	3.7	0.7WTES
2015	713	49	4.1	37.308	-97.472	3.8	1.0WTES
2015	713	442	28.9	37.334	-97.49	0.6	1.0WTES
2015	713	1941	24.2	37.306	-97.474	3.5	0.9WTES
2015	713	2136	59	37.301	-97.461	3.8	0.8WTES
2015	714	348	44.9	37.317	-97.444	15	1.3WTES
2015	714	1205	35.9	37.333	-97.484	5.3	1.2WTES
2015	714	1436	31.6	37.333	-97.481	2.2	0.8WTES
2015	714	1444	27.9	37.335	-97.488	1.1	1.2WTES
2015	716	213	7.5	37.253	-97.605	3.8	2.6WTES
2015	716	1136	38.5	37.33	-97.478	1.6	1.4WTES
2015	716	1719	14.7	37.271	-97.564	4.7	1.6WTES

2015	716	1743	27.7	37.195	-97.549	2.4	1.6WTES
2015	716	2136	52.1	37.237	-97.594	4.4	1.2WTES
2015	718	14	39.1	37.195	-97.545	1.8	1.6WTES
2015	718	352	51.4	37.323	-97.493	2.2	0.8WTES
2015	719	241	34.8	37.302	-97.505	4.8	1.3WTES
2015	719	1902	26	37.325	-97.482	3.5	0.9WTES
2015	719	2141	41	37.324	-97.482	3.4	0.9WTES
2015	720	135	59.8	37.328	-97.486	3.2	1.0WTES
2015	720	1024	2.8	37.325	-97.477	3.7	1.3WTES
2015	720	1313	43.7	37.291	-97.494	5.2	1.2WTES
2015	722	2147	0.4	37.182	-97.542	2.7	1.6WTES
2015	722	2258	45.2	37.321	-97.477	4	1.8WTES
2015	722	2304	54.9	37.181	-97.543	2.2	1.8WTES
2015	723	56	53.1	37.325	-97.483	3.5	1.4WTES
2015	723	227	49.6	37.285	-97.609	5.4	1.6WTES
2015	723	318	14.4	37.179	-97.543	2.7	1.9WTES
2015	723	957	47.6	37.179	-97.543	2.6	1.8WTES
2015	723	1045	5.7	37.243	-97.613	4.6	1.9WTES
2015	723	2125	31.3	37.245	-97.614	4.6	1.5WTES
2015	723	2151	41.3	37.25	-97.609	4.6	1.7WTES
2015	723	2216	40	37.397	-97.715	1.1	1.8WTES
2015	727	429	49.5	37.329	-97.491	2.4	1.2WTES
2015	727	1140	45.9	37.251	-97.607	3.9	2.7WTES
2015	729	633	21.2	37.319	-97.491	3	1.2WTES
2015	729	808	27.5	37.117	-97.478	6.3	1.6WTES
2015	729	1647	6.2	37.327	-97.49	0.8	1.1WTES
2015	729	2032	17.2	37.244	-97.611	4.6	1.5WTES
2015	731	428	31.9	37.265	-97.521	2.8	1.6WTES
2015	731	735	6.5	37.261	-97.519	3.7	1.8WTES
2015	731	1403	53.5	37.312	-97.468	4	1.6WTES
2015	731	1505	52.3	37.32	-97.48	3.3	1.3WTES
2015	731	1507	41.6	37.316	-97.476	3.5	1.1WTES
2015	731	1513	18.2	37.314	-97.47	4.1	1.6WTES
2015	731	1516	32.7	37.31	-97.466	4.3	1.4WTES
2015	731	1518	56.7	37.31	-97.465	4.2	1.6WTES
2015	731	1532	43.1	37.314	-97.474	3.8	1.3WTES
2015	731	1542	35.2	37.313	-97.472	4	1.3WTES

2015	731	1609	29.6	37.308	-97.47	3.7	1.1WTES
2015	731	1610	50.4	37.31	-97.465	4.2	1.6WTES
2015	731	1613	24.4	37.311	-97.468	3.9	1.6WTES
2015	731	1629	20.9	37.316	-97.475	3.6	1.2WTES
2015	731	1630	13.7	37.31	-97.464	4.2	1.6WTES
2015	731	1632	8.1	37.312	-97.472	4	1.2WTES
2015	731	1633	29.1	37.318	-97.475	3.6	1.1WTES
2015	731	1635	28.9	37.318	-97.475	3.5	1.0WTES
2015	731	1705	50.5	37.228	-97.583	15	1.4WTES
2015	731	1709	37.4	37.299	-97.453	3.7	1.2WTES
2015	731	1709	37.4	37.3	-97.456	3.7	0.4WTES
2015	731	1733	5.8	37.318	-97.475	4	1.1WTES
2015	731	1949	14.6	37.312	-97.468	4.1	1.2WTES
2015	731	2309	41.6	37.318	-97.474	4	1.1WTES
2015	731	2350	21.4	37.308	-97.464	4.2	1.7WTES
2015	731	2351	54.8	37.311	-97.465	4.3	1.5WTES
2015	8 1	28	34.6	37.309	-97.466	4	1.3WTES
2015	8 1	35	53.6	37.316	-97.475	4	1.1WTES
2015	8 1	638	31.7	36.951	-97.613	8.6	2.0WTES
2015	8 1	801	19.4	37.306	-97.464	4.1	1.1WTES
2015	8 2	438	56.7	37.318	-97.513	6.5	1.3WTES
2015	8 2	1553	31.9	37.316	-97.475	3.8	1.3WTES
2015	8 2	2205	54.9	37.109	-97.636	7.3	1.9WTES
2015	8 3	141	25.2	37.319	-97.516	5.8	1.3WTES
2015	8 3	622	39.1	37.325	-97.52	4.6	1.2WTES
2015	8 3	1039	51.6	37.319	-97.513	5.9	1.3WTES
2015	8 3	1338	34.7	37.32	-97.513	5.7	1.3WTES
2015	8 3	1350	17.9	37.319	-97.514	5.8	1.5WTES
2015	8 3	1633	10.7	37.317	-97.513	5.9	1.6WTES
2015	8 3	1634	3.6	37.321	-97.516	5.8	1.5WTES
2015	8 3	1943	58.3	37.319	-97.473	4	1.3WTES
2015	8 3	2008	38.1	37.332	-97.488	0.7	1.1WTES
2015	8 3	2009	27.5	37.332	-97.488	0.7	1.1WTES
2015	8 3	2129	13.9	37.325	-97.516	5.7	1.1WTES
2015	8 3	2135	57.5	37.328	-97.483	2.9	1.0WTES
2015	8 3	2225	49.2	37.102	-97.626	5.8	1.5WTES
2015	8 3	2242	43.5	37.331	-97.526	0.2	1.0WTES

2015	8 3	2254	1.3	37.314	-97.515	5.8	1.1WTES
2015	8 4	226	48.6	37.319	-97.513	5.9	1.1WTES
2015	8 4	433	4.2	37.318	-97.515	5.5	2.1WTES
2015	8 4	434	15.6	37.32	-97.513	5.9	1.9WTES
2015	8 4	548	52.2	37.205	-97.537	4	1.3WTES
2015	8 4	558	5.3	37.317	-97.514	6.6	1.1WTES
2015	8 4	751	8.5	37.224	-97.752	8.5	2.0WTES
2015	8 4	950	26.3	37.319	-97.531	3.2	1.5WTES
2015	8 4	1855	24.5	37.32	-97.513	6.3	1.0WTES
2015	8 4	2240	11.7	37.236	-97.594	4.8	1.6WTES
2015	8 5	313	57.3	37.103	-97.63	4.8	2.2WTES
2015	8 5	346	11.8	37.091	-97.709	10.7	2.0WTES
2015	8 5	851	22.1	37.321	-97.515	5.8	1.3WTES
2015	8 5	906	42	37.251	-97.657	4	1.7WTES
2015	8 5	913	58.8	37.319	-97.513	5.9	1.5WTES
2015	8 5	913	58.9	37.321	-97.516	5.3	1.4WTES
2015	8 5	916	59.1	37.318	-97.512	6.1	1.3WTES
2015	8 5	916	59.1	37.32	-97.515	5.8	1.3WTES
2015	8 5	919	31.6	37.318	-97.458	1.8	0.7WTES
2015	8 5	919	31.7	37.315	-97.453	1.8	0.7WTES
2015	8 5	929	35.2	37.32	-97.514	5.8	1.1WTES
2015	8 6	107	24.5	36.99	-97.499	9.6	2.0WTES
2015	8 6	508	27.2	37.325	-97.514	5.7	1.4WTES
2015	8 7	2	46.7	37.326	-97.518	5.8	1.4WTES
2015	8 7	133	41.9	37.328	-97.486	3.3	1.1WTES
2015	8 7	440	5	37.324	-97.481	4	1.2WTES
2015	8 7	926	11.8	37.32	-97.516	5.7	1.3WTES
2015	8 7	928	25.4	37.322	-97.48	3.8	1.0WTES
2015	8 7	1402	48	37.335	-97.498	4	1.2WTES
2015	8 7	1542	55.6	37.319	-97.511	5.6	1.3WTES
2015	8 7	1618	48.3	37.322	-97.478	4.1	1.0WTES
2015	8 7	1635	32.4	37.023	-97.559	7.9	1.9WTES
2015	8 7	1803	25.4	37.321	-97.515	5.6	1.5WTES
2015	8 7	1817	52.8	37.319	-97.514	5.8	1.5WTES
2015	8 7	2258	47.9	37.325	-97.517	5.2	1.3WTES
2015	8 7	2309	25.4	37.324	-97.519	4.1	1.8WTES
2015	8 7	2332	59.7	37.019	-97.555	7.8	1.6WTES

2015	8 7	2332	59.8	37.016	-97.551	4.9	1.7WTES
2015	8 8	17	22.8	37.316	-97.511	7.1	1.0WTES
2015	8 8	27	11.5	37.012	-97.531	2.4	1.4WTES
2015	8 8	801	16.8	37.32	-97.51	6.1	1.3WTES
2015	8 8	838	34	37.326	-97.521	0.2	1.4WTES
2015	8 8	1047	28.9	37.324	-97.522	5	1.0WTES
2015	8 8	1202	26	37.322	-97.479	4	1.2WTES
2015	8 8	1305	44.2	37.328	-97.512	5.1	1.2WTES
2015	8 9	513	54.4	37.332	-97.496	1.7	1.0WTES
2015	8 9	548	19.3	37.323	-97.473	4.1	0.9WTES
2015	8 9	603	2.4	37.274	-97.521	5.2	1.7WTES
2015	8 9	633	58.3	37.275	-97.517	4.6	1.2WTES
2015	8 9	1058	0.8	37.319	-97.476	4.4	0.9WTES
2015	810	1847	24.7	37.109	-97.632	6.7	1.9WTES
2015	810	2150	14.4	37.324	-97.554	6.5	1.1WTES
2015	811	220	52	37.314	-97.491	3.4	1.2WTES
2015	811	353	24	37.319	-97.479	3.9	1.1WTES
2015	811	940	59.1	37.316	-97.513	6.9	1.3WTES
2015	811	1228	24.9	37.101	-97.624	6.3	1.8WTES
2015	811	1810	10.7	37.321	-97.482	3.8	1.0WTES
2015	811	1836	50.7	37.325	-97.489	3.1	1.1WTES
2015	811	2150	46	37.319	-97.479	4.3	1.1WTES
2015	811	2211	26.7	37.323	-97.485	3.7	1.2WTES
2015	811	2229	29	37.321	-97.483	3.9	1.1WTES
2015	811	2231	39.5	37.322	-97.484	3.8	1.5WTES
2015	812	136	11.5	37.33	-97.495	1.7	0.9WTES
2015	812	1417	1	37.328	-97.49	2.7	1.1WTES
2015	813	1137	42.4	37.099	-97.624	4.6	1.7WTES
2015	813	1203	47.6	37.322	-97.481	4.2	1.1WTES
2015	813	1214	25.1	37.325	-97.486	3.3	1.1WTES
2015	813	1643	9.2	37.322	-97.481	4.1	1.2WTES
2015	814	1142	17.8	37.283	-97.428	3	1.0WTES
2015	814	1142	23.2	37.318	-97.478	4.1	1.1WTES
2015	814	1148	54.6	37.308	-97.469	3.6	1.1WTES
2015	814	1149	1.2	37.302	-97.456	4.1	1.1WTES
2015	814	1149	6	37.308	-97.477	3.5	0.8WTES
2015	814	1154	19.2	37.321	-97.479	3.9	1.4WTES

2015	814	1210	55.1	37.319	-97.475	4.6	1.0WTES
2015	814	1212	35.6	37.324	-97.48	3.7	1.7WTES
2015	814	1319	17.5	37.293	-97.442	4.9	0.9WTES
2015	814	1320	52	37.327	-97.488	2.6	1.2WTES
2015	814	1401	25.4	37.3	-97.446	4.7	0.9WTES
2015	814	1429	20.7	37.329	-97.487	2	1.2WTES
2015	814	1649	57.1	37.31	-97.465	4.8	1.1WTES
2015	814	1701	26.5	37.327	-97.488	2.1	1.1WTES
2015	814	1710	32.4	37.328	-97.492	2.1	1.0WTES
2015	814	1712	45.5	37.322	-97.48	4.2	1.0WTES
2015	814	2048	26.8	37.331	-97.489	1.9	1.0WTES
2015	814	2110	17.2	37.325	-97.48	4	1.2WTES
2015	814	2124	35.5	37.33	-97.491	0.2	0.9WTES
2015	814	2152	21.9	37.335	-97.5	0	0.9WTES
2015	814	2234	38.8	37.324	-97.481	3.9	1.1WTES
2015	814	2301	50.4	37.319	-97.473	4.2	1.0WTES
2015	815	236	39.5	37.322	-97.481	4.1	1.6WTES
2015	815	310	56.3	37.321	-97.478	4.1	1.0WTES
2015	815	454	50.9	37.323	-97.481	3.7	1.7WTES
2015	815	622	35.5	37.319	-97.477	4.1	1.1WTES
2015	815	728	52.8	37.322	-97.482	4	2.1WTES
2015	815	730	41.7	37.317	-97.477	4.5	1.2WTES
2015	815	731	18.6	37.318	-97.478	4.7	1.3WTES
2015	815	734	42.4	37.318	-97.476	4.8	1.1WTES
2015	815	739	57.3	37.319	-97.492	2.9	1.3WTES
2015	815	747	12.7	37.332	-97.495	1.5	0.9WTES
2015	815	747	26.2	37.328	-97.496	0.5	0.9WTES
2015	815	755	34.5	37.327	-97.493	1.8	0.9WTES
2015	815	756	19.9	37.324	-97.485	3.6	1.3WTES
2015	815	806	56.3	37.322	-97.484	3.8	1.4WTES
2015	815	816	45.5	37.323	-97.484	3.6	1.0WTES
2015	815	822	6	37.323	-97.486	3.6	1.2WTES
2015	815	912	19.8	37.319	-97.48	4.2	1.2WTES
2015	815	921	55.9	37.329	-97.497	1.6	0.9WTES
2015	815	933	5.2	37.319	-97.48	4.1	1.1WTES
2015	815	934	51.9	37.32	-97.479	4.1	1.4WTES
2015	815	940	29.4	37.317	-97.485	3.1	1.3WTES

2015	815	956	0.7	37.322	-97.485	4	1.7WTES
2015	815	1219	48.4	37.322	-97.486	3.7	1.5WTES
2015	815	1235	31.2	37.329	-97.495	0.6	1.3WTES
2015	815	1249	58.6	37.321	-97.484	3.9	1.4WTES
2015	815	1250	29.5	37.318	-97.477	4.6	1.3WTES
2015	815	1409	2.5	37.322	-97.486	3.9	1.5WTES
2015	815	1451	40.2	37.32	-97.48	4.4	1.0WTES
2015	815	1528	41.4	37.322	-97.477	4.1	1.2WTES
2015	815	1539	19.3	37.325	-97.483	3.6	1.2WTES
2015	815	1545	26.8	37.318	-97.479	4.1	1.1WTES
2015	815	1629	26.7	37.323	-97.484	3.5	1.1WTES
2015	815	1738	56.6	37.329	-97.496	0.7	0.9WTES
2015	815	1832	11.1	37.329	-97.497	0.7	1.0WTES
2015	815	1905	54.4	37.323	-97.485	3.6	1.0WTES
2015	815	2307	58.6	37.253	-97.605	3.4	1.8WTES
2015	816	349	53.9	37.312	-97.47	3.7	1.1WTES
2015	816	648	23.1	37.327	-97.493	2.9	1.1WTES
2015	816	700	50.9	37.325	-97.49	2.8	1.0WTES
2015	816	716	41.7	37.329	-97.492	2.1	0.7WTES
2015	816	720	40.2	37.321	-97.484	3.7	1.1WTES
2015	816	726	53.9	37.306	-97.466	3.6	1.1WTES
2015	816	727	25.2	37.308	-97.461	3.9	1.0WTES
2015	816	746	11.9	37.295	-97.464	3.4	0.9WTES
2015	816	950	45.3	37.318	-97.478	4.4	2.4WTES
2015	816	1006	59	37.327	-97.496	0.4	1.0WTES
2015	816	1008	45.9	37.32	-97.482	4	0.9WTES
2015	816	1013	55.7	37.329	-97.492	2.1	1.0WTES
2015	816	1033	26.8	37.326	-97.489	3.4	1.1WTES
2015	816	1034	21.2	37.32	-97.48	4	1.6WTES
2015	816	1134	51.8	37.328	-97.496	0.7	1.0WTES
2015	816	1212	11.4	37.321	-97.48	4.1	1.8WTES
2015	816	1221	25.3	37.316	-97.47	3.8	1.1WTES
2015	816	1226	2.2	37.315	-97.471	3.7	1.0WTES
2015	816	1235	13.3	37.365	-97.538	0.1	1.2WTES
2015	816	1237	15.9	37.319	-97.48	4.2	1.1WTES
2015	816	1246	44.5	37.328	-97.495	0.7	0.9WTES
2015	816	1305	45.9	37.314	-97.47	3.7	1.4WTES

2015	816	1307	1	37.31	-97.466	4	1.5WTES
2015	816	1308	22	37.312	-97.469	3.8	1.3WTES
2015	816	1310	10.7	37.33	-97.506	8.1	1.1WTES
2015	816	1310	44	37.293	-97.463	1.1	0.7WTES
2015	816	1312	25.1	37.314	-97.47	3.8	1.3WTES
2015	816	1317	38.5	37.309	-97.464	4	1.1WTES
2015	816	1324	1.9	37.315	-97.481	3	1.0WTES
2015	816	1325	56.2	37.31	-97.476	3.5	0.9WTES
2015	816	1326	50.5	37.293	-97.502	2.4	1.2WTES
2015	816	1327	41.2	37.318	-97.476	3.5	1.1WTES
2015	816	1341	29.9	37.307	-97.476	3.6	0.9WTES
2015	816	1341	32.2	37.299	-97.48	3.5	0.9WTES
2015	816	1351	39.7	37.318	-97.494	2.8	0.9WTES
2015	816	1355	29.1	37.315	-97.475	3.4	1.2WTES
2015	816	1411	36.1	37.326	-97.486	3.6	0.9WTES
2015	816	1442	46.1	37.311	-97.477	3.6	0.9WTES
2015	816	1444	19.8	37.308	-97.476	3.6	0.9WTES
2015	816	1444	43.7	37.278	-97.425	2.4	0.9WTES
2015	816	1445	37.9	37.307	-97.507	1.1	1.1WTES
2015	816	1447	22.2	37.314	-97.472	3.5	1.0WTES
2015	816	1447	41.3	37.302	-97.468	3.8	1.0WTES
2015	816	1501	15.9	37.32	-97.478	2.9	1.2WTES
2015	816	1501	35.9	37.316	-97.474	3.8	1.1WTES
2015	816	1504	3.6	37.3	-97.469	3	0.9WTES
2015	816	1505	13.3	37.312	-97.468	3.8	1.6WTES
2015	816	1513	1.3	37.238	-97.566	4.5	1.3WTES
2015	816	1517	16.7	37.306	-97.481	3.5	1.0WTES
2015	816	1521	11.2	37.325	-97.492	2.9	0.9WTES
2015	816	1545	6	37.303	-97.463	4	1.2WTES
2015	816	1601	53.7	37.298	-97.459	3.8	1.6WTES
2015	816	1603	50.4	37.297	-97.449	3.6	1.4WTES
2015	816	1906	25.7	37.408	-97.395	9.1	1.3WTES
2015	817	46	0.5	37.322	-97.482	4	1.0WTES
2015	817	1424	27.8	37.315	-97.474	4.8	1.1WTES
2015	817	1427	24.8	37.318	-97.48	3.9	1.3WTES
2015	817	1800	50.1	37.323	-97.487	3.7	1.5WTES
2015	817	1912	38.2	37.319	-97.478	4.2	1.3WTES

2015	817	2239	3.2	37.364	-97.392	4.3	1.4WTES
2015	817	2340	24.6	37.321	-97.482	4	1.0WTES
2015	818	15	6.4	37.326	-97.489	3.3	1.3WTES
2015	818	17	27.2	37.33	-97.493	2.4	1.4WTES
2015	818	18	17.3	37.326	-97.489	2.7	1.1WTES
2015	818	21	0.5	37.321	-97.482	4	1.4WTES
2015	818	22	33.7	37.323	-97.484	3.5	1.0WTES
2015	818	22	40.1	37.321	-97.48	4.1	1.1WTES
2015	818	37	1	37.321	-97.483	4	1.5WTES
2015	818	39	21.6	37.329	-97.496	0.1	1.0WTES
2015	818	506	42.8	37.324	-97.484	3.6	1.6WTES
2015	818	622	30.6	37.327	-97.489	3.1	0.9WTES
2015	820	928	54.5	37.343	-97.418	10.5	1.6WTES
2015	820	1334	30.5	37.327	-97.486	3.3	1.6WTES
2015	820	1344	57.2	37.314	-97.467	4.3	1.0WTES
2015	820	1354	52.1	37.322	-97.476	4.1	1.3WTES
2015	820	1428	37	37.323	-97.479	3.8	1.2WTES
2015	820	1902	26.9	37.426	-97.472	4.9	1.8WTES
2015	821	1050	17.6	37.252	-97.613	3.9	1.6WTES
2015	821	2030	40.9	37.326	-97.491	2.8	1.2WTES
2015	822	444	47	37.104	-97.637	6.2	1.8WTES
2015	823	1436	19.2	37.322	-97.48	3.9	1.1WTES
2015	824	1137	40.3	37.283	-97.625	4.1	1.5WTES
2015	824	1520	44.4	37.322	-97.515	5.6	1.2WTES
2015	824	1541	57.3	37.323	-97.516	5.3	1.2WTES
2015	824	1919	56.8	37.331	-97.486	2.8	0.9WTES
2015	825	539	40.8	37.234	-97.563	5.5	1.4WTES
2015	825	850	49.6	37.236	-97.587	4.8	1.3WTES
2015	825	1949	45.9	37.327	-97.513	5.1	1.3WTES
2015	825	2230	22	37.323	-97.513	5.5	1.2WTES
2015	825	2322	8.5	37.323	-97.514	5.5	1.5WTES
2015	826	123	44.3	37.276	-97.632	5.6	1.7WTES
2015	826	412	58.7	37.236	-97.566	4.7	1.5WTES
2015	826	515	28.6	37.293	-97.516	6.2	1.5WTES
2015	826	518	6.4	37.318	-97.514	5.6	1.1WTES
2015	826	556	56.2	37.319	-97.515	5.6	1.7WTES
2015	826	815	45.4	37.318	-97.513	5.9	1.1WTES

2015	826	817	35.3	37.319	-97.515	5.7	1.2WTES
2015	826	906	24.1	37.237	-97.565	4.9	1.9WTES
2015	826	1001	38.9	37.24	-97.565	4.6	1.5WTES
2015	826	1002	19.2	37.241	-97.566	4.3	1.2WTES
2015	826	1201	27.8	37.24	-97.566	4.6	1.4WTES
2015	826	1451	40.5	37.347	-97.581	5.1	1.5WTES
2015	826	1758	12.5	37.245	-97.566	4	1.5WTES
2015	826	1801	10.7	37.237	-97.565	4.8	1.4WTES
2015	826	1925	32.3	37.194	-97.56	9.3	1.8WTES
2015	826	2151	16.6	37.276	-97.631	5.7	1.7WTES
2015	827	312	32.7	37.294	-97.515	5.6	1.5WTES
2015	827	649	47.6	37.065	-97.523	4.9	1.8WTES
2015	827	1738	1	37.238	-97.566	4.7	1.6WTES
2015	828	154	13.5	37.241	-97.565	4.2	1.6WTES
2015	828	233	3.6	37.237	-97.564	5.1	1.5WTES
2015	828	939	7.6	37.323	-97.513	5	1.2WTES
2015	828	1010	2	37.32	-97.512	6	1.5WTES
2015	828	1041	28.2	37.323	-97.51	5.3	1.0WTES
2015	828	1104	16.1	37.237	-97.564	4.8	1.9WTES
2015	828	1143	7.4	37.054	-97.529	2	1.4WTES
2015	828	1204	0.2	37.24	-97.564	4.7	1.9WTES
2015	828	1204	5.4	37.24	-97.566	4.8	1.9WTES
2015	828	1439	16.5	37.32	-97.512	5.9	1.7WTES
2015	829	1920	22.4	37.231	-97.573	15	1.7WTES
2015	831	736	3.7	37.315	-97.472	4.5	1.0WTES
2015	831	748	27.5	37.322	-97.48	4	1.3WTES
2015	831	919	58.9	37.32	-97.477	4.3	1.2WTES
2015	831	922	16	37.319	-97.478	4.4	1.4WTES
2015	831	928	50.6	37.319	-97.477	4.3	1.0WTES
2015	831	948	43.4	37.321	-97.478	4.2	1.3WTES
2015	831	950	28.7	37.323	-97.48	3.8	1.4WTES
2015	831	1007	40	37.32	-97.477	4.1	1.3WTES
2015	831	1011	20.5	37.331	-97.491	2	1.1WTES
2015	831	1045	26.8	37.327	-97.495	0.3	1.0WTES
2015	831	1054	18.4	37.327	-97.488	3.3	1.0WTES
2015	831	2105	16.6	37.312	-97.387	3	1.2WTES
2015	9 1	136	47.5	37.059	-97.527	5.7	2.2WTES

2015	9 1	429	17.5	37.062	-97.527	4.7	2.3WTES
2015	9 1	507	57	37.325	-97.481	3.8	1.0WTES
2015	9 1	1149	2.1	37.064	-97.527	3.4	2.5WTES
2015	9 1	1239	45.1	37.243	-97.563	4.1	2.1WTES
2015	9 2	352	56	37.246	-97.568	3.1	1.7WTES
2015	9 3	810	50	37.212	-97.584	15	1.4WTES
2015	9 3	1055	42.3	37.243	-97.564	4.2	2.0WTES
2015	9 3	1101	52.2	37.241	-97.565	4.3	1.3WTES
2015	9 4	435	22.4	37.33	-97.491	2.6	1.2WTES
2015	9 4	1643	48.7	37.32	-97.476	4.2	1.4WTES
2015	9 5	447	20	37.244	-97.565	4.4	1.7WTES
2015	9 5	813	46.5	37.307	-97.511	6.1	1.2WTES
2015	9 5	1034	40.3	37.303	-97.618	5.3	1.8WTES
2015	9 5	2000	22.1	37.24	-97.564	4.7	1.5WTES
2015	9 6	24	10.9	37.057	-97.53	5.6	2.6WTES
2015	9 6	159	31.1	37.24	-97.564	4.7	1.7WTES
2015	9 6	1757	56	37.3	-97.616	3.5	1.7WTES
2015	9 6	1758	25.7	37.3	-97.618	5	1.8WTES
2015	9 7	130	15	37.242	-97.563	4.6	2.8WTES
2015	9 7	207	16.8	37.239	-97.565	4.6	1.6WTES
2015	9 7	208	10.2	37.241	-97.565	4.6	1.6WTES
2015	9 7	221	4.9	37.237	-97.566	4.6	1.4WTES
2015	9 7	221	53.6	37.241	-97.566	4.2	1.4WTES
2015	9 7	932	18.6	37.319	-97.513	6.5	1.1WTES
2015	9 7	1411	18.3	37.244	-97.564	4.2	1.6WTES
2015	9 7	1459	17.7	37.238	-97.599	4.6	1.7WTES
2015	9 7	1702	22.1	37.252	-97.614	4.1	1.5WTES
2015	9 7	1724	24.5	37.317	-97.511	5.8	1.1WTES
2015	9 7	1826	17.5	37.24	-97.566	4.3	1.6WTES
2015	9 7	2013	35.9	37.239	-97.565	4.5	1.9WTES
2015	9 8	309	6.2	37.236	-97.599	4.5	1.4WTES
2015	9 8	1316	47.3	37.233	-97.599	5.1	1.7WTES
2015	9 8	2335	10.9	37.321	-97.509	6.6	1.1WTES
2015	9 8	2355	59.3	37.323	-97.511	5.9	1.1WTES
2015	9 9	235	14.9	37.319	-97.511	5.3	1.4WTES
2015	9 9	510	4.9	37.32	-97.512	5.9	1.5WTES
2015	9 9	747	25	37.299	-97.615	4.2	1.7WTES

2015	9 9	1028	20.1	37.321	-97.515	5.8	1.7WTES
2015	9 9	1349	8.4	37.243	-97.563	4.2	1.3WTES
2015	9 9	1442	40.6	37.32	-97.512	6.3	1.3WTES
2015	9 9	1443	13.6	37.311	-97.51	6.2	1.2WTES
2015	9 9	1448	5.7	37.315	-97.513	5.9	1.8WTES
2015	9 9	1452	57.5	37.317	-97.513	6.4	1.6WTES
2015	9 9	1640	1	37.238	-97.565	4.5	1.4WTES
2015	9 9	1927	54.8	37.322	-97.513	6.6	1.3WTES
2015	9 9	2015	47.9	37.065	-97.522	5.5	1.7WTES
2015	910	320	43	37.325	-97.483	3.3	1.1WTES
2015	910	352	57.5	37.313	-97.516	5.7	1.5WTES
2015	910	416	18	37.283	-97.599	4.4	1.6WTES
2015	910	1202	41.9	37.283	-97.6	4.8	1.8WTES
2015	910	1237	33.6	37.281	-97.6	4.9	1.5WTES
2015	910	1322	48.4	37.331	-97.49	0.6	1.0WTES
2015	910	1533	6	37.323	-97.475	4.1	1.7WTES
2015	910	2208	7.4	37.241	-97.595	4.6	2.2WTES
2015	912	442	53.4	37.313	-97.514	5.9	1.4WTES
2015	912	839	54.7	37.402	-97.423	5.1	1.2WTES
2015	912	1312	31.6	37.248	-97.604	4.3	2.6WTES
2015	912	1323	48	37.299	-97.6	6.7	1.7WTES
2015	912	1820	34.2	37.2	-97.538	3.5	1.5WTES
2015	912	1905	22.6	37.324	-97.518	5.7	1.6WTES
2015	913	404	8.2	37.284	-97.433	4.7	1.4WTES
2015	913	415	55.9	37.061	-97.532	4.8	2.5WTES
2015	913	836	53.2	37.055	-97.534	3.6	1.8WTES
2015	913	845	54.8	37.066	-97.524	4.9	1.7WTES
2015	913	1150	27.6	37.285	-97.607	5	2.0WTES
2015	914	1302	37.7	37.063	-97.531	4.7	2.1WTES
2015	915	327	23.7	37.319	-97.515	6.7	1.3WTES
2015	915	357	33.4	37.283	-97.607	4.3	1.4WTES
2015	915	1111	10.2	37.286	-97.609	5.6	1.8WTES
2015	915	1144	42.5	37.284	-97.611	6.1	1.7WTES
2015	915	1427	7.1	37.287	-97.604	3.8	1.6WTES
2015	915	1518	19.5	37.237	-97.567	4.7	1.7WTES
2015	918	155	18.8	37.243	-97.589	4	1.7WTES
2015	918	155	50.9	37.237	-97.59	5	1.7WTES

2015	918	1505	44.9	37.275	-97.579	5.6	1.6WTES
2015	919	1237	19.6	37.238	-97.597	4.7	1.7WTES
2015	919	1516	20.3	37.31	-97.462	4.5	1.2WTES
2015	919	1516	23.6	37.332	-97.494	1.1	1.1WTES
2015	919	1523	1.3	37.31	-97.462	4.3	1.2WTES
2015	919	1523	34	37.31	-97.464	4.3	1.8WTES
2015	919	1523	41	37.311	-97.465	4	1.7WTES
2015	919	1523	43.8	37.316	-97.487	3.1	1.2WTES
2015	919	1524	14.8	37.307	-97.463	4.2	1.6WTES
2015	919	1524	25.7	37.306	-97.461	4.5	1.1WTES
2015	919	1525	17.1	37.317	-97.47	4	1.0WTES
2015	919	1525	27.6	37.305	-97.458	4.5	1.0WTES
2015	919	1526	11.2	37.309	-97.465	4.1	1.6WTES
2015	919	1526	25.3	37.309	-97.462	4.3	1.0WTES
2015	919	1526	29.2	37.309	-97.463	4.3	1.2WTES
2015	919	1527	32.2	37.31	-97.465	4.4	1.6WTES
2015	919	1527	44.2	37.311	-97.462	4.4	1.4WTES
2015	919	1530	30.2	37.309	-97.462	4.4	1.5WTES
2015	919	1536	31.1	37.307	-97.458	4.3	1.1WTES
2015	919	1540	29.1	37.316	-97.472	4	1.1WTES
2015	919	1556	32.1	37.308	-97.459	4.4	1.3WTES
2015	919	1613	43.1	37.308	-97.461	4.6	1.4WTES
2015	919	1622	39.6	37.126	-97.558	3.9	2.1WTES
2015	919	1650	49.7	37.304	-97.468	3.8	0.9WTES
2015	919	2258	35.5	37.32	-97.511	5.8	1.3WTES
2015	920	1442	29	37.295	-97.51	2.7	1.0WTES
2015	921	1521	59.3	37.237	-97.563	4.9	1.6WTES
2015	923	251	20.4	37.32	-97.515	5.7	1.8WTES
2015	923	253	36.4	37.319	-97.516	5.8	1.8WTES
2015	923	336	8.2	37.322	-97.516	6	1.5WTES
2015	923	345	16.9	37.321	-97.516	5.9	1.1WTES
2015	923	1855	20.2	37.327	-97.509	4.7	1.2WTES
2015	924	1025	50.9	37.245	-97.562	4.2	2.1WTES
2015	924	1606	33.7	37.238	-97.566	4.5	1.5WTES
2015	925	20	17.6	37.102	-97.699	4.9	2.3WTES
2015	926	1936	51.2	37.32	-97.515	5.7	1.2WTES
2015	926	1937	12.5	37.321	-97.513	5.8	1.3WTES

2015	926	1944	7.6	37.319	-97.512	6.3	1.1WTES
2015	926	1946	37.3	37.319	-97.511	6.2	1.1WTES
2015	926	2009	22.3	37.305	-97.509	6.7	1.1WTES
2015	926	2022	49.9	37.323	-97.48	3.9	1.3WTES
2015	926	2122	37.1	37.321	-97.477	3.9	1.0WTES
2015	927	718	47.3	37.331	-97.493	1.7	1.1WTES
2015	927	719	10.6	37.305	-97.459	4.9	1.0WTES
2015	927	747	30.1	37.328	-97.491	2.2	1.0WTES
2015	927	1410	43	37.323	-97.483	3.7	0.9WTES
2015	927	1938	31.3	37.322	-97.482	3.7	1.9WTES
2015	927	1939	7.8	37.329	-97.493	0.8	1.2WTES
2015	927	1941	16.2	37.318	-97.477	4	1.3WTES
2015	927	1942	58	37.32	-97.474	4.7	1.0WTES
2015	927	1956	44.7	37.327	-97.488	2.7	0.9WTES
2015	927	2004	30.3	37.328	-97.487	2.7	1.1WTES
2015	927	2008	54.3	37.329	-97.493	1.7	1.0WTES
2015	927	2025	19.8	37.319	-97.488	3.8	1.4WTES
2015	927	2030	37.5	37.315	-97.478	4.3	1.2WTES
2015	928	610	23.5	37.24	-97.562	4.1	1.4WTES
2015	930	905	24	37.243	-97.561	4.4	2.7WTES
2015	930	2346	20.9	37.323	-97.486	3.6	1.2WTES
2015	10 1	19	10.7	37.321	-97.483	3.6	1.1WTES
2015	10 1	36	42	37.321	-97.48	4	1.2WTES
2015	10 1	40	33.9	37.325	-97.489	3.2	1.2WTES
2015	10 1	2334	12.8	37.306	-97.427	5	1.0WTES
2015	10 2	605	41.2	37.32	-97.509	6.4	1.6WTES
2015	10 2	1418	33.1	37.283	-97.626	4.2	1.8WTES
2015	10 2	1727	19.8	37.322	-97.51	5.1	1.1WTES
2015	10 2	1844	12.2	37.331	-97.522	0.1	1.0WTES
2015	10 2	2320	5.8	37.321	-97.508	5.9	1.5WTES
2015	10 2	2328	25.1	37.301	-97.601	6.3	1.7WTES
2015	10 3	405	43.2	37.302	-97.603	6.5	1.8WTES
2015	10 3	511	58.5	37.103	-97.701	5.2	3.2WTES
2015	10 3	627	10.6	37.321	-97.507	6.3	1.5WTES
2015	10 3	1713	4.9	37.323	-97.508	7	1.6WTES
2015	10 3	2038	46.1	37.321	-97.51	5.6	1.2WTES
2015	10 3	2140	57.8	37.32	-97.508	6	1.2WTES

2015	10 4	44	47.9	37.325	-97.51	5.1	1.1WTES
2015	10 4	328	31.1	37.332	-97.52	0	2.7WTES
2015	10 4	614	38.2	37.325	-97.511	6.2	1.2WTES
2015	10 4	656	27.4	37.321	-97.51	6.9	1.2WTES
2015	10 4	741	34.2	37.32	-97.508	5.9	1.9WTES
2015	10 4	912	21.1	37.322	-97.512	5.7	1.6WTES
2015	10 4	1018	13.8	37.325	-97.505	7.6	1.3WTES
2015	10 4	1043	42.6	37.321	-97.509	5.3	1.3WTES
2015	10 4	1123	51.4	37.317	-97.5	6.2	1.0WTES
2015	10 4	1430	12.4	37.319	-97.506	6.5	1.5WTES
2015	10 4	1733	1.3	37.321	-97.511	6.1	1.9WTES
2015	10 4	1846	54.2	37.324	-97.509	5.7	1.3WTES
2015	10 4	1922	25.4	37.329	-97.508	5.9	2.3WTES
2015	10 5	414	49	37.324	-97.507	6.6	1.5WTES
2015	10 5	644	57.8	37.206	-97.521	2.9	1.5WTES
2015	10 5	1011	4.3	37.322	-97.505	6.7	1.1WTES
2015	10 5	1017	33.2	37.324	-97.507	5.7	1.2WTES
2015	10 5	2008	53.9	37.326	-97.507	6.3	1.4WTES
2015	10 5	2117	40.7	37.322	-97.506	6.3	1.1WTES
2015	10 6	221	30.6	37.354	-97.482	5	1.5WTES
2015	10 6	224	53	37.353	-97.48	5.5	1.3WTES
2015	10 6	340	4.8	37.36	-97.493	2.8	1.2WTES
2015	10 6	413	36.8	37.323	-97.504	6.5	1.4WTES
2015	10 6	611	11.9	37.323	-97.508	6.8	1.2WTES
2015	10 6	612	2.8	37.061	-97.519	4.1	1.6WTES
2015	10 6	1509	2.3	37.264	-97.305	1.1	1.7WTES
2015	10 6	1621	52.5	37.344	-97.507	5.7	2.2WTES
2015	10 6	1653	33.7	37.325	-97.51	5.1	1.4WTES
2015	10 7	12	52.2	37.322	-97.508	5.6	1.3WTES
2015	10 7	39	54.1	37.327	-97.506	5.9	2.4WTES
2015	10 7	124	52.3	37.322	-97.516	0.3	1.0WTES
2015	10 7	237	5.1	37.321	-97.51	5.7	1.5WTES
2015	10 7	239	30.8	37.321	-97.508	6.2	1.3WTES
2015	10 7	240	13.2	37.319	-97.508	5.7	1.2WTES
2015	10 7	329	8.7	37.319	-97.503	6	1.2WTES
2015	10 7	331	47.7	37.324	-97.508	6.3	1.5WTES
2015	10 7	501	35.6	37.321	-97.51	6	1.7WTES

2015	10 7	920	26.9	37.237	-97.568	4.4	1.9WTES
2015	10 7	1229	24.2	37.328	-97.514	4.5	1.1WTES
2015	10 7	1448	37.7	37.235	-97.567	4.5	1.8WTES
2015	10 7	1737	18.7	37.342	-97.54	0.1	1.2WTES
2015	10 7	1833	53.9	37.321	-97.515	5.6	1.2WTES
2015	10 7	1848	55.5	37.323	-97.51	6.9	1.2WTES
2015	10 7	2118	15.4	37.319	-97.512	5.3	1.0WTES
2015	10 7	2122	42.1	37.32	-97.511	5.9	1.1WTES
2015	10 7	2238	20.6	37.326	-97.517	5.4	1.4WTES
2015	10 7	2350	56.9	37.324	-97.512	5.4	1.1WTES
2015	10 8	340	38.3	37.321	-97.512	5.6	1.5WTES
2015	10 8	403	42	37.323	-97.515	5.6	1.1WTES
2015	10 8	1136	59.9	37.209	-97.522	2.4	1.4WTES
2015	10 8	1511	0.6	37.346	-97.579	4.3	1.3WTES
2015	10 8	1558	28.4	37.344	-97.581	5.4	1.5WTES
2015	10 8	1843	2.4	37.22	-97.585	3.5	1.8WTES
2015	10 8	1921	57.3	37.216	-97.583	3.8	1.4WTES
2015	10 8	2112	11.1	37.331	-97.494	1.8	1.2WTES
2015	10 8	2144	8.7	37.318	-97.475	4.2	1.0WTES
2015	10 8	2149	57.4	37.32	-97.477	4.1	1.3WTES
2015	10 8	2251	26.1	37.328	-97.486	2.7	1.3WTES
2015	10 8	2347	3.3	37.327	-97.486	3.2	1.1WTES
2015	10 8	2348	24.5	37.326	-97.486	3.3	1.2WTES
2015	10 8	2348	27.3	37.329	-97.495	0.6	1.1WTES
2015	10 8	2349	31.9	37.328	-97.495	0.1	1.0WTES
2015	10 8	2349	35.1	37.327	-97.486	3.5	1.0WTES
2015	10 8	2350	16.3	37.322	-97.483	3.7	1.1WTES
2015	10 9	40	9.5	37.32	-97.479	4.1	1.3WTES
2015	10 9	2252	6.6	37.29	-97.495	4.3	1.2WTES
2015	1010	143	6.3	37.313	-97.473	15	1.2WTES
2015	1010	208	49.4	37.181	-97.638	5.1	1.7WTES
2015	1010	220	0.5	37.185	-97.639	3.1	1.7WTES
2015	1010	1136	35	37.291	-97.492	5.2	1.7WTES
2015	1011	103	2.1	37.365	-97.397	4.5	1.4WTES
2015	1011	338	43.2	37.356	-97.395	5.7	1.3WTES
2015	1012	13	26.9	37.21	-97.522	2.8	1.5WTES
2015	1012	357	34.3	37.188	-97.637	4.7	2.3WTES

2015	1012	827	48.2	37.184	-97.64	4.9	1.9WTES
2015	1012	1320	13.2	37.189	-97.637	4.8	2.2WTES
2015	1012	2309	20.4	37.399	-97.72	1.5	1.8WTES
2015	1013	632	19	37.244	-97.564	4.6	2.2WTES
2015	1013	639	4.5	37.238	-97.564	4.8	1.4WTES
2015	1013	803	48.5	37.24	-97.565	4.5	1.5WTES
2015	1014	924	52.1	37.239	-97.566	4.9	1.8WTES
2015	1014	931	59.3	37.241	-97.565	4.6	1.3WTES
2015	1017	246	17.5	37.297	-97.6	4.1	1.2WTES
2015	1017	437	17.8	37.396	-97.712	1	1.6WTES
2015	1017	445	9.3	37.213	-97.528	4	1.9WTES
2015	1017	2025	51.5	37.061	-97.526	5.7	2.3WTES
2015	1018	708	19.9	37.061	-97.529	5.4	2.6WTES
2015	1018	851	18.6	37.062	-97.531	5.8	1.7WTES
2015	1019	8	50.9	37.12	-97.62	3.4	3.2WTES
2015	1019	734	54	37.241	-97.563	4.8	1.9WTES
2015	1019	1014	43.1	37.124	-97.618	3.4	2.5WTES
2015	1019	1217	2.9	37.306	-97.468	4.9	1.0WTES
2015	1021	1419	37.1	37.187	-97.64	4.8	2.2WTES
2015	1021	2002	14.8	37.123	-97.62	3.3	2.8WTES
2015	1021	2256	51.6	37.25	-97.61	4.4	2.5WTES
2015	1022	552	50.7	37.193	-97.251	0.1	1.7WTES
2015	1022	1039	58	37.247	-97.563	3.8	1.5WTES
2015	1023	1312	41.3	37.241	-97.562	4.8	1.7WTES
2015	1023	1717	41.3	37.239	-97.564	4.9	1.5WTES
2015	1023	2316	25.6	37.208	-97.523	3	1.4WTES
2015	1024	520	26.5	37.274	-97.496	4.1	1.3WTES
2015	1025	449	20.2	37.325	-97.485	3.4	0.8WTES
2015	1026	608	34.9	37.071	-97.532	4	2.4WTES
2015	1026	2023	27	37.311	-97.463	4.5	1.2WTES
2015	1026	2024	44.9	37.311	-97.465	4.2	0.8WTES
2015	1026	2024	56.3	37.317	-97.471	3.9	0.9WTES
2015	1026	2026	30	37.314	-97.468	4.3	1.0WTES
2015	1027	221	47.7	37.124	-97.618	3.5	3.2WTES
2015	1027	306	49.6	37.124	-97.619	3.5	3.5WTES
2015	1027	753	2.1	37.124	-97.621	3.6	2.6WTES
2015	1027	1227	41.8	37.154	-97.622	4.1	2.7WTES

2015	1027	2227	48.6	37.242	-97.563	4.6	1.5WTES
2015	1027	2235	33.2	37.117	-97.617	4.4	1.9WTES
2015	1029	0	43.5	37.117	-97.621	5.1	2.7WTES
2015	1029	2	14.3	37.117	-97.621	4.9	2.1WTES
2015	1029	1905	31.4	37.242	-97.562	4.6	1.4WTES
2015	1030	437	2.4	37.152	-97.621	4	3.5WTES
2015	1030	1209	17.6	37.32	-97.506	6.7	1.4WTES
2015	1030	1242	59.7	37.12	-97.623	3.7	2.2WTES
2015	1030	2003	49.2	37.062	-97.526	5.6	2.7WTES
2015	1030	2108	32.7	37.128	-97.617	3.5	2.3WTES
2015	1031	948	8	37.123	-97.621	6.1	1.7WTES
2015	11 1	222	13.2	37.125	-97.617	3.1	2.8WTES
2015	11 1	1247	16.8	37.242	-97.565	4.5	1.2WTES
2015	11 2	515	26.9	37.064	-97.525	5.1	2.4WTES
2015	11 2	643	27.6	37.316	-97.292	7.1	1.8WTES
2015	11 2	644	1.9	37.297	-97.287	3.4	1.4WTES
2015	11 2	645	36.8	37.24	-97.566	4.8	1.3WTES
2015	11 2	726	55.3	37.057	-97.533	5.4	2.7WTES
2015	11 2	1110	32.3	37.053	-97.542	0.1	1.4WTES
2015	11 2	1116	44.4	37.059	-97.533	5.3	2.5WTES
2015	11 2	1444	5.3	37.238	-97.552	4	1.3WTES
2015	11 2	2253	57.5	37.065	-97.52	5.6	1.8WTES
2015	11 3	134	56.2	36.964	-97.467	5.1	1.6WTES
2015	11 3	501	58.4	37.054	-97.539	5.9	1.9WTES
2015	11 3	525	1.6	37.049	-97.54	2.8	2.0WTES
2015	11 3	824	9	37.058	-97.534	6.4	2.1WTES
2015	11 3	1933	6.2	37.055	-97.53	3.9	2.3WTES
2015	11 3	2128	52.5	37.062	-97.528	6.2	2.3WTES
2015	11 6	1830	32.5	37.155	-97.621	4.9	1.7WTES
2015	11 7	134	25.2	37.138	-97.557	1.1	1.9WTES
2015	11 7	435	0.4	37.058	-97.531	3.5	1.6WTES
2015	11 7	808	47.2	37.345	-97.581	5.2	1.5WTES
2015	11 8	25	1.9	37.257	-97.597	4.2	2.3WTES
2015	11 8	129	52.8	37.248	-97.602	5.1	1.8WTES
2015	11 8	655	46.4	37.249	-97.603	5	1.5WTES
2015	11 8	2220	51.1	37.186	-97.803	7.5	2.2WTES
2015	11 9	351	52.2	37.321	-97.294	7.3	1.6WTES

2015	11 9	1617	31.5	37.136	-97.567	2.8	1.9WTES
2015	11 9	1714	33.8	37.141	-97.567	3.6	2.3WTES
2015	11 9	1838	11.2	37.328	-97.494	2	1.1WTES
2015	11 9	1902	5.7	37.142	-97.569	3.8	2.2WTES
2015	11 9	2242	6.8	37.115	-97.607	3	3.8WTES
2015	11 9	2335	18	37.129	-97.617	5.2	2.5WTES
2015	1110	10	47.9	37.063	-97.529	6	2.3WTES
2015	1110	31	39	37.063	-97.527	6.3	2.6WTES
2015	1110	924	44.8	37.244	-97.564	4.4	1.5WTES
2015	1110	1046	16.1	37.057	-97.532	5.7	2.3WTES
2015	1110	2258	35.1	37.346	-97.582	3.5	1.4WTES
2015	1111	417	0	37.126	-97.613	4.8	2.6WTES
2015	1113	1348	51.7	37.327	-97.48	3.5	1.2WTES
2015	1113	1718	55.6	37.329	-97.482	3	1.0WTES
2015	1114	956	33.4	37.137	-97.564	3.6	2.0WTES
2015	1114	1020	37.5	37.331	-97.488	1.7	0.9WTES
2015	1114	2121	51.8	37.3	-97.503	5.4	1.4WTES
2015	1115	732	49	37.197	-97.543	2.9	1.5WTES
2015	1115	841	7.1	37.318	-97.461	15	2.3WTES
2015	1115	846	38.1	37.314	-97.512	5.3	1.3WTES
2015	1115	911	57.7	37.318	-97.518	5	1.5WTES
2015	1115	922	5.4	37.313	-97.512	5.3	1.5WTES
2015	1115	1152	27.4	37.313	-97.511	5.5	2.0WTES
2015	1115	1539	11.8	37.318	-97.516	5	1.1WTES
2015	1115	1610	7.4	37.318	-97.516	5.3	1.5WTES
2015	1115	1610	23.4	37.314	-97.513	5	1.3WTES
2015	1115	1634	0.6	37.31	-97.509	6.1	1.3WTES
2015	1115	2013	16.9	37.323	-97.519	3.9	1.4WTES
2015	1115	2305	16.4	37.311	-97.515	5.3	1.2WTES
2015	1115	2306	53.8	37.296	-97.517	5.5	1.1WTES
2015	1119	705	58.7	37.124	-97.597	3.6	2.0WTES
2015	1119	2057	32.1	37.142	-97.566	3	2.2WTES
2015	1122	932	46.1	37.142	-97.569	3.3	2.0WTES
2015	1122	1208	34.9	37.276	-97.496	3.5	1.3WTES
2015	1122	1518	42.2	37.348	-97.505	0.8	1.2WTES
2015	1122	2044	36	37.308	-97.523	2.3	1.1WTES
2015	1123	1126	41.9	37.142	-97.569	2.8	2.6WTES

2015	1123	1856	5.3	37.119	-97.617	2.6	2.1WTES
2015	1123	2226	26.1	37.33	-97.415	2.1	1.0WTES
2015	1124	640	57.7	37.331	-97.416	2	0.9WTES
2015	1125	332	59.6	37.33	-97.413	1.9	1.4WTES
2015	1125	538	51.9	37.317	-97.521	4.8	1.2WTES
2015	1125	703	57.3	37.33	-97.414	2.1	1.0WTES
2015	1125	829	7.7	37.33	-97.42	2.2	1.0WTES
2015	1125	1203	31.4	37.333	-97.417	1.8	1.1WTES
2015	1126	245	33.3	37.324	-97.404	8.1	1.5WTES
2015	1126	1114	44.2	37.273	-97.493	2.9	0.8WTES
2015	1126	1535	58.7	37.297	-97.591	4.4	1.6WTES
2015	1126	1615	11.9	37.331	-97.418	2.3	0.9WTES
2015	1126	1742	28.6	37.326	-97.416	2.3	1.0WTES
2015	1126	1835	52	37.331	-97.414	1.7	1.0WTES
2015	1127	2	49.7	37.321	-97.412	2.6	1.3WTES
2015	1127	1119	50.8	37.286	-97.487	4.3	1.3WTES
2015	1127	1158	12.2	37.288	-97.491	3.9	1.7WTES
2015	1128	732	15.8	37.245	-97.555	6.5	1.8WTES
2015	12 2	1014	45.4	37.246	-97.586	4.3	1.7WTES
2015	12 3	911	0.9	37.3	-97.494	6.9	1.3WTES
2015	12 4	550	50.6	37.262	-97.399	12.6	1.5WTES
2015	12 4	1001	29	37.272	-97.382	2	1.2WTES
2015	12 4	1048	19.7	37.189	-97.263	0	1.9WTES
2015	12 4	2045	38.7	37.273	-97.462	21.8	1.7WTES
2015	12 6	737	13.5	37.19	-97.257	1.9	2.2WTES
2015	1210	2242	46.6	37.301	-97.463	4.2	1.1WTES
2015	1210	2324	5.4	37.304	-97.465	4.3	1.3WTES
2015	1212	1215	18.5	37.302	-97.426	4.8	1.0WTES
2015	1213	720	31.5	37.431	-97.392	7	1.3WTES
2015	1213	1307	9.9	37.328	-97.416	2.6	0.8WTES
2015	1214	224	44.4	37.324	-97.481	3.7	1.4WTES
2015	1215	352	56.2	37.436	-97.393	5.6	1.3WTES
2015	1216	901	38.2	37.279	-97.624	5.9	2.0WTES
2015	1216	922	46.4	37.274	-97.625	4.6	2.1WTES
2015	1216	1239	20.4	37.277	-97.625	4.9	2.0WTES
2015	1216	1239	53.6	37.28	-97.626	5.1	2.1WTES
2015	1216	1240	17.6	37.279	-97.625	5	1.5WTES

2015	1221	1430	54.5	37.02	-97.551	1	2.5WTES
2015	1222	7	24.8	37.111	-97.64	5.5	2.2WTES
2015	1222	449	41.8	37.395	-97.716	0.7	2.6WTES
2015	1222	2114	25.3	37.401	-97.728	8.1	2.0WTES
2015	1224	33	14.6	37.157	-97.619	3.2	2.4WTES
2015	1224	141	47.6	37.156	-97.62	3.5	2.3WTES
2015	1224	926	48.7	37.326	-97.417	1.9	0.9WTES
2015	1224	1634	28.7	37.308	-97.459	3.2	1.1WTES
2015	1225	217	46.5	37.303	-97.465	2.9	0.8WTES
2015	1225	1734	56.5	37.315	-97.497	6.1	0.9WTES
2015	1226	756	37.7	37.394	-97.715	1.1	2.1WTES
2015	1226	2139	10.1	37.321	-97.51	5.9	1.9WTES
2015	1226	2146	33.3	37.317	-97.51	5.5	1.8WTES
2015	1227	1106	24.7	37.324	-97.516	4	1.8WTES
2015	1227	1330	32.1	37.321	-97.52	3.6	1.7WTES
2015	1227	1410	58	37.327	-97.517	4.9	1.5WTES
2015	1227	2039	47.9	37.324	-97.504	5.5	1.5WTES
2015	1227	2229	18.5	37.394	-97.715	0.9	2.2WTES
2015	1228	659	4.5	37.327	-97.506	5.9	2.1WTES
2015	1229	30	22.9	37.328	-97.507	5.4	0.9WTES
2015	1229	158	36	37.322	-97.504	5.7	0.9WTES
2015	1229	623	0.6	37.302	-97.507	6	0.9WTES
2015	1229	654	2.6	37.268	-97.637	5.3	1.4WTES
2015	1229	740	2.7	37.268	-97.633	4.1	1.2WTES
2015	1229	743	6.8	37.267	-97.632	3.8	1.1WTES
2015	1229	811	48.1	37.266	-97.639	5.3	1.3WTES
2015	1229	820	52.5	37.267	-97.637	5.2	1.4WTES
2015	1229	1000	12.1	37.267	-97.639	5.5	1.5WTES
2015	1229	1006	5.3	37.267	-97.638	5.2	1.2WTES
2015	1229	1219	56.5	37.313	-97.506	5.5	0.9WTES
2015	1229	1240	49	37.267	-97.636	4.9	1.5WTES
2015	1229	1406	8.7	37.268	-97.636	4.9	1.5WTES
2015	1229	1603	15.2	37.323	-97.507	5.7	1.0WTES
2015	1229	1611	43.7	37.327	-97.509	5.2	1.1WTES
2015	1229	1746	14.6	37.265	-97.634	5.1	2.6WTES
2015	1229	1927	4.3	37.267	-97.637	4.8	1.7WTES
2015	1229	2135	2.2	37.321	-97.505	6	0.8WTES

2015	1230	726	59.1	37.265	-97.634	5	2.1WTES
2015	1230	1246	49.2	37.322	-97.499	0.1	1.0WTES
2015	1230	1303	45.7	37.319	-97.488	3.8	0.8WTES
2015	1230	1538	40.1	37.321	-97.494	2.9	0.9WTES
2015	1230	1628	16.4	37.323	-97.506	5.6	1.0WTES
2015	1230	2211	12.1	37.324	-97.508	5	1.4WTES
2015	1231	355	43.3	37.326	-97.435	2.3	1.3WTES
2015	1231	414	59.4	37.391	-97.72	5	1.9WTES
2015	1231	602	26.3	37.324	-97.439	2.6	0.9WTES
2015	1231	1416	43.8	37.137	-97.654	6.6	2.8WTES
2015	1231	1631	32.5	37.133	-97.652	6.5	2.7WTES
2016	1 1	1421	40.9	37.244	-97.611	4.7	1.7WTES
2016	1 1	1852	37.9	37.135	-97.653	7.4	1.4WTES
2016	1 2	46	53	37.27	-97.413	2.3	1.0WTES
2016	1 2	503	9.3	37.276	-97.42	4.1	1.1WTES
2016	1 2	821	46.6	37.252	-97.606	3.9	1.9WTES
2016	1 2	825	45.5	37.252	-97.605	4	1.8WTES
2016	1 2	1417	19.1	37.236	-97.561	3.8	1.8WTES
2016	1 2	2114	11.5	37.317	-97.484	4.1	1.0WTES
2016	1 3	5	26.4	37.316	-97.487	4	0.9WTES
2016	1 3	46	54.6	37.238	-97.563	3.7	1.4WTES
2016	1 3	157	33	37.316	-97.487	3.9	1.1WTES
2016	1 3	706	6.2	37.318	-97.486	4.1	1.0WTES
2016	1 3	1736	50.7	37.328	-97.442	3.1	0.7WTES
2016	1 3	1928	47.6	37.311	-97.463	3	1.1WTES
2016	1 4	538	52.7	37.288	-97.461	5.8	0.9WTES
2016	1 4	626	19.1	37.237	-97.562	3.8	1.7WTES
2016	1 4	857	2.2	37.238	-97.563	3.6	1.6WTES
2016	1 4	2248	40.8	37.131	-97.657	6.3	2.0WTES
2016	1 6	825	2.5	37.237	-97.561	3.9	1.6WTES
2016	1 7	1357	39	37.322	-97.424	2.8	0.7WTES
2016	1 8	1440	25	37.256	-97.572	5.1	1.3WTES
2016	1 8	1507	43.5	37.258	-97.571	4.7	1.7WTES
2016	1 8	1511	31.1	37.257	-97.571	5.1	1.4WTES
2016	1 9	34	29.4	37.3	-97.48	5.5	1.3WTES
2016	112	1209	13.3	37.275	-97.42	3.8	1.0WTES
2016	114	240	17	37.493	-97.786	15	2.6WTES

2016	114	544	23.8	37.278	-97.493	4.2	1.5WTES
2016	114	1314	36	37.278	-97.491	4.2	1.2WTES
2016	115	206	30.8	36.956	-97.805	7.5	3.4WTES
2016	115	206	31.4	36.969	-97.779	11.8	2.8WTES
2016	115	329	25.4	36.986	-97.791	14	2.2WTES
2016	115	2057	38.6	37.283	-97.486	4.2	1.1WTES
2016	116	9	51.7	36.979	-97.791	15.8	2.5WTES
2016	116	901	47.3	37.276	-97.423	4.2	1.3WTES
2016	116	1308	25.7	37.282	-97.487	4.3	1.4WTES
2016	116	1859	23.2	37.595	-97.322	8.2	2.4WTES
2016	116	2013	18.5	37.569	-97.728	2.1	2.2WTES
2016	116	2337	47.6	37.308	-97.457	3.2	0.8WTES
2016	117	652	43.3	37.368	-97.421	2.2	1.1WTES
2016	117	2122	22.8	37.304	-97.475	2.4	0.9WTES
2016	117	2224	19.4	37.371	-97.435	0.4	1.0WTES
2016	117	2242	7.3	37.36	-97.405	2.5	1.2WTES
2016	117	2329	31.9	37.307	-97.456	3.4	0.9WTES
2016	118	36	55.9	37.354	-97.403	3.2	1.2WTES
2016	118	236	17.1	37.278	-97.429	4.2	1.2WTES
2016	118	248	31.6	37.271	-97.412	2.3	1.1WTES
2016	118	427	59.9	37.274	-97.418	3.7	1.4WTES
2016	118	531	4.8	37.366	-97.421	2.7	1.0WTES
2016	118	609	38.8	37.278	-97.424	4.2	1.4WTES
2016	118	649	20.7	37.266	-97.435	2.9	0.9WTES
2016	120	924	51.8	37.005	-97.466	0.5	2.2WTES
2016	120	1536	38.5	36.874	-97.817	21.4	2.0WTES
2016	120	1905	45.6	37.245	-97.555	3.6	1.5WTES
2016	120	2024	23.1	37.273	-97.413	3.3	1.1WTES
2016	120	2034	25	37.279	-97.421	4.2	1.4WTES
2016	120	2036	20.7	37.273	-97.408	2.9	1.1WTES
2016	121	47	9.6	37.276	-97.416	3.9	1.0WTES
2016	121	329	49.2	37.272	-97.413	2.7	1.2WTES
2016	121	728	16.6	37.282	-97.423	4.1	1.1WTES
2016	121	801	44.9	37.188	-97.532	2.9	1.3WTES
2016	121	1551	3.4	37.248	-97.857	8.7	2.4WTES
2016	121	1619	48	37.392	-97.354	3.9	1.7WTES
2016	122	926	27.8	37.229	-97.224	6.9	1.4WTES

2016	122	1020	54.9	37.39	-97.352	5	1.5WTES
2016	122	1448	25.8	37.392	-97.353	5	1.2WTES
2016	123	1240	8.1	37.283	-97.502	0	1.1WTES
2016	123	1304	41.2	37.181	-97.808	5.6	1.9WTES
2016	123	1651	34.8	37.243	-97.562	4.5	1.5WTES
2016	123	1927	7.8	37.244	-97.561	4.5	1.5WTES
2016	123	2125	53.9	37.243	-97.562	4.5	1.6WTES
2016	123	2331	4.2	37.242	-97.563	4.4	2.0WTES
2016	124	36	10.5	37.24	-97.563	4.6	1.7WTES
2016	124	37	55.2	37.242	-97.564	4.4	2.0WTES
2016	124	1001	41.3	36.933	-97.638	7.9	3.8WTES
2016	124	1531	2.1	37.286	-97.434	4.9	0.6WTES
2016	124	1819	41.5	36.957	-97.813	16.9	2.3WTES
2016	125	246	46.4	37.242	-97.564	4.2	1.3WTES
2016	125	806	43.1	37.274	-97.421	3.8	0.8WTES
2016	126	17	36.6	37.281	-97.428	4.5	1.0WTES
2016	126	601	27.5	37.358	-97.387	4.4	1.4WTES
2016	127	622	36.4	37.076	-97.719	8.3	2.1WTES
2016	128	1438	23.8	37.328	-97.418	2.4	0.8WTES
2016	131	1327	19.1	37.318	-97.604	4	1.7WTES
2016	2 1	600	45.1	37.435	-97.544	0.1	1.4WTES
2016	2 1	745	28.9	37.057	-97.519	4.7	1.5WTES
2016	2 1	837	6.6	37.229	-97.586	4.3	1.2WTES
2016	2 1	951	30.1	37.24	-97.557	3.9	1.5WTES
2016	2 2	21	59.1	37.222	-97.585	4.3	1.6WTES
2016	2 2	111	34.9	37.133	-97.658	2	2.1WTES
2016	2 2	940	33.1	37.125	-97.611	4.9	1.5WTES
2016	2 3	2132	19.9	37.219	-97.586	4.6	1.5WTES
2016	2 3	2250	13.7	37.217	-97.585	4.7	1.6WTES
2016	2 4	41	43.5	37.217	-97.586	4.6	1.4WTES
2016	2 4	243	30.2	37.328	-97.417	2.5	1.2WTES
2016	2 4	639	41.9	37.219	-97.585	4.6	1.6WTES
2016	2 4	1806	59.1	37.23	-97.588	4	2.6WTES
2016	2 5	820	41.1	37.206	-97.602	15	1.7WTES
2016	2 5	1341	28.6	37.269	-97.415	3.8	1.0WTES
2016	2 5	1354	20.5	37.272	-97.42	3.6	1.3WTES
2016	2 5	1937	21.4	37.219	-97.588	4.5	1.6WTES

2016	2 6	151	8.9	37.269	-97.411	3.2	0.9WTES
2016	2 6	315	29.2	37.269	-97.409	3.6	0.9WTES
2016	2 6	1351	12.6	37.276	-97.416	4.5	1.2WTES
2016	2 6	1948	40.9	37.285	-97.407	4.5	1.1WTES
2016	2 7	346	10	37.311	-97.414	6.4	1.0WTES
2016	2 7	355	0.9	37.276	-97.418	3.8	1.1WTES
2016	2 7	521	59.4	37.266	-97.418	3.5	0.9WTES
2016	2 7	731	34.4	37.274	-97.416	4.3	1.0WTES
2016	2 7	912	17.8	37.276	-97.432	4.8	1.1WTES
2016	2 7	915	21	37.277	-97.425	4.4	1.1WTES
2016	2 8	1048	50.4	37.269	-97.479	4.8	1.5WTES
2016	2 9	1007	32.3	37.273	-97.412	3.2	1.1WTES
2016	2 9	1012	19.8	37.268	-97.409	2	0.7WTES
2016	2 9	1026	31.3	37.263	-97.405	1.5	1.0WTES
2016	2 9	1138	12.3	37.278	-97.418	4.4	0.9WTES
2016	2 9	1420	10.1	37.221	-97.584	4.5	1.7WTES
2016	2 9	2333	32.6	37.219	-97.583	4.9	2.6WTES
2016	2 9	2350	42.9	37.223	-97.585	4.8	2.4WTES
2016	210	217	15.3	37.221	-97.583	4.9	2.1WTES
2016	210	338	24.1	37.221	-97.584	4.5	1.5WTES
2016	210	730	43.7	37.222	-97.586	4.7	1.5WTES
2016	210	823	44	37.22	-97.583	4.9	1.6WTES
2016	210	837	35.4	37.221	-97.585	4.2	1.5WTES
2016	210	937	39.8	37.222	-97.583	4.6	1.6WTES
2016	210	1027	40.2	37.01	-97.614	11.2	2.0WTES
2016	210	1218	13	37.221	-97.586	4.9	1.6WTES
2016	210	1314	8.6	37.221	-97.584	4.9	1.9WTES
2016	210	1917	18.9	37.22	-97.585	5	1.7WTES
2016	210	1919	23.3	37.218	-97.583	5	1.9WTES
2016	211	445	57.2	37.221	-97.582	4.8	1.6WTES
2016	212	335	47.8	37.35	-97.52	7.2	1.4WTES
2016	212	422	36.4	37.346	-97.517	7	1.1WTES
2016	212	956	30.1	37.221	-97.585	4.7	1.5WTES
2016	212	1512	11.2	37.221	-97.584	4.5	1.7WTES
2016	213	40	59.4	37.347	-97.581	5	1.4WTES
2016	213	1346	21.6	37.221	-97.585	5	2.4WTES
2016	213	1349	33.9	37.22	-97.585	4.7	1.9WTES

2016	213	1540	13.5	37.274	-97.565	3.7	1.2WTES
2016	213	1707	7.8	36.137	-98.274	38.4	5.1WTES
2016	213	1840	27.5	37.221	-97.585	4.4	1.7WTES
2016	214	1851	35.8	37.219	-97.586	4.4	1.5WTES
2016	215	444	39.3	37.351	-97.582	4.1	1.3WTES
2016	215	627	51.8	37.351	-97.581	4	1.6WTES
2016	215	1606	9.7	37.097	-97.686	7.6	1.7WTES
2016	216	338	41.6	37.349	-97.582	4.6	1.4WTES
2016	216	1539	28.6	37.388	-97.742	5.4	1.9WTES
2016	216	1641	59.6	37.225	-97.583	4.3	1.7WTES
2016	216	1715	15.1	37.223	-97.584	4.3	1.9WTES
2016	216	1815	12.7	37.221	-97.585	4.8	2.6WTES
2016	217	447	9.6	37.287	-97.5	2.3	1.3WTES
2016	217	1414	52.6	37.063	-97.182	12.2	1.8WTES
2016	218	254	29	37.279	-97.502	2.8	0.9WTES
2016	218	332	56.7	37.283	-97.488	4.7	1.2WTES
2016	218	333	4.2	37.282	-97.487	4.8	1.3WTES
2016	218	333	11.3	37.262	-97.44	4.9	0.6WTES
2016	218	440	12.4	37.224	-97.581	4.2	1.6WTES
2016	218	808	59.1	37.115	-97.588	8.5	1.8WTES
2016	218	817	38.2	37.288	-97.497	5.3	1.0WTES
2016	218	853	29.9	37.282	-97.489	4.7	1.5WTES
2016	218	1119	2.1	37.288	-97.496	4.5	1.4WTES
2016	218	1136	13.3	37.256	-97.458	0.9	1.0WTES
2016	218	1450	56.3	37.282	-97.487	4.7	1.6WTES
2016	218	1711	24.8	37.436	-97.392	5.8	1.9WTES
2016	218	2327	3.2	37.33	-97.423	2.3	1.0WTES
2016	219	604	4.8	37.289	-97.499	5.3	1.6WTES
2016	219	821	3.9	37.289	-97.498	5.6	1.2WTES
2016	219	936	23.8	37.22	-97.582	4.8	1.7WTES
2016	219	1050	38.9	37.293	-97.503	4.7	1.0WTES
2016	219	1317	50.7	37.29	-97.498	5.3	1.8WTES
2016	219	1405	38.9	37.282	-97.492	5.3	1.1WTES
2016	219	1626	1.1	37.292	-97.502	5.1	1.3WTES
2016	219	1730	25.3	37.291	-97.5	5.3	1.5WTES
2016	219	1806	28.4	37.295	-97.505	4.8	1.2WTES
2016	219	2116	24.9	37.285	-97.497	5.1	1.2WTES

2016	220	722	7.9	37.282	-97.479	4.9	1.0WTES
2016	220	1721	59.5	37.631	-97.075	11.6	1.9WTES
2016	220	1937	13.8	37.327	-97.418	2.6	0.7WTES
2016	220	2018	31.5	37.221	-97.586	4.7	1.6WTES
2016	220	2021	18.9	37.221	-97.585	4.9	1.6WTES
2016	220	2212	19	37.303	-97.506	3.4	0.7WTES
2016	221	10	49.9	37.299	-97.502	3.6	1.0WTES
2016	221	127	22.6	37.359	-97.389	4	1.0WTES
2016	221	334	40.9	37.321	-97.497	4.4	1.6WTES
2016	221	339	7.5	37.322	-97.499	4.3	1.2WTES
2016	221	357	55.1	37.32	-97.499	4.1	1.3WTES
2016	221	453	38.6	37.319	-97.497	4.5	1.2WTES
2016	221	913	45.2	37.362	-97.401	4.6	0.8WTES
2016	221	1118	39.8	37.368	-97.394	4	0.8WTES
2016	221	1424	40.8	37.318	-97.495	5.1	1.2WTES
2016	221	1724	53	37.304	-97.563	6.2	1.4WTES
2016	221	1727	13.3	37.305	-97.563	6.2	1.3WTES
2016	221	2215	9.7	37.285	-97.49	4.7	1.4WTES
2016	221	2215	17.5	37.276	-97.48	4.8	1.0WTES
2016	221	2215	26.5	37.277	-97.494	3.2	0.9WTES
2016	221	2314	34.6	37.366	-97.397	4.7	1.2WTES
2016	221	2347	9.5	37.368	-97.398	4.7	1.3WTES
2016	221	2352	14.8	37.13	-97.655	4.4	2.7WTES
2016	222	15	59.4	37.367	-97.396	4.5	1.5WTES
2016	222	25	58.5	37.366	-97.394	4.5	2.0WTES
2016	222	241	12.7	37.289	-97.502	3	1.6WTES
2016	222	242	21	37.284	-97.483	5.1	1.0WTES
2016	222	242	28.2	37.289	-97.506	2.9	1.2WTES
2016	222	243	7	37.302	-97.504	3.8	0.9WTES
2016	222	250	20.6	37.291	-97.491	4.5	1.0WTES
2016	222	407	50.8	37.361	-97.383	4.3	0.8WTES
2016	222	531	40.7	37.361	-97.381	4	1.2WTES
2016	222	1406	27.8	37.291	-97.491	4.5	1.3WTES
2016	222	1446	9	37.257	-97.643	3.9	2.2WTES
2016	222	1939	52.2	37.307	-97.564	6.5	1.4WTES
2016	224	205	11.9	37.244	-97.558	4.3	1.4WTES
2016	224	1001	29.7	37.286	-97.432	4.7	1.0WTES

2016	224	1008	30.9	37.271	-97.415	3.5	1.0WTES
2016	224	1147	34.1	37.433	-97.39	6.4	1.3WTES
2016	224	2006	21.5	37.435	-97.391	5.6	1.4WTES
2016	224	2025	40.2	37.272	-97.415	3.6	1.1WTES
2016	224	2227	45.7	37.283	-97.426	4.8	1.1WTES
2016	224	2235	9.3	37.33	-97.416	2.3	0.9WTES
2016	225	10	18.1	37.33	-97.414	2.5	1.4WTES
2016	225	52	0.3	37.435	-97.39	6.2	1.5WTES
2016	225	1425	43.7	37.329	-97.417	2.4	1.3WTES
2016	225	1536	31	37.332	-97.417	2.2	1.0WTES
2016	226	230	19.2	37.281	-97.423	4.7	0.9WTES
2016	227	530	34	37.244	-97.557	4.3	2.0WTES
2016	227	535	50.7	37.275	-97.42	3.8	1.1WTES
2016	227	1117	26.4	37.438	-97.395	5.7	1.7WTES
2016	227	1150	25.9	37.434	-97.388	6.5	1.7WTES
2016	227	1425	37.2	37.244	-97.603	5	1.4WTES
2016	227	1638	54.6	37.246	-97.602	4.8	1.6WTES
2016	228	1210	48.5	37.317	-97.472	4.5	0.8WTES
2016	228	1217	2.8	37.317	-97.473	4.3	1.0WTES
2016	228	1246	8.8	37.058	-97.724	8.8	2.0WTES
2016	228	1623	5.6	37.319	-97.478	4.2	1.3WTES
2016	228	1630	24.8	37.333	-97.49	1.7	1.1WTES
2016	229	835	46	37.267	-97.573	12.1	1.8WTES
2016	229	2323	8.7	37.218	-97.586	4.6	2.5WTES
2016	3 1	0	38.1	37.221	-97.586	4.6	1.8WTES
2016	3 1	253	30.3	37.274	-97.631	3.5	2.2WTES
2016	3 1	345	59.7	37.217	-97.589	4.5	1.5WTES
2016	3 1	347	36.9	37.276	-97.63	3.5	1.8WTES
2016	3 1	549	47.5	37.131	-97.658	5.7	1.6WTES
2016	3 1	948	25.2	37.292	-97.602	5	1.7WTES
2016	3 1	1142	44.8	37.29	-97.602	5.3	1.6WTES
2016	3 1	1215	20.1	37.217	-97.587	4.7	2.3WTES
2016	3 1	1411	50.6	37.256	-97.573	5.1	1.6WTES
2016	3 1	1804	29.7	37.218	-97.589	4.5	2.2WTES
2016	3 1	2017	20.5	37.22	-97.589	4.3	1.8WTES
2016	3 2	426	30.3	37.291	-97.602	4.8	1.6WTES
2016	3 2	625	3.4	37.288	-97.601	6	2.0WTES

2016	3 2	657	36.4	37.296	-97.596	4.1	2.0WTES
2016	3 2	704	14.9	37.294	-97.599	4.7	1.6WTES
2016	3 2	714	57.1	37.292	-97.598	3.6	1.5WTES
2016	3 2	721	17.5	37.293	-97.598	4.9	1.7WTES
2016	3 2	806	0.2	37.222	-97.586	4.6	2.0WTES
2016	3 2	848	40.6	37.293	-97.596	4.7	1.7WTES
2016	3 2	850	5	37.292	-97.6	5.3	1.7WTES
2016	3 2	903	22.1	37.29	-97.599	5.1	1.9WTES
2016	3 2	928	41.2	37.292	-97.6	4.7	1.7WTES
2016	3 2	1237	31.7	37.292	-97.599	4.8	2.0WTES
2016	3 2	1255	39.4	37.291	-97.601	5.4	1.9WTES
2016	3 2	1316	56.2	37.292	-97.599	4.9	1.6WTES
2016	3 2	1609	38.1	37.219	-97.589	4.2	1.7WTES
2016	3 2	1929	38.8	37.294	-97.599	4.5	1.6WTES
2016	3 3	139	21.9	37.292	-97.603	4.9	1.7WTES
2016	3 3	716	19.7	37.155	-97.421	4.9	1.4WTES
2016	3 3	1558	1.3	37.068	-97.156	4.1	2.2WTES
2016	3 3	2224	32.6	37.29	-97.602	5.5	1.7WTES
2016	3 3	2228	14.7	37.292	-97.599	4.4	1.8WTES
2016	3 3	2233	15.8	37.292	-97.598	4.9	1.8WTES
2016	3 3	2317	45.6	37.291	-97.601	4.2	1.6WTES
2016	3 3	2328	52.1	37.292	-97.596	5	1.5WTES
2016	3 4	41	35.2	37.291	-97.603	5.2	2.0WTES
2016	3 4	128	52	37.291	-97.6	4.2	2.0WTES
2016	3 5	7	3.2	37.217	-97.585	4.7	1.5WTES
2016	3 5	104	59.6	37.218	-97.588	4.7	1.4WTES
2016	3 5	105	29.3	37.221	-97.588	4.5	1.6WTES
2016	3 5	328	58.9	37.294	-97.598	4.8	1.7WTES
2016	3 5	1334	18.4	37.293	-97.597	1.1	1.8WTES
2016	3 5	1712	34.7	37.289	-97.598	4.7	2.3WTES
2016	3 5	1719	25.6	37.218	-97.727	2.1	2.5WTES
2016	3 5	1810	20.2	37.291	-97.603	4.6	1.7WTES
2016	3 5	1817	20.6	37.284	-97.611	15	1.8WTES
2016	3 5	1820	42.7	37.292	-97.6	4.2	1.6WTES
2016	3 5	1846	42.9	37.294	-97.6	3.2	1.6WTES
2016	3 5	1901	51.7	37.292	-97.595	0.1	1.4WTES
2016	3 5	1902	27.4	37.291	-97.601	5.4	1.5WTES

2016	3 5	1923	51.2	37.293	-97.599	4.6	2.1WTES
2016	3 5	1938	7.2	37.293	-97.601	3.3	1.5WTES
2016	3 5	2017	23.7	37.276	-97.42	4.2	1.4WTES
2016	3 5	2231	57.2	37.292	-97.604	4.7	1.5WTES
2016	3 5	2357	15.3	37.292	-97.602	4.5	1.5WTES
2016	3 6	829	22.9	37.29	-97.611	6.4	1.7WTES
2016	3 6	1023	28.9	37.291	-97.602	3	1.6WTES
2016	3 6	1023	52.5	37.292	-97.604	4.3	1.7WTES
2016	3 6	1059	6.1	37.294	-97.599	5	2.1WTES
2016	3 6	1116	59.3	37.29	-97.607	5.3	1.6WTES
2016	3 6	1130	55.6	37.29	-97.606	5	1.7WTES
2016	3 6	1313	20	37.251	-97.607	4.6	1.6WTES
2016	3 6	1421	55.7	37.291	-97.602	4.2	2.1WTES
2016	3 6	1513	33.5	37.291	-97.603	4.4	1.8WTES
2016	3 6	2022	59.7	37.292	-97.597	4.3	2.1WTES
2016	3 7	236	13.9	37.291	-97.597	4.9	2.2WTES
2016	3 7	335	36.4	37.293	-97.598	4.3	2.2WTES
2016	3 7	350	48.1	37.295	-97.6	3.9	1.7WTES
2016	3 7	352	31.7	37.291	-97.599	3.7	1.8WTES
2016	3 7	631	8.6	37.292	-97.603	4.9	1.9WTES
2016	3 7	1052	21.2	37.279	-97.421	4.3	1.2WTES
2016	3 7	1115	48.7	37.291	-97.597	5.2	1.9WTES
2016	3 8	211	22.3	37.322	-97.497	4.4	1.5WTES
2016	3 8	224	35.3	37.324	-97.497	4.3	1.2WTES
2016	3 8	1027	38.6	37.296	-97.601	1	1.8WTES
2016	3 8	1028	59.8	37.229	-97.546	7.7	1.4WTES
2016	3 9	1032	47.1	37.278	-97.49	4.3	2.5WTES
2016	3 9	1157	37.1	37.323	-97.497	3.9	1.0WTES
2016	3 9	1508	46.7	37.074	-97.155	8.3	1.7WTES
2016	3 9	2342	58	37.266	-97.617	15	2.0WTES
2016	3 9	2349	33.2	37.293	-97.604	3.8	1.5WTES
2016	310	434	4.6	37.284	-97.501	2.3	1.0WTES
2016	310	1325	49.6	37.21	-97.446	4.3	1.4WTES
2016	310	1350	17.4	37.285	-97.496	3	1.0WTES
2016	311	834	32.9	37.28	-97.615	15	1.9WTES
2016	311	852	18.2	37.305	-97.61	3.9	1.6WTES
2016	311	2106	10.4	37.284	-97.625	15	1.9WTES

2016	311	2106	19.1	37.303	-97.612	4	1.7WTES
2016	311	2118	22.3	37.304	-97.611	3.5	1.7WTES
2016	312	319	17.9	37.306	-97.611	3.4	1.4WTES
2016	313	37	36.2	37.331	-97.411	1.7	1.1WTES
2016	313	538	49.2	37.331	-97.427	3.4	0.8WTES
2016	315	537	54.5	37.238	-97.561	4.1	1.4WTES
2016	315	941	6.7	37.333	-97.42	1.3	0.7WTES
2016	316	11	3.2	37.307	-97.612	4	1.4WTES
2016	316	16	48.7	37.305	-97.61	3.6	1.7WTES
2016	316	1420	29.4	37.126	-97.286	7.8	1.9WTES
2016	316	1823	42.7	37.229	-97.622	3.1	1.6WTES
2016	317	615	3.5	37.295	-97.593	4.8	1.4WTES
2016	319	549	46.1	37.244	-97.565	3.2	1.8WTES
2016	319	2252	44.7	37.32	-97.498	4.2	2.3WTES
2016	322	1743	3.4	37.246	-97.593	4.6	1.9WTES
2016	324	356	6.5	37.324	-97.499	3.5	1.3WTES
2016	324	1702	45.7	37.324	-97.5	3.8	1.9WTES
2016	324	1902	31.3	37.321	-97.496	4.6	1.5WTES
2016	325	319	33.6	37.321	-97.497	4.3	1.4WTES
2016	325	333	12.1	37.322	-97.498	4	1.2WTES
2016	325	2345	51.6	37.327	-97.523	5.2	1.4WTES
2016	326	245	2.3	37.323	-97.499	4.1	1.4WTES
2016	327	601	47.5	36.641	-97.831	26.7	3.3WTES
2016	327	1312	7.2	37.335	-97.416	2.9	1.1WTES
2016	327	1312	7.3	37.335	-97.416	2.8	1.2WTES
2016	328	129	54.9	37.336	-97.423	3	0.9WTES
2016	328	545	14.6	37.365	-97.396	4.7	1.1WTES
2016	328	721	7.7	37.327	-97.502	3	1.1WTES
2016	328	834	49.7	37.276	-97.632	4.4	1.6WTES
2016	329	453	2.3	36.041	-97.66	0.4	4.3WTES
2016	330	623	27.2	37.243	-97.557	3.9	2.3WTES
2016	330	805	2.9	37.24	-97.557	4	1.1WTES
2016	330	1141	18.7	37.242	-97.555	4.2	2.0WTES
2016	330	1143	3.8	37.242	-97.554	4	2.2WTES
2016	330	1532	10.8	37.275	-97.494	4.1	1.3WTES
2016	331	239	17.4	37.24	-97.559	4.2	1.5WTES
2016	331	250	11	37.327	-97.436	3.1	0.9WTES

2016	331	521	29.4	37.241	-97.556	4	1.3WTES
2016	331	1026	19.3	37.556	-97.235	7.5	2.1WTES
2016	4 1	1431	29.8	37.294	-97.455	4	0.9WTES
2016	4 1	1432	56.8	37.29	-97.446	3.1	0.8WTES
2016	4 1	1433	0	37.297	-97.469	3.7	0.9WTES
2016	4 1	1433	15.2	37.306	-97.491	8	1.0WTES
2016	4 1	1433	39.9	37.275	-97.434	0.1	0.9WTES
2016	4 1	1434	6.4	37.314	-97.471	3.8	1.1WTES
2016	4 1	1434	13.6	37.302	-97.476	3.5	0.7WTES
2016	4 1	1439	33.8	37.313	-97.458	5.4	1.8WTES
2016	4 1	1443	0.3	37.314	-97.468	3.8	1.4WTES
2016	4 1	1505	24.7	37.322	-97.497	3.9	1.1WTES
2016	4 1	1529	59.2	37.31	-97.465	3.9	1.1WTES
2016	4 1	1634	57.9	37.321	-97.499	4.2	2.1WTES
2016	4 2	207	7.9	37.322	-97.502	3.9	1.4WTES
2016	4 2	914	15.8	37.326	-97.481	3.3	1.2WTES
2016	4 2	1002	12.2	37.324	-97.483	3.1	1.2WTES
2016	4 2	1033	7.8	37.239	-97.551	4.2	1.4WTES
2016	4 2	1210	53.8	37.322	-97.473	4.4	1.5WTES
2016	4 2	1748	17.5	37.42	-97.42	4.5	1.7WTES
2016	4 3	334	40.6	37.317	-97.496	5.2	1.2WTES
2016	4 3	654	11.3	37.405	-97.411	9.3	1.1WTES
2016	4 3	1046	55.9	37.314	-97.476	4.1	1.0WTES
2016	4 3	1139	11.8	37.33	-97.489	1.8	1.1WTES
2016	4 4	124	55.1	37.422	-97.419	5.4	1.2WTES
2016	4 8	55	20	37.294	-97.591	4.8	2.2WTES
2016	4 8	141	20.2	37.297	-97.592	4.1	1.2WTES
2016	4 9	413	3.3	37.146	-97.666	5.7	2.1WTES
2016	4 9	439	17	37.137	-97.67	6.5	1.7WTES
2016	4 9	753	5	37.144	-97.668	6.4	2.2WTES
2016	4 9	1927	21.3	36.867	-97.36	1.9	2.3WTES
2016	4 9	2155	44.7	36.907	-97.661	2.4	3.7WTES
2016	410	243	58.9	37.135	-97.665	5.4	2.3WTES
2016	410	453	43.7	37.14	-97.669	3.6	2.2WTES
2016	410	2014	39.5	37.137	-97.668	7.2	1.6WTES
2016	411	216	37.6	37.302	-97.616	4.1	1.5WTES
2016	411	708	6.3	37.136	-97.672	4.6	1.9WTES

2016	412	251	3.2	37.416	-97.418	6.3	1.4WTES
2016	412	728	4.2	37.351	-97.77	1.5	1.7WTES
2016	414	2044	9.3	37.124	-97.681	6.6	2.1WTES
2016	414	2223	43.6	37.118	-97.684	6	2.1WTES
2016	415	248	49.4	37.12	-97.68	5.8	1.7WTES
2016	415	1949	47.3	37.272	-97.515	3.3	1.3WTES
2016	417	852	14	36.934	-97.49	7.8	1.7WTES
2016	419	825	29.2	37.312	-97.473	3.5	1.1WTES
2016	419	1726	26.4	37.052	-97.455	7.4	1.9WTES
2016	420	2219	41.5	37.26	-97.445	4.1	1.1WTES
2016	421	1112	19	37.368	-97.373	3.2	1.1WTES
2016	422	634	9.3	37.22	-97.584	4.9	1.8WTES
2016	422	638	8.2	37.221	-97.584	4.8	1.9WTES
2016	422	643	35.6	37.22	-97.584	4.6	2.1WTES
2016	422	648	50.1	37.221	-97.583	4.6	1.4WTES
2016	422	805	3.5	37.22	-97.584	4.8	2.1WTES
2016	422	806	26.1	37.219	-97.583	4.8	2.0WTES
2016	422	1539	21.7	37.22	-97.585	4.4	1.8WTES
2016	423	35	46.4	37.188	-97.55	3.8	1.4WTES
2016	423	716	41.5	37.315	-97.599	3.7	1.6WTES
2016	424	147	22.4	37.302	-97.611	5.4	1.8WTES
2016	424	939	38.8	37.295	-97.637	15	1.5WTES
2016	424	2137	3.6	37.278	-97.619	15	1.9WTES
2016	425	1332	21.3	37.322	-97.5	3.9	1.3WTES
2016	425	1534	8.3	37.304	-97.61	4.9	1.9WTES
2016	426	30	43.4	37.221	-97.583	4.5	1.5WTES
2016	427	1917	38.7	37.251	-97.579	4.4	1.5WTES
2016	427	1956	23.7	37.236	-97.56	4.5	1.6WTES
2016	428	24	2.6	37.267	-97.524	0.7	1.2WTES
2016	430	116	22	37.318	-97.604	3.5	1.6WTES
2016	5 1	537	39.9	37.221	-97.876	7.8	3.4WTES
2016	5 1	1912	24.8	37.359	-97.369	4.2	1.9WTES
2016	5 1	1923	0.3	37.369	-97.382	4.4	1.3WTES
2016	5 2	531	27.6	37.366	-97.374	4.2	0.9WTES
2016	5 2	701	56.1	37.277	-97.488	4.3	1.3WTES
2016	5 2	855	33.4	37.277	-97.49	4	1.2WTES
2016	5 3	102	26.4	37.248	-97.552	4.2	1.4WTES

2016	5 3	224	14.6	37.278	-97.49	4	1.3WTES
2016	5 3	418	25.7	37.277	-97.49	3.9	1.1WTES
2016	5 3	955	23.4	37.231	-97.573	15	1.7WTES
2016	5 3	1945	42.2	37.214	-97.618	5.1	2.4WTES
2016	5 3	2020	55.7	37.214	-97.619	5.2	2.7WTES
2016	5 3	2045	11.4	37.214	-97.618	4.7	1.8WTES
2016	5 3	2131	16.3	37.218	-97.62	4.7	1.6WTES
2016	5 3	2221	42.9	37.431	-97.431	4.3	1.5WTES
2016	5 6	1530	16	37.367	-97.391	3.9	1.2WTES
2016	5 6	1642	14.6	37.367	-97.39	3.9	1.1WTES
2016	5 6	1656	19.1	37.281	-97.494	3	1.2WTES
2016	5 8	936	45.9	37.313	-97.506	5.5	1.3WTES
2016	5 8	1119	5.6	37.315	-97.603	3.7	1.6WTES
2016	510	1727	17.8	36.313	-96.921	0.6	2.9WTES
2016	514	638	34.3	37.502	-97.759	30.1	2.7WTES
2016	514	1904	36.9	37.071	-97.717	6.4	2.7WTES
2016	516	633	38.1	36.281	-97.262	0.2	2.3WTES
2016	516	1446	44.7	37.068	-97.728	7.9	1.8WTES
2016	516	1604	25.4	37.36	-97.5	5.6	1.0WTES
2016	516	2027	29.3	37.317	-97.49	5.1	1.0WTES
2016	518	722	29.8	37.234	-97.519	2.6	1.2WTES
2016	520	611	26.8	37.267	-97.671	1.5	1.8WTES
2016	520	1616	10.7	37.26	-97.581	15	1.4WTES
2016	520	1619	56.5	37.243	-97.558	4.1	1.2WTES
2016	520	1621	56.6	37.28	-97.579	5	1.6WTES
2016	520	1655	37.6	37.279	-97.58	4.5	1.2WTES
2016	521	112	46.5	37.276	-97.581	5.4	1.5WTES
2016	521	117	42.4	37.278	-97.582	5	1.3WTES
2016	521	122	42.6	37.279	-97.581	4.5	1.5WTES
2016	521	240	16.1	37.278	-97.582	5	1.8WTES
2016	521	256	2.4	37.276	-97.582	5.7	1.5WTES
2016	521	305	28.3	37.276	-97.581	5.1	1.3WTES
2016	521	452	46.5	37.275	-97.581	5.6	1.5WTES
2016	521	504	30.5	37.193	-97.649	5.7	1.6WTES
2016	521	548	33.6	37.277	-97.581	5.3	1.4WTES
2016	521	601	29.9	37.28	-97.582	4.4	1.5WTES
2016	521	706	21.6	37.281	-97.58	3.3	1.4WTES

2016	521	731	16.3	37.276	-97.581	5.3	1.7WTES
2016	521	744	16.4	37.287	-97.577	1.1	1.2WTES
2016	521	801	42.1	37.276	-97.58	5.3	1.8WTES
2016	521	1624	56.8	37.276	-97.582	5.5	1.5WTES
2016	522	237	43.1	37.28	-97.581	4.8	1.3WTES
2016	522	1016	47.3	37.278	-97.582	5.1	1.4WTES
2016	522	1656	44.9	37.275	-97.582	4.9	1.5WTES
2016	523	2	15.5	37.349	-97.485	2.5	1.2WTES
2016	523	631	49.2	37.141	-97.579	3.5	1.6WTES
2016	523	1936	25.5	37.278	-97.582	5	1.5WTES
2016	524	425	54.9	37.282	-97.492	3.6	1.1WTES
2016	524	640	40.7	37.281	-97.578	2.4	1.4WTES
2016	524	2146	43.5	37.303	-97.826	5.7	2.3WTES
2016	524	2245	34.1	37.308	-97.603	6.1	1.5WTES
2016	525	227	0.6	37.273	-97.578	6.3	1.5WTES
2016	525	908	50.6	37.348	-97.485	2.2	1.3WTES
2016	526	2302	25.1	37.208	-97.512	3.8	2.2WTES
2016	526	2348	5.3	37.277	-97.486	4.3	1.3WTES
2016	527	222	5	37.278	-97.575	5	1.5WTES
2016	527	808	25.5	37.344	-97.49	2.4	1.1WTES
2016	527	929	22.9	37.279	-97.572	4.9	2.1WTES
2016	527	1236	28.4	37.278	-97.574	4.9	1.5WTES
2016	528	1141	53.8	37.28	-97.573	4	1.6WTES
2016	528	1224	9.3	37.278	-97.572	4.6	1.5WTES
2016	528	1245	60	37.28	-97.572	4.1	2.0WTES
2016	528	1412	44.3	37.278	-97.572	4.4	1.7WTES
2016	528	1436	37.4	37.277	-97.572	5	1.7WTES
2016	529	621	37.4	37.335	-97.47	4.9	1.1WTES
2016	529	821	8.3	37.376	-97.733	6.8	2.5WTES
2016	529	1534	6	37.277	-97.486	4.2	1.5WTES
2016	529	1936	5.2	37.278	-97.487	4.2	1.2WTES
2016	530	110	24.4	37.346	-97.777	2.7	1.7WTES
2016	530	1535	58.7	37.239	-97.587	5.2	1.5WTES
2016	530	1612	40.6	37.239	-97.588	5.2	1.5WTES
2016	531	530	3.7	37.314	-97.485	4.1	0.9WTES
2016	531	1844	9.2	37.277	-97.488	4.3	1.1WTES
2016	6 1	1756	1	37.164	-97.46	10.5	1.9WTES

2016	6 3	522	41	37.238	-97.588	5.4	1.5WTES
2016	6 3	750	25.1	37.238	-97.588	5.4	1.4WTES
2016	6 4	1700	47.9	37.316	-97.487	3.9	1.2WTES
2016	6 4	1825	36.1	37.316	-97.56	1.1	1.4WTES
2016	6 4	2204	6	37.278	-97.484	4.2	1.2WTES
2016	6 5	2036	22.5	37.299	-97.509	3.6	1.1WTES
2016	6 5	2058	27	37.279	-97.485	4.3	1.0WTES
2016	6 6	833	28.7	37.277	-97.483	4.2	1.1WTES
2016	6 6	1101	35.2	37.28	-97.488	4.2	1.0WTES
2016	6 6	1745	46.5	37.299	-97.621	4.1	1.5WTES
2016	6 7	352	26.3	37.282	-97.485	4	0.5WTES
2016	6 7	958	4.9	37.313	-97.504	5.7	0.9WTES
2016	6 7	1527	27	37.293	-97.47	15	1.4WTES
2016	6 7	1922	38.7	37.301	-97.447	27.2	1.5WTES
2016	6 8	1627	25	37.281	-97.484	4	1.4WTES
2016	6 8	1855	21.9	37.308	-97.504	5.6	1.2WTES
2016	6 9	105	21.1	37.282	-97.484	4	1.1WTES
2016	6 9	2256	2.3	37.282	-97.619	1.2	1.7WTES
2016	610	141	40.2	37.285	-97.491	4.6	1.4WTES
2016	610	1142	46.1	37.281	-97.485	4.4	1.4WTES
2016	611	524	20.4	37.211	-97.73	8.3	2.1WTES
2016	611	727	2.7	37.213	-97.729	8.2	3.2WTES
2016	611	1108	49	37.28	-97.485	4	1.3WTES
2016	611	1114	12.7	37.214	-97.729	8.3	1.9WTES
2016	611	1416	32.6	37.279	-97.485	4.3	1.5WTES
2016	611	1842	23.5	37.342	-97.429	2.6	1.6WTES
2016	611	1913	11.5	37.206	-97.541	4.6	1.5WTES
2016	611	2225	23.3	37.34	-97.428	2.6	1.1WTES
2016	612	13	51.3	37.206	-97.559	15	2.0WTES
2016	612	22	57.2	37.208	-97.54	4.6	1.5WTES
2016	612	154	52.7	37.133	-97.531	5.4	1.7WTES
2016	612	1135	43.1	37.211	-97.728	8.3	2.2WTES
2016	612	1801	45.9	37.341	-97.427	2.9	1.8WTES
2016	613	126	21.2	37.209	-97.541	4.5	1.6WTES
2016	613	1632	5.5	37.286	-97.495	3.9	1.0WTES
2016	614	1736	23	37.278	-97.485	4.1	1.3WTES
2016	615	1256	43.9	37.403	-97.357	5.8	1.5WTES

2016	616	1012	14.7	37.256	-97.442	5.2	1.0WTES
2016	617	1715	23.6	37.318	-97.499	4.1	1.6WTES
2016	617	2030	0.1	37.315	-97.507	4.9	1.8WTES
2016	618	438	2.1	37.279	-97.487	4	1.1WTES
2016	618	932	2.9	37.209	-97.539	4.7	1.8WTES
2016	618	935	34	37.211	-97.54	4.4	1.8WTES
2016	618	944	27.2	37.21	-97.54	4.7	1.5WTES
2016	618	1247	54.3	37.21	-97.541	4	1.6WTES
2016	620	448	4.5	37.397	-97.416	9.2	1.5WTES
2016	620	558	18.3	37.368	-97.315	5.2	1.4WTES
2016	620	635	11.8	37.262	-97.443	5.2	2.1WTES
2016	620	1341	16.3	37.279	-97.486	4.5	1.8WTES
2016	622	828	33.8	37.258	-97.387	0.2	1.4WTES
2016	623	823	57.1	37.278	-97.483	5.9	1.0WTES
2016	623	2143	59.4	37.325	-97.482	3.1	1.0WTES
2016	624	734	12	37.275	-97.484	4.4	1.6WTES
2016	624	757	59.3	37.277	-97.485	4.1	2.3WTES
2016	624	956	54.1	37.273	-97.472	6.9	1.4WTES
2016	624	1234	15.5	37.284	-97.491	4.4	1.1WTES
2016	624	1615	45.5	37.284	-97.488	3.4	1.2WTES
2016	624	1658	19.8	37.275	-97.484	4.5	1.7WTES
2016	624	1722	49.7	37.279	-97.488	4.1	1.5WTES
2016	624	2139	20.3	37.302	-97.511	3	1.2WTES
2016	625	53	46.8	37.278	-97.573	5.3	1.9WTES
2016	625	1803	22.8	37.023	-97.557	7.5	3.1WTES
2016	626	1255	42.2	37.284	-97.43	3.9	0.8WTES
2016	626	1719	52.2	37.275	-97.484	4.4	2.1WTES
2016	627	21	38.2	37.28	-97.424	3.3	0.9WTES
2016	628	18	10.4	37.266	-97.304	2.9	1.7WTES
2016	630	128	14.6	37.315	-97.472	4.2	0.7WTES
2016	630	736	57.1	37.318	-97.477	4.6	1.0WTES
2016	630	743	46.2	37.327	-97.489	2.8	1.0WTES
2016	630	748	24.3	37.322	-97.482	3.6	1.7WTES
2016	630	756	7.7	37.328	-97.492	0.6	0.9WTES
2016	630	855	27.5	37.317	-97.476	4.2	1.0WTES
2016	630	950	4.1	37.32	-97.477	4.2	1.2WTES
2016	630	1027	10	37.319	-97.475	4.2	1.0WTES

2016	630	1037	54.1	37.324	-97.483	3.4	1.4WTES
2016	630	1041	11	37.325	-97.484	3.1	0.9WTES
2016	630	1113	19	37.325	-97.485	2.8	1.3WTES
2016	630	1857	58.4	37.29	-97.498	4	1.1WTES
2016	7 1	2357	11.8	37.286	-97.433	4.1	0.8WTES
2016	7 2	1505	20.3	37.275	-97.486	4.4	1.7WTES
2016	7 3	1755	29.3	37.277	-97.492	1.3	1.0WTES
2016	7 4	1556	48	37.381	-97.389	8	1.7WTES
2016	7 4	1708	59.9	37.404	-97.444	3.9	1.0WTES
2016	7 4	1713	51.3	37.399	-97.433	4.9	1.7WTES
2016	7 5	1751	4.8	37.409	-97.394	5.5	1.3WTES
2016	7 5	1751	21.1	37.417	-97.391	3.4	1.1WTES
2016	7 5	2059	39.6	37.416	-97.398	4.6	1.9WTES
2016	7 5	2113	38.2	37.408	-97.393	6.1	1.7WTES
2016	7 5	2212	36	37.412	-97.39	5.3	1.5WTES
2016	7 6	14	35.5	37.415	-97.394	5.1	1.5WTES
2016	7 6	814	59	37.413	-97.396	5.4	1.2WTES
2016	7 6	905	28.1	37.413	-97.392	5.3	1.4WTES
2016	7 6	908	5.6	37.409	-97.394	4.9	1.3WTES
2016	7 6	1013	37.7	37.411	-97.394	5.4	1.8WTES
2016	7 6	1222	46.8	37.412	-97.389	4.8	1.6WTES
2016	7 6	1301	8.4	37.412	-97.392	5.7	1.6WTES
2016	7 6	1635	26.5	37.279	-97.487	4.2	1.6WTES
2016	7 6	1855	39.7	37.273	-97.479	5	1.3WTES
2016	7 6	1924	16.7	37.411	-97.394	5.5	1.8WTES
2016	7 7	826	3.7	37.28	-97.485	4.3	1.2WTES
2016	7 8	811	49.3	37.322	-97.5	3.5	2.3WTES
2016	7 8	1020	42.4	37.325	-97.495	4.8	1.4WTES
2016	7 8	1310	14.2	37.319	-97.495	4.5	1.2WTES
2016	7 8	1629	53.8	37.242	-97.559	4.8	1.3WTES
2016	7 8	1818	50	37.317	-97.474	5	1.4WTES
2016	7 8	1846	55.4	37.322	-97.481	4.4	1.5WTES
2016	7 8	1947	57.5	37.282	-97.493	3.4	1.0WTES
2016	7 8	1950	20.7	37.42	-97.404	2.4	2.0WTES
2016	7 8	2140	3.3	37.32	-97.48	4	2.1WTES
2016	7 8	2145	57	37.317	-97.474	4.8	1.0WTES
2016	7 8	2155	25.8	37.316	-97.484	3.9	1.0WTES

2016	7 8	2155	52	37.324	-97.486	3.3	1.3WTES
2016	7 8	2156	16.6	37.321	-97.481	3.8	0.9WTES
2016	7 8	2201	40.7	37.322	-97.482	3.9	1.4WTES
2016	7 8	2204	55.2	37.321	-97.48	4	0.8WTES
2016	7 8	2205	16.5	37.302	-97.458	5	0.9WTES
2016	7 8	2205	34.9	37.327	-97.489	3.3	1.0WTES
2016	7 8	2214	11.5	37.323	-97.483	3.8	0.9WTES
2016	7 8	2223	45.6	37.321	-97.477	3.8	1.0WTES
2016	7 8	2232	40.4	37.323	-97.485	3.5	1.4WTES
2016	7 8	2310	0.7	37.32	-97.476	4.1	1.0WTES
2016	7 8	2311	37.9	37.328	-97.49	1.9	1.3WTES
2016	7 9	126	0.3	37.322	-97.483	3.8	1.5WTES
2016	7 9	131	40.4	37.325	-97.488	3.2	1.2WTES
2016	7 9	142	55.5	37.285	-97.498	0.1	1.3WTES
2016	7 9	230	59.2	37.276	-97.484	4.6	1.5WTES
2016	7 9	329	13.9	37.292	-97.498	1.1	1.1WTES
2016	7 9	1125	49.2	37.329	-97.496	1.7	1.1WTES
2016	7 9	1623	53.1	37.413	-97.401	5.3	2.4WTES
2016	7 9	1714	59.8	37.409	-97.391	5.9	1.6WTES
2016	7 9	1901	30.6	37.409	-97.396	4.9	1.6WTES
2016	7 9	2022	5.1	37.39	-97.398	7.6	1.3WTES
2016	710	47	38.5	37.321	-97.501	3.9	2.3WTES
2016	710	1254	21.3	37.264	-97.465	4.4	1.3WTES
2016	712	726	47.6	37.445	-97.417	5.5	2.0WTES
2016	713	1017	48.6	37.283	-97.487	2.8	1.0WTES
2016	714	748	22.9	37.32	-97.499	4.2	1.1WTES
2016	715	1216	6.8	37.134	-97.596	4.3	2.0WTES
2016	716	508	30.4	37.29	-97.426	4.2	1.1WTES
2016	716	603	50.9	37.421	-97.396	3.5	1.3WTES
2016	716	915	5.7	37.32	-97.499	4.4	1.6WTES
2016	716	1217	58.5	37.414	-97.393	5.4	2.1WTES
2016	716	1921	59.2	37.343	-97.432	8.1	1.0WTES
2016	718	141	24.5	37.324	-97.498	3.9	1.4WTES
2016	718	651	35.3	37.359	-97.398	4	1.2WTES
2016	718	820	20.4	37.413	-97.396	4.6	1.4WTES
2016	719	117	56.4	37.1	-97.658	3.6	1.8WTES
2016	719	1255	11.8	37.333	-97.396	2.9	0.9WTES

2016	719	2202	59.6	37.335	-97.398	3	0.7WTES
2016	719	2340	25.1	37.342	-97.39	0	0.8WTES
2016	719	2352	52.9	37.331	-97.397	3.2	1.0WTES
2016	720	4	27.3	37.323	-97.399	3.8	0.8WTES
2016	720	58	54	37.337	-97.395	2.8	0.6WTES
2016	720	108	36.5	37.335	-97.396	2.9	1.2WTES
2016	720	124	35.7	37.335	-97.395	2.7	1.4WTES
2016	720	156	38.9	37.297	-97.437	4.8	0.9WTES
2016	720	235	49	37.298	-97.436	4.6	1.0WTES
2016	720	339	18.5	37.293	-97.434	4.3	1.0WTES
2016	720	524	22.9	37.331	-97.402	3.5	1.1WTES
2016	720	853	38.2	37.29	-97.43	4.1	1.0WTES
2016	720	947	34.8	37.326	-97.604	5	1.3WTES
2016	720	1123	12.3	37.325	-97.604	5	1.5WTES
2016	721	542	17	37.189	-97.568	2.4	1.7WTES
2016	721	1250	6.9	37.285	-97.425	3.8	1.1WTES
2016	721	1534	25.7	37.283	-97.42	3.7	1.3WTES
2016	722	1139	58.1	37.264	-97.437	4.6	1.2WTES
2016	723	546	23.2	37.289	-97.426	4.1	1.0WTES
2016	723	600	43.4	37.332	-97.426	2.8	1.4WTES
2016	723	622	19.6	37.29	-97.427	4.1	1.2WTES
2016	723	1137	55.5	37.289	-97.427	4	0.8WTES
2016	723	1254	17	37.295	-97.431	4.4	0.9WTES
2016	723	1308	6.9	37.29	-97.427	4	0.9WTES
2016	724	1245	7.1	37.329	-97.424	2.9	0.8WTES
2016	725	447	22.2	37.272	-97.509	2.4	1.2WTES
2016	726	305	47.1	37.289	-97.429	4.6	1.8WTES
2016	726	1628	38	37.285	-97.4	4	1.0WTES
2016	727	224	53	37.329	-97.428	2.9	1.1WTES
2016	727	1011	32.2	37.33	-97.436	2.7	0.9WTES
2016	727	1313	14.8	37.268	-97.441	4.7	1.1WTES
2016	728	744	29.8	37.262	-97.499	4.3	1.1WTES
2016	728	1926	29.1	37.286	-97.437	4	1.0WTES
2016	729	446	35.5	37.244	-97.659	4.3	2.2WTES
2016	729	2158	7	37.265	-97.438	4.4	1.2WTES
2016	731	301	49	37.281	-97.575	4.7	1.3WTES
2016	8 3	820	20.1	37.416	-97.406	4.3	1.8WTES

2016	8 3	853	49.7	37.414	-97.396	4.6	1.8WTES
2016	8 3	1140	12.4	37.415	-97.41	0.2	1.4WTES
2016	8 3	1140	45.2	37.414	-97.406	0.1	1.4WTES
2016	8 3	1951	7.6	37.283	-97.502	4.1	1.6WTES
2016	8 3	1951	21	37.28	-97.499	1.1	1.2WTES
2016	8 3	2121	37.4	37.246	-97.659	4.1	1.9WTES
2016	8 4	538	16.8	37.275	-97.493	4.2	1.3WTES
2016	8 4	1034	12.2	37.274	-97.493	4.5	1.5WTES
2016	8 4	1226	19.3	37.281	-97.499	7	1.2WTES
2016	8 4	1344	0.6	37.304	-97.608	6.2	1.7WTES
2016	8 5	1420	43.7	37.329	-97.426	2.9	1.1WTES
2016	8 5	1527	36.8	37.272	-97.611	15	1.5WTES
2016	8 5	1713	13.5	37.305	-97.608	6.2	1.4WTES
2016	8 5	1750	3.7	37.304	-97.608	5.7	1.1WTES
2016	8 5	1807	36.3	37.258	-97.649	4.3	1.3WTES
2016	8 6	335	13.9	37.275	-97.579	5.8	0.9WTES
2016	8 6	346	44	37.275	-97.578	5.9	0.7WTES
2016	8 7	246	52.6	37.277	-97.577	5.6	1.5WTES
2016	8 7	1642	15.4	37.237	-97.561	4.5	1.4WTES
2016	8 9	1323	8.7	37.293	-97.515	6	1.5WTES
2016	8 9	1548	5.7	37.279	-97.43	3.5	0.9WTES
2016	8 9	1654	12.8	37.279	-97.626	4.4	1.5WTES
2016	810	1847	8.7	37.28	-97.629	15	1.7WTES
2016	811	614	57.8	37.289	-97.614	6.1	1.5WTES
2016	811	1602	5.3	37.293	-97.612	5.2	2.0WTES
2016	811	1603	48	37.292	-97.611	5.8	2.0WTES
2016	811	1928	12.3	37.296	-97.595	5.1	1.6WTES
2016	811	2005	4	37.29	-97.611	5.7	1.9WTES
2016	811	2350	15.9	37.294	-97.597	5.8	1.4WTES
2016	812	1356	1.7	37.291	-97.611	5.4	2.4WTES
2016	812	1433	32.5	37.29	-97.611	5.6	1.6WTES
2016	812	1740	37.4	37.29	-97.611	5.8	1.5WTES
2016	812	1740	51.4	37.292	-97.608	5.5	1.8WTES
2016	812	2039	5	37.292	-97.611	5.7	2.4WTES
2016	813	1245	18	37.29	-97.611	5.9	1.3WTES
2016	813	1825	42.9	37.286	-97.617	6.3	1.4WTES
2016	815	1412	10.7	37.246	-97.657	3.9	1.9WTES

2016	815	1908	35.4	37.33	-97.486	2.5	0.8WTES
2016	816	1110	8.9	37.275	-97.425	4.2	0.9WTES
2016	817	218	4.5	37.402	-97.431	5.1	1.2WTES
2016	817	601	53.7	37.432	-97.716	0	1.5WTES
2016	817	604	18.9	37.428	-97.712	1	1.8WTES
2016	817	634	47.2	37.428	-97.713	1.1	1.8WTES
2016	817	1454	16.9	37.292	-97.613	5.8	2.0WTES
2016	818	39	44.4	37.613	-97.119	0.1	2.0WTES
2016	819	354	44.8	37.608	-97.13	6.3	1.6WTES
2016	819	1421	59.1	37.964	-96.573	7.3	2.1WTES
2016	820	632	44	37.294	-97.433	4.9	0.9WTES
2016	820	1532	54	37.295	-97.43	4.2	1.2WTES
2016	821	46	27.7	37.558	-97.264	7.6	1.7WTES
2016	821	1029	35.4	37.559	-97.267	7.7	1.9WTES
2016	821	1031	35.2	37.56	-97.28	0.3	1.9WTES
2016	821	1340	34.5	37.423	-97.7	1	1.9WTES
2016	821	1348	53.7	37.562	-97.278	7.4	1.9WTES
2016	821	1410	16.4	37.558	-97.27	7.7	2.4WTES
2016	822	455	59.7	37.285	-97.419	3.6	1.2WTES
2016	822	1112	3.6	37.232	-97.443	4.9	1.3WTES
2016	822	1435	45.6	37.304	-97.609	6.1	1.5WTES
2016	822	1511	47.2	37.305	-97.606	5.9	1.5WTES
2016	822	1906	24.8	37.306	-97.607	5.5	1.4WTES
2016	823	2123	24.8	37.413	-97.398	5.3	1.7WTES
2016	824	258	24.8	37.307	-97.601	0.1	1.4WTES
2016	824	542	4.7	37.243	-97.663	4.2	1.7WTES
2016	824	641	44.8	37.041	-97.835	8.1	2.2WTES
2016	824	717	44.2	37.244	-97.665	5.1	1.7WTES
2016	824	1613	32	37.279	-97.395	2.3	1.0WTES
2016	825	729	26.6	37.303	-97.481	3.3	1.2WTES
2016	826	423	34.3	37.056	-97.525	5.4	2.8WTES
2016	826	935	40.8	37.31	-97.473	3.8	1.0WTES
2016	826	937	26.5	37.308	-97.469	4.4	1.0WTES
2016	826	1649	32.3	37.38	-97.39	4.8	1.2WTES
2016	827	622	31.3	37.244	-97.412	0.1	1.2WTES
2016	827	1432	37.3	37.291	-97.589	5.8	1.3WTES
2016	828	313	31.9	37.282	-97.425	3.5	0.9WTES

2016	828	830	25.8	37.257	-97.576	15	1.9WTES
2016	828	1217	13.5	37.288	-97.422	3.4	1.0WTES
2016	830	138	49	37.057	-97.538	6.7	2.4WTES
2016	9 1	219	51.3	37.061	-97.534	6.5	2.9WTES
2016	9 1	1457	27.1	37.249	-97.58	5.3	2.0WTES
2016	9 3	718	25.4	37.423	-97.704	5.1	1.6WTES
2016	9 3	1202	42.5	36.296	-96.947	33.6	5.4WTES
2016	9 4	1152	28.5	37.262	-97.43	6.8	1.3WTES
2016	9 6	637	20.8	37.311	-97.497	4.8	1.7WTES
2016	9 6	1341	19.1	37.352	-97.479	2.7	1.6WTES
2016	9 6	1531	2.1	37.347	-97.488	2.4	1.4WTES
2016	9 6	1642	59	37.347	-97.488	2.4	1.5WTES
2016	910	802	14.7	37.279	-97.631	3.3	1.3WTES
2016	911	303	36.9	37.244	-97.587	9.8	1.6WTES
2016	911	2229	51.3	37.259	-97.608	9.1	1.5WTES
2016	912	21	17.8	37.352	-97.573	1.1	1.7WTES
2016	914	218	4.2	37.496	-97.355	0.1	1.6WTES
2016	915	616	46	37.411	-97.397	4.7	1.5WTES
2016	917	152	42.7	37.419	-97.405	4.5	1.9WTES
2016	917	314	25	37.243	-97.56	4.1	1.7WTES
2016	917	525	40.6	37.331	-97.453	2.6	0.9WTES
2016	917	1207	50.8	37.418	-97.402	3	1.5WTES
2016	917	1318	17	37.411	-97.393	4.6	2.7WTES
2016	917	1404	22.7	37.419	-97.389	3.8	1.5WTES
2016	917	2309	16.5	37.42	-97.4	4.6	1.5WTES
2016	918	1759	19.8	37.286	-97.629	4.5	1.7WTES
2016	919	816	10.9	37.211	-97.269	4.4	1.4WTES
2016	920	129	11.7	37.408	-97.389	5.5	1.8WTES
2016	920	131	16.4	37.423	-97.405	3.1	1.7WTES
2016	920	1042	27.6	37.357	-97.505	2.2	1.9WTES
2016	920	1111	36.6	37.353	-97.501	3.6	1.2WTES
2016	920	1120	30.9	37.347	-97.508	0.3	1.3WTES
2016	920	2041	57.1	37.211	-97.269	5.2	1.7WTES
2016	920	2121	23.5	37.209	-97.266	2.8	1.5WTES
2016	921	1934	40.8	37.232	-97.288	11.7	1.6WTES
2016	921	2121	20.5	37.217	-97.274	6.8	1.6WTES
2016	921	2243	6.8	37.225	-97.28	9.9	1.3WTES

2016	922	816	37.3	37.417	-97.4	4.7	1.4WTES
2016	922	823	25.1	37.203	-97.552	4.3	1.5WTES
2016	922	1146	50.7	37.206	-97.56	5.1	1.5WTES
2016	924	458	19.9	37.221	-97.277	8.8	1.7WTES
2016	924	2357	19.5	37.174	-97.455	12.4	1.7WTES
2016	925	411	7.8	37.212	-97.272	6.2	1.5WTES
2016	925	1015	30.5	37.415	-97.398	4.8	1.6WTES
2016	926	339	40.2	37.265	-97.514	5	1.4WTES
2016	926	649	12.4	37.24	-97.558	3.8	1.3WTES
2016	926	934	54.5	37.327	-97.485	3	1.6WTES
2016	926	1344	14.3	37.352	-97.497	4.3	1.1WTES
2016	926	1447	31.4	37.326	-97.489	2.7	1.1WTES
2016	927	2345	7.1	37.325	-97.482	3.5	1.0WTES
2016	927	2359	39.5	37.331	-97.492	0.6	1.5WTES
2016	10 1	2050	54.2	37.565	-97.234	18.7	1.7WTES
2016	10 2	101	7.3	37.266	-97.526	2.6	1.5WTES
2016	10 3	1219	51.9	37.007	-97.546	15	2.8WTES
2016	10 3	2341	15.1	37.416	-97.393	3.8	1.6WTES
2016	10 4	1741	53	37.356	-97.502	2.7	1.4WTES
2016	10 7	643	21.8	37.307	-97.609	2.8	1.4WTES
2016	10 7	644	21.9	37.282	-97.583	9.6	1.4WTES
2016	10 7	725	33.8	37.3	-97.597	1.8	1.6WTES
2016	10 7	817	51.1	37.302	-97.6	3.9	2.0WTES
2016	10 7	1609	44.8	36.948	-97.688	1.8	2.5WTES
2016	10 7	1842	44.2	37.049	-97.667	5.3	2.2WTES
2016	10 8	423	36.8	37.228	-97.286	11.1	1.6WTES
2016	10 8	512	12.7	37.212	-97.271	5.5	1.7WTES
2016	10 9	2304	30.4	37.604	-97.102	1.7	2.2WTES
2016	1010	428	21.1	37.379	-97.43	12.1	1.2WTES
2016	1010	1104	26.7	37.408	-97.425	4.4	1.3WTES
2016	1010	1954	27.1	37.402	-97.428	4.5	1.7WTES
2016	1012	829	27.4	37.421	-97.396	1.7	1.9WTES
2016	1013	227	46.2	37.33	-97.527	0.6	1.4WTES
2016	1013	248	42.6	36.859	-98.343	6.3	3.6WTES
2016	1013	1430	18.4	37.365	-97.414	0.8	1.2WTES
2016	1014	2252	48.8	36.905	-97.822	1.6	2.8WTES
2016	1015	1441	17.3	37.403	-97.431	4.7	1.9WTES

2016	1015	1545	14.6	37.407	-97.437	0.8	1.5WTES
2016	1015	2340	10.3	37.39	-97.426	3.7	1.4WTES
2016	1017	909	54.6	37.089	-97.69	10.1	2.3WTES
2016	1017	2048	52.5	37.434	-97.843	0.4	2.7WTES
2016	1018	115	39.9	36.977	-97.877	12.2	2.5WTES
2016	1019	2107	16.9	36.825	-97.663	1.4	2.4WTES
2016	1019	2233	35.9	36.839	-97.858	18.7	3.2WTES
2016	1020	106	26.6	37.093	-97.531	0.8	1.9WTES
2016	1020	124	46.7	37.295	-97.435	4.7	1.7WTES
2016	1020	1214	8.6	36.927	-97.595	1.5	3.2WTES
2016	1022	2244	34.1	37.423	-97.414	1.6	1.3WTES
2016	1022	2309	17.8	37.412	-97.399	5.3	1.4WTES
2016	1023	146	31.6	37.386	-97.419	4.7	1.1WTES
2016	1023	225	8.9	37.328	-97.493	0.8	1.1WTES
2016	1023	618	5.1	37.226	-97.286	10.6	1.6WTES
2016	1024	33	34.6	36.818	-97.55	6.5	3.0WTES
2016	1024	1325	55.2	37.13	-97.797	13.2	3.2WTES
2016	1024	1342	1.1	36.986	-97.723	17.5	2.2WTES
2016	1024	1350	13.8	37.039	-97.705	11.7	2.8WTES
2016	1024	1404	42.9	37.416	-97.435	1.2	2.0WTES
2016	1024	2310	5.9	37.406	-97.422	4.3	1.4WTES
2016	1025	248	19.4	37.41	-97.426	4	1.7WTES
2016	1025	1559	8.1	37.123	-97.792	13	2.5WTES
2016	1026	2339	25.2	37.688	-97.254	5.9	1.9WTES
2016	1026	2340	9.1	37.69	-97.226	9.8	2.0WTES
2016	1026	2352	58	37.694	-97.262	0.1	2.1WTES
2016	1027	1033	9.8	37.094	-97.589	13.7	1.9WTES
2016	1027	1124	56.3	36.925	-97.603	2.5	2.3WTES
2016	1028	1757	5.8	37.406	-97.675	14.2	2.1WTES
2016	1028	2104	39.9	37.424	-97.705	8	1.8WTES
2016	1028	2211	11.3	37.406	-97.418	5.2	1.3WTES
2016	1029	1443	17.5	37.009	-97.541	1.8	2.2WTES
2016	1029	1533	11.7	37.265	-97.315	5.4	1.5WTES
2016	1029	1652	18.4	37.424	-97.706	0.1	2.0WTES
2016	1029	1835	3.8	37.423	-97.703	8.8	2.2WTES
2016	1029	2256	36.8	37.291	-97.424	4	1.5WTES
2016	1030	402	23.8	37.286	-97.425	3.5	1.0WTES

2016	1030	503	55	37.293	-97.434	4.4	0.8WTES
2016	1030	509	56.5	37.291	-97.433	4.1	0.9WTES
2016	1030	1631	53.2	37.289	-97.424	3.8	1.4WTES
2016	1030	2058	36.5	37.292	-97.426	4.1	1.9WTES
2016	1030	2106	16.1	37.03	-97.57	12.8	2.2WTES
2016	1031	2152	1.1	37.227	-97.526	4.4	1.6WTES
2016	11 1	2229	53.5	37.393	-97.369	1.8	1.5WTES
2016	11 1	2235	9.4	37.395	-97.372	1.8	1.3WTES
2016	11 2	2238	36.4	37.288	-97.418	4.5	1.4WTES
2016	11 2	2330	4.7	37.288	-97.417	4.2	1.1WTES
2016	11 3	151	40.2	37.285	-97.415	3.9	1.4WTES
2016	11 3	400	47.6	37.287	-97.417	4.1	1.3WTES
2016	11 3	514	45.6	37.285	-97.414	4	1.2WTES
2016	11 3	620	25	37.285	-97.413	3.7	1.4WTES
2016	11 3	706	53.9	37.288	-97.414	3.9	1.4WTES
2016	11 3	743	14.1	37.282	-97.413	3.4	1.4WTES
2016	11 3	1036	50.2	37.281	-97.411	3.4	1.2WTES
2016	11 3	2211	3.5	37.289	-97.418	4.6	1.5WTES
2016	11 5	202	7.1	37.36	-97.726	8.8	2.4WTES
2016	11 5	920	21	37.367	-97.717	12.8	3.0WTES
2016	11 6	311	7.4	37.409	-97.402	4.3	1.8WTES
2016	11 6	850	59.6	37.396	-97.657	8.1	1.8WTES
2016	11 6	1133	37.9	37.246	-97.664	4.9	1.7WTES
2016	11 7	41	58.5	37.286	-97.426	3.6	1.0WTES
2016	11 7	144	25	35.969	-96.812	23.2	5.0WTES
2016	11 7	452	35.1	37.391	-97.752	8.1	3.0WTES
2016	11 7	701	43.3	37.166	-97.819	9.1	2.7WTES
2016	11 9	1040	50.9	37.331	-97.486	2.8	1.3WTES
2016	11 9	1048	17.9	37.288	-97.426	3.7	1.1WTES
2016	11 9	1728	0.9	37.221	-97.598	4.4	1.5WTES
2016	11 9	2137	37.1	37.329	-97.485	2.6	1.0WTES
2016	1110	203	52.4	37.326	-97.439	2.5	0.9WTES
2016	1112	255	51.9	36.906	-97.478	7.4	2.5WTES
2016	1112	521	49.5	37.335	-97.399	2.8	1.2WTES
2016	1112	1511	33.7	37.326	-97.479	3.6	1.0WTES
2016	1113	1355	9.7	36.931	-97.534	19.9	2.0WTES
2016	1114	135	2.9	37.215	-97.278	7.7	1.6WTES

2016	1114	1627	24.3	37.017	-97.559	8.3	2.2WTES
2016	1114	1734	6.2	37.072	-97.155	1.8	2.0WTES
2016	1114	2059	8.7	37.292	-97.422	4.1	1.6WTES
2016	1116	902	16.8	37.211	-97.57	3.2	1.7WTES
2016	1117	534	38.7	37.278	-97.637	4.6	1.7WTES
2016	1117	712	6.3	37.291	-97.422	3.5	1.3WTES
2016	1117	939	4.3	37.402	-97.427	4.4	1.5WTES
2016	1118	2326	53.4	36.852	-97.698	12.3	2.5WTES
2016	1124	1329	15.2	37.33	-97.577	1	1.4WTES
2016	1125	1519	36.4	36.859	-97.75	15.3	3.9WTES
2016	1125	2133	30.2	36.953	-97.737	21	2.6WTES
2016	1126	253	55.9	37.242	-97.652	2.1	2.0WTES
2016	1126	257	16	37.249	-97.658	3.8	2.9WTES
2016	1126	621	6.6	37.247	-97.661	4.1	2.0WTES
2016	1126	1414	14.4	37.352	-97.62	1.1	1.4WTES
2016	1126	1948	13.3	37.242	-97.661	4.3	1.6WTES
2016	1127	837	25	37.246	-97.668	5.6	1.7WTES
2016	1127	1329	13.1	37.413	-97.392	5.1	2.2WTES
2016	1127	1330	10.9	37.416	-97.412	0.4	2.1WTES
2016	1127	2032	20.8	37.418	-97.401	5	1.9WTES
2016	1127	2244	5.3	37.411	-97.387	5.5	2.4WTES
2016	1128	50	8.2	37.418	-97.394	1.1	1.6WTES
2016	1128	1135	5.5	37.41	-97.379	5.1	1.5WTES
2016	1129	132	2.5	37.409	-97.385	5	2.6WTES
2016	1129	901	24.8	37.416	-97.391	4.5	1.4WTES
2016	1130	657	55.3	37.225	-97.508	2.2	1.1WTES
2016	1130	810	13.7	37.139	-97.575	10.7	1.6WTES
2016	1130	1340	17.7	37.26	-97.548	3.3	1.2WTES
2016	1130	1406	3.3	37.252	-97.541	4	1.2WTES
2016	12 1	408	59.6	37.416	-97.405	0.5	1.6WTES
2016	12 1	454	34.6	37.419	-97.404	1.6	1.6WTES
2016	12 1	723	57.5	37.295	-97.436	4.8	1.2WTES
2016	12 1	1126	50.4	37.291	-97.431	4.6	1.4WTES
2016	12 2	852	49	37.423	-97.406	0.8	2.1WTES
2016	12 2	943	35.5	37.421	-97.399	4	1.5WTES
2016	12 2	1348	31.5	37.25	-97.539	4.6	1.8WTES
2016	12 2	1417	6.5	37.25	-97.539	4.6	1.6WTES

2016	12 2	1441	19.7	37.265	-97.556	3.7	1.5WTES
2016	12 2	1443	25	37.259	-97.547	4	1.5WTES
2016	12 2	1445	56.9	37.251	-97.539	4.5	1.4WTES
2016	12 2	1747	7.3	37.423	-97.406	2.2	1.3WTES
2016	12 3	419	27.3	37.08	-98.005	8	2.3WTES
2016	12 3	2109	47	37.292	-97.415	3.4	1.0WTES
2016	12 3	2147	31.3	37.201	-97.655	4.5	2.1WTES
2016	12 3	2307	44.4	37.147	-97.592	12	1.6WTES
2016	12 4	331	7.2	37.198	-97.653	5.3	1.9WTES
2016	12 4	845	40	37.346	-97.489	2	1.3WTES
2016	12 4	1726	49.2	37.356	-97.326	5.1	1.2WTES
2016	12 5	43	34	37.418	-97.394	4	1.7WTES
2016	12 5	216	20.4	37.418	-97.395	3.5	1.4WTES
2016	12 6	208	28	37.408	-97.4	7	1.3WTES
2016	12 6	214	42.3	37.421	-97.404	3.1	1.3WTES
2016	12 6	429	4.4	37.415	-97.402	5	1.4WTES
2016	12 6	429	29.7	37.411	-97.393	5.6	1.6WTES
2016	12 7	733	6.4	37.423	-97.418	0.1	1.4WTES
2016	12 7	1951	55.9	37.291	-97.433	4.2	1.1WTES
2016	12 7	2340	37.5	37.293	-97.426	4.3	1.5WTES
2016	12 8	503	9.2	37.294	-97.425	4.1	0.9WTES
2016	12 8	2312	43.4	37.293	-97.437	4.5	0.8WTES
2016	12 9	117	27.3	37.308	-97.6	4.5	1.3WTES
2016	12 9	340	2.3	37.403	-97.444	0.1	1.5WTES
2016	12 9	1049	53.6	37.408	-97.439	1.7	1.7WTES
2016	12 9	1120	48.7	37.412	-97.385	6.1	1.5WTES
2016	12 9	1531	21.9	37.404	-97.429	4.7	1.3WTES
2016	12 9	1611	17.1	37.408	-97.437	1.8	1.2WTES
2016	12 9	1904	40.8	37.405	-97.432	4.4	1.6WTES
2016	1210	1023	23.4	37.362	-97.612	4.2	1.5WTES
2016	1210	1800	52	37.172	-97.63	6	1.9WTES
2016	1211	1128	36.7	37.413	-97.384	4.7	1.7WTES
2016	1211	1440	45.7	37.242	-97.525	4.3	1.5WTES
2016	1211	1449	16.2	37.256	-97.544	4.1	1.2WTES
2016	1211	1531	9.7	37.239	-97.525	4.6	1.5WTES
2016	1212	108	51	37.412	-97.389	5.2	1.8WTES
2016	1212	715	34.2	37.404	-97.429	4.5	1.5WTES

2016	1212	734	55.9	37.411	-97.445	1	1.3WTES
2016	1212	1410	57.2	37.408	-97.447	0.9	1.3WTES
2016	1214	620	24.8	37.243	-97.523	4.2	1.3WTES
2016	1214	2342	43.7	37.202	-97.639	6.6	1.3WTES
2016	1215	139	12.8	37.401	-97.738	0.2	2.5WTES
2016	1215	209	58.7	37.413	-97.388	5.1	1.8WTES
2016	1215	302	45.6	37.395	-97.743	1.7	2.2WTES
2016	1215	1621	30.2	37.392	-97.712	10	1.9WTES
2016	1215	1937	28.9	37.329	-97.431	0.9	0.5WTES
2016	1216	438	59.8	37.243	-97.527	4.4	1.3WTES
2016	1216	1316	37.3	37.111	-97.649	4.3	2.0WTES
2016	1216	1729	54.3	37.273	-97.858	6.8	2.3WTES
2016	1216	2345	39	37.199	-97.612	4	1.4WTES
2016	1218	30	2.2	37.341	-97.493	3.8	1.4WTES
2016	1218	1515	12.6	36.903	-97.493	7.7	2.4WTES
2016	1218	2031	27.9	37.244	-97.528	4.2	1.1WTES
2016	1218	2355	37.3	37.21	-97.257	8.8	2.1WTES
2016	1219	749	12.1	37.2	-97.611	3.8	1.8WTES
2016	1219	928	33.8	37.242	-97.528	4.5	1.3WTES
2016	1221	653	39.8	37.24	-97.529	4.7	1.3WTES
2016	1221	751	45.6	37.239	-97.529	4.8	1.2WTES
2016	1221	757	45.9	37.244	-97.529	4.6	1.8WTES
2016	1221	820	54.4	37.242	-97.529	4.5	1.8WTES
2016	1221	1138	7.1	37.245	-97.526	4.5	1.4WTES
2016	1221	1512	49.3	37.563	-97.8	15	3.1WTES
2016	1222	1446	57.3	37.241	-97.844	7.7	2.7WTES
2016	1222	1525	31.8	37.317	-97.617	5.9	1.6WTES
2016	1222	1547	10.8	37.413	-97.395	5.3	1.4WTES
2016	1222	1606	46.3	37.414	-97.395	4.8	1.7WTES
2016	1222	2343	35.4	37.167	-97.535	9.5	1.5WTES
2016	1223	254	28.2	37.314	-97.618	6.2	1.2WTES
2016	1223	1405	6.9	37.416	-97.396	4.2	2.0WTES
2016	1223	1719	59.5	37.244	-97.528	4.5	1.5WTES
2016	1223	2012	21	37.243	-97.526	4.6	1.5WTES
2016	1224	1211	54.2	37.419	-97.396	4.3	2.5WTES
2016	1224	1318	34.3	36.911	-97.507	14.7	2.1WTES
2016	1224	1521	15.4	37.409	-97.424	4.6	1.6WTES

2016	1224	1755	40.4	37.408	-97.422	4.4	1.9WTES
2016	1224	1757	31	37.408	-97.417	5.1	1.6WTES
2016	1225	1741	58.7	37.217	-97.572	4	1.4WTES
2016	1226	351	19.7	37.258	-97.531	4.3	1.7WTES
2016	1226	1404	12.2	37.43	-97.428	4	1.3WTES
2016	1226	1642	31.8	37.191	-97.524	2.6	1.5WTES
2016	1226	1819	0.9	37.265	-97.536	2.6	1.5WTES
2016	1226	2124	45.4	37.42	-97.398	1.6	1.4WTES
2016	1226	2129	53.7	37.42	-97.413	0.1	1.3WTES
2016	1227	922	50.2	36.869	-97.729	10.2	2.3WTES
2016	1227	1729	29.9	36.963	-97.641	10.6	2.4WTES
2016	1228	1112	56.9	37.182	-97.525	1.8	1.4WTES
2016	1228	1936	52.7	37.404	-97.434	3.9	1.5WTES
2016	1228	2229	55.6	37.416	-97.394	4.4	1.7WTES
2016	1229	550	23.8	37.298	-97.566	6.4	1.5WTES
2016	1229	1056	41.3	37.314	-97.619	6.6	1.2WTES
2016	1229	2314	20.9	37.3	-97.567	6.3	1.6WTES
2016	1230	212	40.1	37.301	-97.562	6.4	1.1WTES
2016	1230	457	24.7	37.216	-97.575	3.7	1.3WTES
2016	1230	1809	25.7	37.445	-97.941	1.9	2.3WTES
2016	1231	2115	9	37.579	-97.802	1.8	2.6WTES